UC Riverside
UC Riverside Electronic Theses and Dissertations

Title

Fire Interactions and Pulsation - Theoretical and Physical Modeling

Permalink

https://escholarship.org/uc/item/851832j6

Author

Maynard, Trevor

Publication Date

2013

Peer reviewed|Thesis/dissertation

UNIVERSITY OF CALIFORNIA
RIVERSIDE

Fire Interactions and Pulsation – Theoretical and Physical Modeling

A Dissertation submitted in partial satisfaction
of the requirements for the degree of

Doctor of Philosophy

in

Mechanical Engineering

by

Trevor Brian Maynard

August 2013

Dissertation Committee:
Dr. Marko Princevac, Chairperson
Dr. Heejung Jung
Dr. David Weise

The Dissertation of Trevor Brian Maynard is approved:

_____

_____

_____

Committee Chairperson

University of California, Riverside

ACKNOWLEDGEMENTS

The completion of this dissertation would not have been possible without the help of many individuals throughout the duration of my graduate studies. First and foremost, I would like to thank my advisor, Professor Marko Princevac. He tirelessly supported my work from day one, through the good and the bad. He always made time for me, and he always listened to my ideas, even when they didn't make much sense. I will forever admire the passion and enthusiasm he has for science and for life in general, and I am truly fortunate to have had him as an advisor and friend.

I would also like to thank another faculty member, Professor Shankar Mahalingam, for his support during my first two years as a graduate student. He went far above and beyond what could be reasonably expected of any professor to help ensure my success, and I am certain that I could not have completed this endeavor without his guidance. He provided me with sage advice in mathematics and fluid mechanics, but more importantly, he helped me to believe in myself, which is something I will carry with me throughout the rest of my life.

I also had a great deal of assistance from other members of the faculty and research community. David Weise of the USDA Forest Service Pacific Southwest Research Station, who served on my committee, went to great lengths to support my research and provided the motivation for much of the material described in this dissertation. He never hesitated to provide assistance or lend an ear when I had questions. Professor Heejung Jung served as a member of my committee and was very supportive of me when I worked on the SERDP smoke emissions project. Professors Chris Dames and David Cocker served on my qualifying exam committee and provided excellent feedback on my early work. Mark Finney, Jack Cohen, Sara McAllister, and Jason Forthofer of the USDA Forest Service Rocky Mountain Research Station spent a great deal

This work is dedicated to wildland firefighters, who endure long hours,

weeks away from home, and dreadful working conditions to help protect life,

property, and our natural resources. It is the author's hope that the

information presented here will someday be of use to them.

ABSTRACT OF THE DISSERTATION

Fire Interactions and Pulsation – Theoretical and Physical Modeling

by

Trevor Brian Maynard

Doctor of Philosophy, Graduate Program in Mechanical Engineering
University of California, Riverside, August 2013
Dr. Marko Princevac, Chairperson

The study of fire behavior has numerous applications, from the control of destructive wildfires to the design of more efficient combustion engines. Two phenomena of freely burning flames, fire pulsation and flame interaction, have significant consequences for the understanding and control of fire.

Fire pulsation is a feature of freely burning flames, and is characterized by periodic, large scale fluctuations in flame structure which appear to be only dependent on the scale of the fire. To help understand the origins of these pulsations, both laminar and turbulent pool fires were filmed using a high speed camera. Fluctuations in image intensity, which occur throughout the pulsation cycle, were quantitatively analyzed to identify the existence of dominant pulsation frequencies. The measured pulsation frequencies agreed well with existing experiments from the literature. The imagery was also used to support a new theoretical model which proposes that pulsation is initially triggered by thermals, discrete convective instabilities which develop at the base of the flame before rising and disturbing the flame structure.

Fire interactions occur when two or more flames are placed adjacent to each other. Flame height, angle of tilt, burning intensity, and rate of spread have all been observed to increase as proximate fires converge. To explain the flame tilting phenomena, a model based on the conservation of linear momentum is developed, and it is shown that entrainment in the inner

region between flames is restricted as a result of flame configuration. The model is validated by using cross-correlation image analysis to analyze the behavior of passive tracer smoke placed in the entrainment field of two stationary pool fires. In addition, the heat transfer aspects of flame merging are discussed in detail, and modifications to existing fire spread models to accommodate an adjacent flame front are proposed.

TABLE OF CONTENTS

LIST OF FIGURES

1. INTRODUCTION

Since the dawn of civilization, fire has played a dichotomous role in society, its significance in the survival of man rivaled only by the magnitude of its destructive potential. For centuries, humans have attempted to both understand and control fire, capitalizing on its benefits while simultaneously struggling to live with its adverse effects.

Given its significance to human development, fire has attracted the attention of the research community for centuries, and its science spans a wide breadth of disciplines. At its core, combustion is a complex series of chemical reactions, its understanding best suited to the physical chemist. However, fire behavior is greatly affected by heat transfer and external factors such as wind, subjects which require the expertise of the physicist. Interpreting the consequences of fire involves even more specialists, be it the engineer who wishes to design a fire safe consumer product, or the forester who desires to understand the impact of wildfires on forest ecology. Though their backgrounds are diverse, these researchers all share the same goal – to understand and predict the behavior of fire.

1.1 The hazards of fire

Despite advances in fire protection technology and public awareness, the direct impacts of fire continue to plague even the most developed nations. In the United States, the National Fire Protection Association (NFPA) estimates fires claimed 3,005 civilian lives and left 17,500 injured in 2011 alone (Karter, 2012). In the same year, 30 firefighters were killed in on-duty accidents not related to cardiac arrest (Fahy et al., 2012). Fatalities occurred during structure, wildland, and vehicle fires in 2011, and there were 23 mass-casualty fires (claiming five or more lives) which resulted in 114 deaths. (Badger, 2012).

Aside from the human toll, the economic consequences of fire are substantial. Cox (1999) estimates that fire costs developed nations approximately 1% of gross domestic product (GDP) each year. In 2009, this number exceeded 2% of GDP in the United States (Hall, 2012). Interestingly, direct property loss only accounts for approximately 5% of this figure – the remainder went toward insurance coverage and injury/fatality claims, fire protection and prevention services, and fire protection technology in homes and buildings. The cost of fire department staffing alone, not including the monetary value of time donated by volunteer fire departments, reached nearly $40 billion USD in 2009, exceeding the annual budgets of the United States Departments of Agriculture, Interior, and Commerce combined (United States Government, 2009). Even a single fire event can have staggering financial implications. The Grand Prix, Old, and Padua wildfires, which merged in the southern California foothills in October 2003, were estimated to cost over $1 billion USD when considering the costs of fire suppression, post-fire rehabilitation and recovery, and insurance claims (Dunn et al., 2005).

Though casualties and economic losses are the most apparent impacts of fire, the secondary effects on human health and climate are also of concern. Smoke from vegetation fires is comprised primarily of CO, CO_2, volatile organic carbon compounds, and particulate matter (PM) (Langmann et al., 2009). Exposures to CO and PM, both acute and chronic, have been shown to cause numerous health issues (Astrup, 1972; Eftim et al., 2008). Vegetation fires also affect the earth's climate by producing greenhouse gases and aerosols which modify the atmospheric radiation budget while simultaneously eliminating biomass, a carbon reservoir (Langmann et al., 2009).

1.2   The benefits of fire

Despite its negative impacts, the presence of fire has been largely beneficial to society. It has been proposed that using fire to prepare food contributed to the rapid increase in human brain size, as more net energy can be obtained by eating cooked versus raw food, which has physiological consequences on brain development (Fonseca-Azevedo and Herculano-Houzel, 2012). Of human engineering achievements, the ability to control combustion has been arguably one of the most significant, allowing for the development of mass transportation, electrical power generation, and ultimately, globalization. Fire also serves a vital purpose in nature. One does not have to look far into the literature to find numerous studies citing the benefits of natural fire on the earth's ecosystems. For example, longleaf pine (*pinus palustris* Mill), a pine tree common to the southeastern United States, is relatively resistant to fire and relies on periodic low-intensity burning to eliminate competition from other plant species (Glitzenstein et al., 1995). In forests, the natural fire cycle is an important component of resource management, supporting biodiversity and creating a natural mosaic of trees and plants which vary in age and species (Gauthier et al., 1996). Additionally, low intensity fire can act as a housekeeper of sorts, consuming leaf litter and other surface fuels under manageable conditions. Without periodic burning, fuels can accumulate in quantities conducive to high intensity, destructive wildfires (Brown et al., 2003).

1.3   The role of fluid mechanics in fire behavior

The scientific community has long been cognizant of the impact of fluid mechanics on fire behavior. In Book VIII of his famous *Physics*, written in 350 BC, Aristotle speaks in depth about the "upward motion" of fire – clearly an early recognition of the buoyancy force which characterizes the behavior of flames. In fact, much of modern combustion science incorporates fluid dynamics as a principle topic, at both large and small scales. For example, at small scale, the

3

basic propagation of flame over a surface is inherently a boundary layer problem, where the expansion of reacting gases interacts with bulk fluid motion near the surface (Fernandez-Pello and Hirano, 1983). Also, in turbulent flames, turbulence and vorticity are critical mechanisms for the mixing of fuel and air. Combustion produces density gradients which induce rotation across the spectrum of length scales, and the turbulent structures generated are capable of entraining air far into the flame (Tieszen, 2001). The strong vertical motion of the flame causes it to behave in a manner similar to a free shear flow, spawning eddies which further enhance mixing (Weckman and Strong, 1996). At larger scale, the entire flame as a whole is often treated as a turbulent plume or jet, and many theoretical and engineering models for flame behavior are based on their familiar similarity solutions. Lastly, most modern numerical fire models, such as the widely-used Fire Dynamics Simulator (FDS) (McGrattan et al., 2000), are computational fluid dynamics (CFD) models modified to account for the reacting nature of combustion flows. Clearly, the underlying physics of fluid mechanics plays a critical role in the behavior of fire.

1.4   Scope of research

This dissertation focuses on two unique fire behavior problems that result from fluid mechanics – fire pulsation and fire interaction.

1.4.1   Fire pulsation

The phenomenon of fire pulsation is characterized by a periodic disturbance that begins near the base of the flame and propagates upwards, distorting the flame structure as it rises (Figure 1-1). The feature is quite visible to the naked eye, particularly for larger fires, which pulse at a slower rate. The frequency of pulsation is surprisingly independent of fuel type, and appears to be primarily a function of fire diameter (Cetegen and Ahmed, 1993). Though many ideas have been proposed, no universally accepted theory exists to explain the origin of pulsation. An

understanding of this phenomenon is critical in the understanding of air entrainment, flame behavior, and potentially fire propagation.
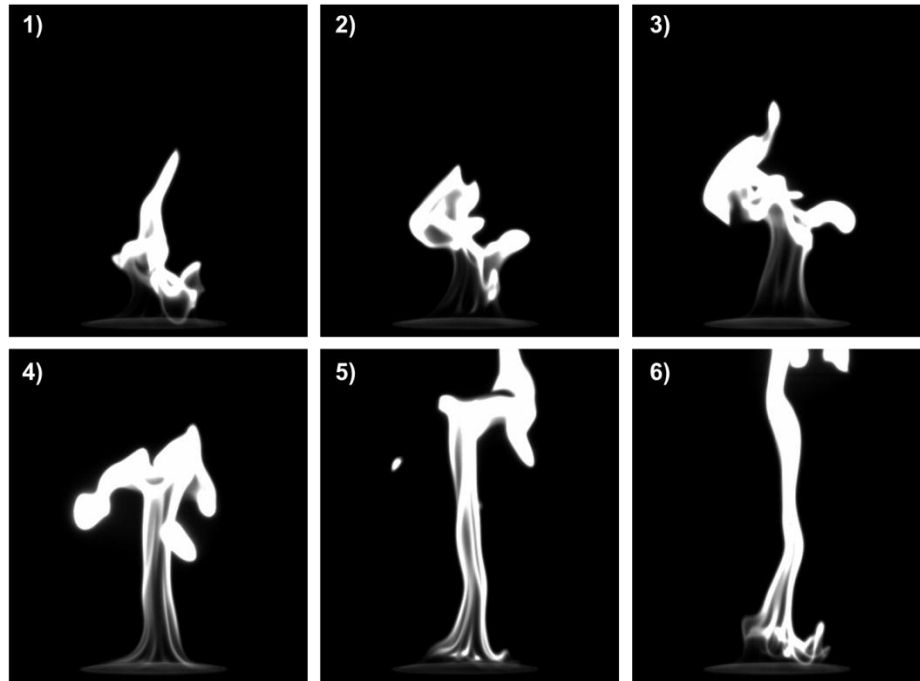
Figure 1-1: Pulsation cycle of a 125 mm diameter ethyl alcohol fire (time between frames is 25 ms). In frame 6, the cycle starts again with a disturbance at the base of the flame.

In this dissertation, it is proposed that pulsations originate from convective instabilities called thermals. Thermals are discrete buoyant structures which form in fluid layers when heated from below. The thermal itself is a packet of fluid which is less dense than its surroundings, but is initially held to the surface by viscous and thermal damping forces. Eventually, its buoyancy overcomes these restraints, and the thermal breaks free from the surface, rising into the surrounding fluid.

As will be discussed in Section 3, the surface of a pool fire (a stationary fire burning freely in a horizontal fuel bed) appears to be conducive to forming thermals. We discuss the use

5

of high speed imagery to quantify pulsation rate and identify thermal-like instabilities at the base of the flame. Experimental results are discussed in context of thermals, and two different models are proposed to explain their behavior in pool fires.

1.4.2   Fire interaction

Pulsation is a natural feature of freely burning flames and is almost always present, regardless of fire configuration. Fire interaction, in contrast, only occurs when two or more fires burn in close proximity to each other. Flame height, flame angle, heat release rate, and rate of spread (for spreading fires) have been observed to change as neighboring flames approach one another (Finney and McAllister, 2011). These effects are principally believed to be a result of interacting air entrainment fields (Baldwin et al., 1964) and enhanced heat feedback to fuels (Liu et al., 2009), but few studies have explored the combined effects of fluid dynamics and heat transfer in merging natural fires.

The interaction of flames is common in both wildland and structural fires. In vegetation fires, flame merging can occur naturally, or can be induced as part of a fire suppression or fire management plan. Common merging scenarios (Figure 1-2) include the convergence of fires generated from multiple point source ignitions, or the joining of a purposely-lit backfire with the primary flame front, which can be an effective method of fire suppression (Green, 1977). In closely spaced urban areas and wildland areas with urban development (the wildland urban interface, or WUI), burning structures can interact with each other and the surrounding fires (Rehm and Mell, 2009). An understanding of the physical process governing merging fire effects is necessary for the advancement of fire suppression and fire management models and strategies.

Figure 1-2: Examples of common scenarios for fire interaction in prescribed burns. Converging spot fires (left) and merging strip-head fires (right).

In this dissertation, we discuss the physical aspects of fire merging, namely the interaction of the flow fields of neighboring fires and its effect on fire behavior. We develop a simple flow model based on momentum conservation and potential flow theory, and test its practicality by observing the behavior of adjacent line fires. The model is validated using optical flow analysis, a method of quantitative visualization that allows indirect measurement of the flow field surrounding the fires. Additionally, we consider the potential effects of flame merging on radiative and convective heat transfer to intervening fuels, and we share the results of field observations on flame merging at large scale.

2. THE BEHAVIOR OF TURBULENT DIFFUSION FLAMES AND FIRE PLUMES (BACKGROUND)

To explore the behavior of both pulsating and interacting fires, some prior knowledge on the behavior of flames is necessary. In this section, we discuss the general characteristics of flames from natural fires and introduce the physical concepts which govern their behavior. The emphasis of this section is on the large scale fluid dynamics which control the flame structure.

2.1 The role of buoyancy

Buoyancy provides the impetus for the bulk vertical motion of the flame, and its significance to fire behavior cannot be understated. Buoyancy is the body force which arises from density inhomogeneities between adjacent fluids. In fires, the density difference is caused by temperature gradients between the flame and its surroundings, which results in the combusting gases being lifted. Buoyancy is usually represented as a force per unit volume:

$$B = g(\rho_\infty - \rho) \tag{2-1}$$

where ρ_∞ - ρ is the density difference between the ambient and rising fluid. To some extent, from a dynamics perspective, buoyancy can be thought of as the end product of combustion. Fire is a series of exothermic chemical reactions which produce heat; this heat drives the density deficiency that generates fluid motion. In this section, and throughout this dissertation, we largely ignore the specifics of combustion and make the assumption that fire is, in essence, a "buoyancy engine" which produces fluid accelerations in its surroundings. This notion is supported in the literature, at least in the study of large scale combustion-driven fluid dynamics surrounding the flame (Buckmaster and Peters, 1988; Yuan et al., 1994; Quintiere, 1989), which is our focus. This

approach would not be appropriate for the study of small scale turbulent motions within the flame, which are bidirectionally coupled with combustion reactions and have characteristic time scales which are much closer to reaction time scales (Tieszen, 2001; Bray, 1996).

2.2   Classification of flame types

In combustion science, a distinction is made between premixed and diffusion flames. In premixed flames, the oxidizer required for combustion is mixed with the fuel prior to ignition, usually by molecular diffusion (McAllister et al., 2011). Conversely, in diffusion flames, the flame obtains oxygen only from its surroundings by entrainment, and combustion occurs only after sufficient natural mixing of fuel and oxidizer has occurred (Drysdale, 2011). For laminar diffusion flames, air entrainment is primarily through molecular diffusion, while for turbulent flames, air is entrained by mixing from turbulent eddies (McCaffrey, 1983). Since the focus of this dissertation is the behavior of flames from natural fires, we will consider only the characteristics of diffusion flames in this section.

Diffusion flames with significant initial momentum (i.e., combusting gas emanating from a process stack at high flow rate) are usually jet-like in behavior, while those with negligible starting momentum behave as buoyant plumes. The momentum of the jet is forced, typically through an upstream pressure drop in a nozzle or orifice, while the turbulent plume obtains all of its momentum from body forces produced by density inhomogeneities (List, 1982). The appearance of diffusion flames can either be laminar or turbulent. For freely-burning diffusion flames, the transition to turbulence is primarily a function of fuel surface area, where flames become fully turbulent around at a diameter of 0.1 m (Corlett, 1974). For a very large fuel area, a single flame cannot be maintained, and the fire breaks up into multiple flames, called a "mass fire" (Figure 2-1). These scales are not only relevant to flame appearance – they also affect how

the flame consumes fuel. As discussed by Orloff et al. (1975), laminar flames are primarily controlled by conduction and convection at the edges of the flame, so the burning rate (per unit area) decreases as the flame grows larger. In the intermediate and larger scales, burning rate becomes increasingly affected by radiation and eventually becomes independent of fire size. Since most fires of practical concern are in the turbulent regime, we only focus on fully turbulent diffusion flames in this section.
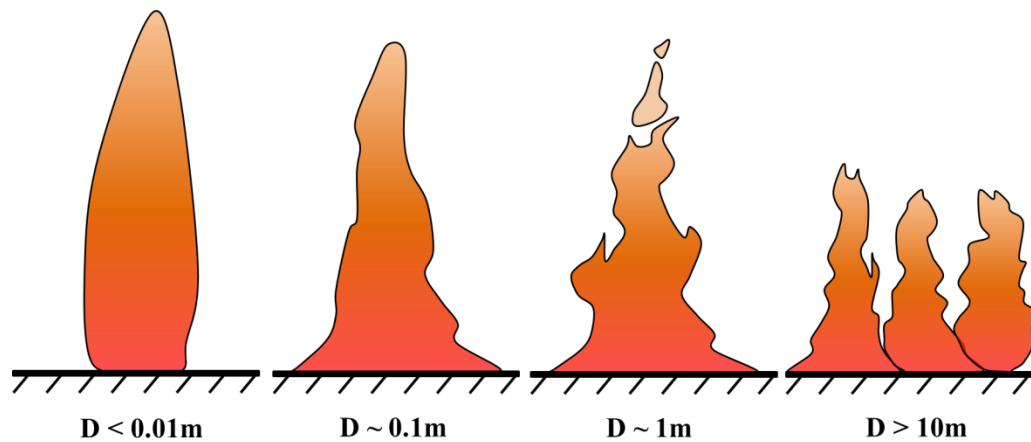
Figure 2-1: Schematic of transition from laminar to turbulent flame and eventually mass fire (adapted from Drysdale, 2011).

2.3   Structure of the turbulent diffusion flame

A schematic of the turbulent diffusion flame is shown in Figure 2-2. McCaffrey (1979) described these flames as having three distinct zones – the continuous flame zone, the intermittent flame zone, and the thermal plume. At the base of the flame, the gases have little momentum and the flame has a laminar (but not necessarily steady) appearance. In this region, the flame appears "anchored" to the fuel surface, but experiences some fluctuations in shape due to the existence of

10

a recirculation/stagnation zone where combustion products accumulate (Corlett, 1974). As pyrolysis gases rise, more oxygen is introduced and combustion activity increases, causing the plume to accelerate. For flames of sufficient size, acceleration triggers the eventual transition from laminar to turbulent flow (Weckman and Strong, 1996). In the intermittent flame zone, the visible flame tip fluctuates fairly rapidly; the upper part of this zone is what is typically perceived as the flame height. Above the intermittent zone is the thermal plume, where combustion products continue to rise due to their density deficiency relative to the surrounding air.
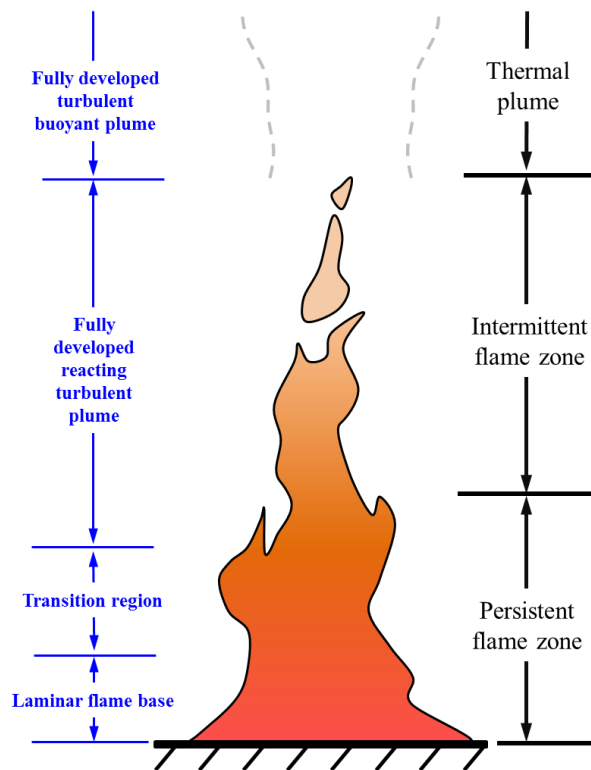
Figure 2-2: Structure of a typical diffusion flame (adapted from Bouhafid et al., 1989)

2.4 Governing equations and simplifying assumptions

The turbulent diffusion flame consists of rising, turbulent gases which also give motion to the surrounding fluid through advection. As such, the usual forms of the mass and momentum conservation equations can be applied (Tennekes and Lumley, 1976). Using index notation, these are given as:

Conservation of mass:

$$\frac{\partial \rho}{\partial t} + \frac{\partial \rho u_i}{\partial x_j} = 0 \tag{2-2}$$

Conservation of momentum:

$$\rho\left(\frac{\partial u_i}{\partial t} + \frac{\partial u_i u_j}{\partial x_j}\right) = -\frac{\partial p}{\partial x_i} + \rho g_i + \mu \frac{\partial^2 u_i}{\partial x_j \partial x_j} \tag{2-3}$$

where u is the fluid velocity, p is the fluid pressure, and μ is the dynamic viscosity. Since we are discussing turbulent flows, all vector and scalar quantities consist of mean and fluctuating components. In order for these equations to be of practical use, fire researchers often use special assumptions and approximations to recast them in a simplified form.

In buoyancy-driven flows, one commonly used simplification is the Boussinesq approximation, which assumes that density variations are only important in terms where they are multiplied by gravitational acceleration (Incropera and DeWitt, 2007). Consequently, density differences in the conservation equations are ignored, except where they affect buoyancy. Using the Boussinesq approximation, the momentum equation becomes:

$$\frac{\partial u_i}{\partial t} + \frac{\partial u_i u_j}{\partial x_j} = \frac{-1}{\rho_\infty} \frac{\partial p}{\partial x_i} - \frac{T - T_\infty}{T_\infty} g_\mathbf{i} + \nu \frac{\partial^2 u_i}{\partial x_j \partial x_j} \tag{2-4}$$

where ν is the kinematic viscosity (μ/ρ) and the equation of state for an ideal gas has been used to express the buoyancy force as a function of temperature. Though the Boussinesq approximation is helpful for simplifying the momentum equation, its underlying assumption of small density variation is questionable for fires. Flame temperatures in liquid pool fires can exceed 1400 K (Schneider and Kent, 1989; Koseki and Hayasaka, 1989). At this temperature, the density of air is less than a third of its value at ambient temperature. However, these extreme temperatures have been shown to be largely localized to the gases in the center of the flame (Fischer et al., 1987; Davis et al., 1991), while the surroundings remain relatively cool. Thus, the Boussinesq approximation is often useful for studying far-field entrainment into fires (Smith et al., 1975) and the thermal plume above the flame (Zukoski et al., 1981; Heskestad, 1998), both of which will be discussed in further detail later.

Since the Boussinesq approximation is not appropriate for the flow within and very near the flame, others have applied more complex assumptions to make the governing equations more amenable to analytical or numerical solutions. One widely-used approach was developed by Rehm and Baum (1978), who derived conservation equations for thermally-driven buoyant flows with localized heat addition. In essence, their model suggests that the timescale of heat addition (and buoyancy effects) is much slower than that of acoustic disturbances, meaning acoustic effects in the conservation equations can be filtered out. Though the model does not use the Boussinesq approximation, they showed that if small heat addition is assumed, their model

collapses to the Boussinseq conservation equations. This is the model employed by the widely-used NIST Fire Dynamics Simulator (FDS) (McGrattan et al., 2000).

One initial assumption Rehm and Baum's (1978) model is that the gas is inviscid. They based this assumption on the value of the Grashof number for turbulent flames. The Grashof number is a ratio of buoyant and viscous forces, and is essentially the natural convection equivalent of the Reynolds number:

$$\mathrm{Gr}_\delta = \frac{g\beta\Delta T\delta^3}{\nu^2} \tag{2-5}$$

where β is the thermal expansion coefficient of the fluid, α is the thermal diffusivity, and δ is a length scale. For turbulent diffusion flames, Grashof numbers exceeding 10^9 are commonly observed (Thomas, 1963; Yedinak et al., 2010), which is regarded as the upper threshold for turbulent natural convection (Quintiere, 2006).

2.5   The role of turbulence and vorticity

By definition, turbulent diffusion flames are characterized by random fluctuations in fluid properties. As illustrated in Figure 2-3, the visible structure of the turbulent flame indicates a high level of disorder across the spectrum of length scales.

Figure 2-3: Flames from a vegetation fire burning in a pine needle fuel bed (left); close up of flame structure (right)

To the naked eye, turbulent flames, both large and small, appear as pulsating towers of luminous gas which generate and shed turbulent eddies as they undulate (Figure 2-4). These large scale structures are responsible for much of the oxidizer entrainment needed for combustion to occur in turbulent diffusion flames (Pitsch, 2006). Unlike molecular diffusion, this form of entrainment is non-uniform and leads to strong species concentration gradients which facilitate mixing and diffusion at progressively smaller scales (Kuo and Acharya, 2012). The degree of interaction between turbulence and combustion reactions is dependent on their respective timescales (Bray, 1996).
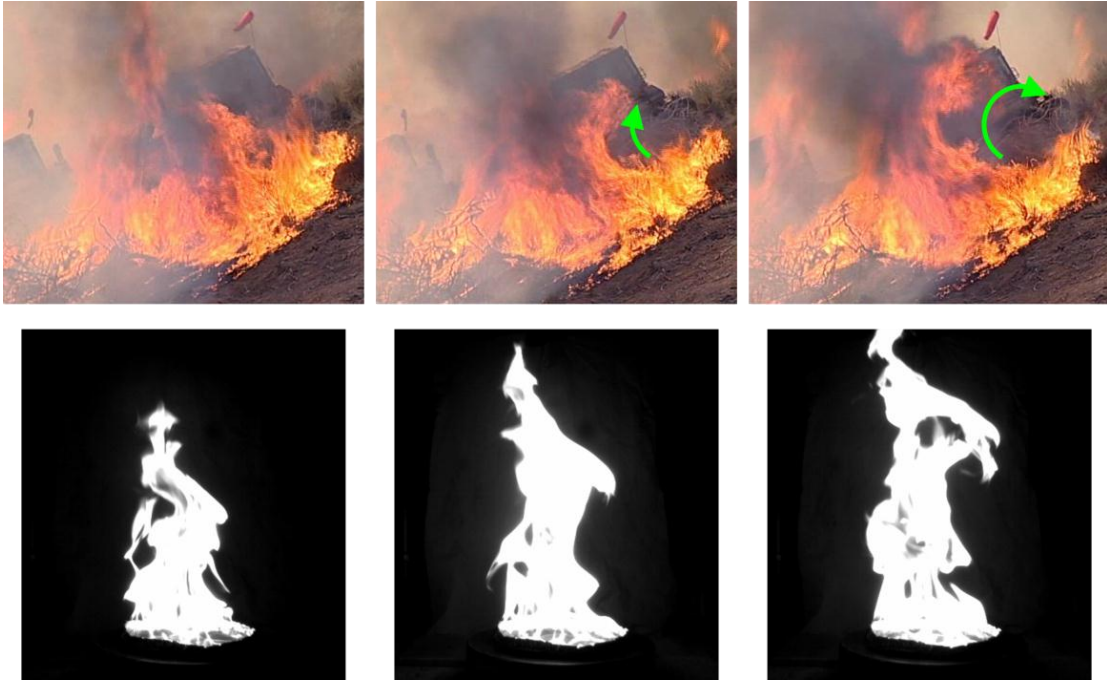
Figure 2-4: Evolution of a large eddy during an experimental vegetation fire (upper) and presence of eddies in a 20 cm ethyl alcohol pool fire (lower) (upper image courtesy of the USDA Forest Service San Dimas Technology and Development Center).

Vorticity is one of the most important concepts in turbulent combustion, as it characterizes the rotation of eddies which facilitate mixing. The vorticity equation is obtained by taking the curl of the momentum equation. In index notation, this is given by:

$$\frac{D\omega_i}{Dt} = \underbrace{\omega_j \frac{\partial u_i}{\partial x_j}}_{(1)} - \underbrace{\omega_i \frac{\partial u_j}{\partial x_j}}_{(2)} + \underbrace{-\upsilon \frac{\partial^2 \omega_i}{\partial x_j \partial x_j}}_{(3)} + \underbrace{\frac{1}{\rho^2} \varepsilon_{ijk} \frac{\partial \rho}{\partial x_i} \frac{\partial p}{\partial x_k}}_{(4)} \tag{2-6}$$

where ω is the vorticity vector. The first term represents *vortex stretching*; it results in amplification of vorticity due to strain rate and plays a major role in the turbulent energy cascade (Tennekes and Lumley, 1976). In turbulent flames, vortex stretching is thought to affect reactant

16

consumption by reducing the thickness and increasing the area over which the vortex entrains (Karagozian and Marble, 1986). Term two is related to fluid expansion, and can be positive or negative depending on whether the fluid is contracting or expanding. In fires, heat release causes rapid expansion, which can act as a sink of vorticity in the reaction zone (McMurtry et al., 1989). The third term is viscous diffusion of vorticity, which is significant only at the smallest scales where viscosity is relevant. For fire, the fourth term, *baroclinic torque*, is quite important. Physical interpretation of the baroclinic term is easier when expressed in vector notation:

$$\vec{B} = \nabla \frac{1}{\rho} \times \nabla p \qquad (2\text{-}7)$$

Baroclinic vorticity arises when the density and pressure gradients are misaligned. In the flame, the pressure gradient is hydrostatic and the density gradient points horizontally outward, which causes the cross product in (Eq. 2-7) to be nonzero. Since the only term in the vorticity equation (Eq. 2-6) that is not a function of *existing* vorticity is the baroclinic term, it is theorized that baroclinicity gives rise to the initial vorticity in the flame (Cheung and Yeoh, 2006).

2.6   Important dimensionless groups

Williams (1969) derived 28 dimensionless groups which are theoretically relevant to fire behavior. Not surprisingly, one of the most significant is the Froude number, which is widely used in the study of buoyancy-induced flows. For flames, the Froude number is given as:

$$Fr = \frac{U^2}{gl} \qquad (2\text{-}8)$$

where U is the characteristic flame velocity and l is a characteristic length scale, typically the flame height or the linear dimension of the flame at its base. The Froude number is the ratio of the characteristic and gravitational wave velocities, and is often used as the principle dimensionless

group for laboratory scaling of fires, as it appears to be the best method to emphasize convective processes (Quintiere, 1989). Since it serves as a comparison of inertial and gravitational forces, the Froude number also has significance in the behavior of wind-blown flames. When exposed to an external flow, flames tilt in the direction of the wind. The angle of tilt results from a balance of horizontal momentum flux (from the imposed wind) and the vertical momentum from buoyancy. Albini (1981) showed that the flame angle is proportional to the square root of the Froude number using flame height as the length scale and wind speed as the characteristic velocity. Flame angle has special relevance in spreading fires, as it modifies the flame's radiation view factor and may lead to other convective effects which can accelerate fire spread (Weise and Biging, 1996). This will be discussed in more detail in Sections 4 and 5.

For fires, the rate of energy release is an important parameter, as it affects flame height and entrainment rate. Zukowski (1995) defined the dimensionless energy release rate as:

$$Q^* = \frac{\dot{Q}}{\rho_\infty c_p T_\infty \sqrt{g}\, \ell^{5/2}} \tag{2-9}$$

where Q is the rate of heat release, c_p is the specific heat of air at constant pressure, T_∞ is the ambient air temperature, and ℓ is a length scale, usually the fire diameter. Physically, Q^* represents the heat release rate relative to the rate of buoyant convection, and it is important in determining entrainment rate and flame height.

In the study of wind-aided fire spread, another significant dimensionless quantity is the convection number, introduced by Byram (1959). The convection number represents the rate at which thermal energy is converted to kinetic energy in the buoyant plume above the fire, relative to the horizontal flux of kinetic energy from the mean wind:

18

$$N_C = \frac{2gI}{\rho_\infty c_p T_\infty u_a{}^3} \tag{2-10}$$

where I is the "fireline intensity" (the energy released per unit length of fire front), c_p is the specific heat of air at constant pressure, T is the air temperature, and u_a is the ambient wind velocity. The convection number has been used as an indicator of the effect of wind on fires – a small convection number indicates the flame is strongly influenced by the wind, which can cause propagation rate to accelerate. Albini (1981) and Nelson et al. (2012) showed that the convection number can be represented as the inverse of a Froude number based on buoyancy flux:

$$Fr_F = 2N_C{}^{-1} = \frac{u_a{}^3}{b_F} \tag{2-11}$$

where b_F is the flux of buoyancy per unit length of flame front:

$$b_F = \frac{g\Delta\rho q}{\rho} \tag{2-12}$$

and q is the volume flow rate of rising fluid per length of flame front.

Lastly, though not often used for large scale fire behavior, another dimensionless number used in natural convection, the Rayleigh number, is important in fire pulsation:

$$\text{Ra}_\delta = \text{Gr}_\delta \, \text{Pr} = \frac{g\beta\Delta T\delta^3}{\nu\alpha} \tag{2-13}$$

where Pr is the Prandtl number, a fluid property which represents the ratio of momentum to thermal diffusivity:

$$Pr = \frac{\nu}{\alpha} \tag{2-14}$$

The Rayleigh number is a ratio of buoyancy to viscous and thermal damping, and is a common metric used to study the stability of fluid layers subject to heat flux from below. The critical Rayleigh number serves as a demarcation between conduction and convection dominated heat transfer, and indicates the point where the fluid layer becomes unstable (Bergé and Dubois, 1984). As will be discussed in the section on fire pulsation, convective instabilities are suggested to be the initial trigger for the pulsation mechanism in pool fires.

2.7 The behavior of flames from vegetation fires

Though most of the studies of flame structure mentioned thus far have considered only stationary liquid pool fires, many of the same principles apply for vegetation fires. The primary difference between the two is in the mechanics of fire propagation. In pool fires, the flame quickly spreads over the available surface, and the entire fuel surface burns simultaneously to depletion. Dominant mechanisms for flame spread in liquid fuels are surface tension and gas phase properties (Sirignano and Glassman, 1970). In solid fuels, the spread of flame is much slower, and the fire typically consists of a single flame front which propagates through the available fuel.

In general, wildland fire science has remained largely separated from other combustion research. In the author's opinion, this is largely due to the scale and complexity of the wildland fire problem, which necessitates the inclusion of additional influences outside of traditional

combustion research. To completely understand wildland fire, one would need to by a physicist, botanist, atmospheric scientist, and physical chemist, among others. Examples of external factors which have a major effect on wildland fire behavior are micro- and mesoscale weather conditions, local geography, and forest ecology (Pyne et al., 1996). In addition, the urgent need for predictive operational tools has driven much of the research toward models which are only quasi-physical, but incorporate decades of empirical data from experiments and field observations used to fine-tune their performance. Successful examples which incorporate several existing empirical, physical, and statistical models include FARSITE (Finney, 2004) and BEHAVE (Andrews, 2007).

Given the breadth of variables which control wildland fire behavior, here we discuss only the topics relevant to the work described in this dissertation. Thorough treatments of the subject are given by Brown and Davis (1973) and Pyne et al. (1996).

2.7.1 Rate of spread

Since vegetation fires have the ability to spread, sometimes uncontrollably, much of wildland fire science has been dedicated to understanding how fast the fire will move and in what direction. The rate of propagation (commonly called rate of spread or ROS) is dependent on many factors, including (but not limited to) fuel characteristics (composition, arrangement, moisture content), terrain, and wind (Anderson, 1982; Rothermel, 1983; Baines, 1990).

To date, many of the physical models developed to explain fire spread have assumed radiation heat transfer to be the principal mechanism of heat transfer to fuels adjacent to the flame, and detailed radiation-based models can be found throughout the literature (Emmons, 1964; Van Wagner, 1967; Albini, 1985; De Mestre et al., 1989). However, as highlighted by Finney et al. (2012), numerous models and experiments have demonstrated that radiation alone is

generally incapable of heating fuels to ignition. In Baines' (1990) discussion of the radiation model of De Mestre et al. (1989), he notes that the predicted fuel surface temperatures are over 100K below what is required for the ignition of their fuel particles, which is likely a result of convective cooling. Additionally, experiments by Fang and Steward (1969), Vogel and Williams (1970), Yedinak et al. (2010), and others have shown that ignition in discontinuous fuel beds only occurs after flame contact, which indicates that convection heat transfer must play a key role in fuel particle ignition. Recent experiments at the USDA Forest Service Rocky Mountain Research Station (Finney et al., 2013; Adam et al., 2013) have suggested that convection drives fire spread in discontinuous fuel beds, primarily by the advection of fluctuating longitudinal vortices which penetrate the flame front, convectively heating the fuels ahead of it. Though the problem of fire spread is far from solved, it is gradually becoming more apparent that fluid mechanics plays an important, perhaps principal, role in the process.

2.7.2   The effect of wind

Wind is one of the most important factors affecting fire spread. Fires burning with the wind (head fires) are generally more intense and spread faster than those burning against the wind (backing fires) (Figure 2-5). Wind affects spread rate by enhancing both radiative and convective heat transfer to fuels ahead of the flame (Weise and Biging, 1996), and by increasing the frequency and distance of spot fires, which are caused by burning embers being advected onto receptive fuels ahead of the main flame front (Albini, 1983).

<div align="center">

Head fire
- Tilted in the direction of the wind
- Enhanced radiation and convection → faster ROS
- More spot fires

Backing fire
- Tilted away from wind
- Slower ROS
- More easily controlled

</div>
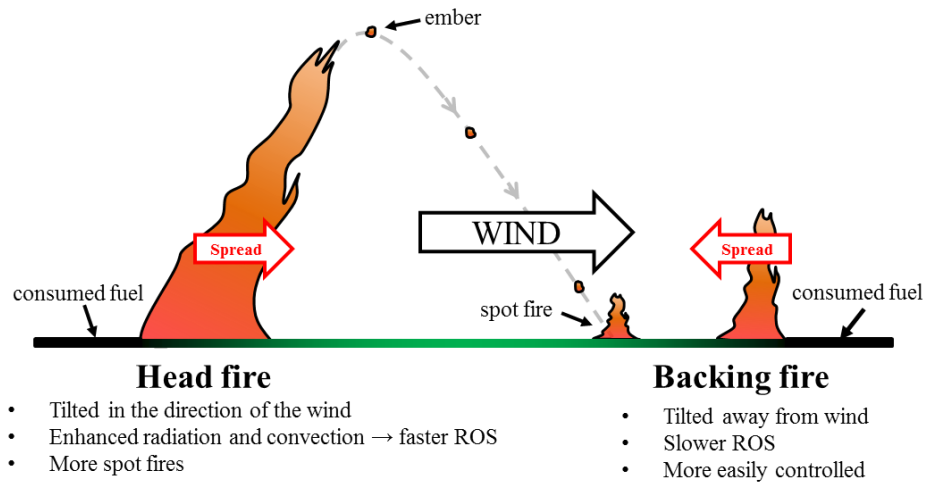
Figure 2-5: Wind-aided (head) fire versus wind-opposed (backing) fire

The angle of the wind-blown flame relative to the surface is important in determining the amount of heat transferred to fuels ahead of the flame. As discussed previously, both radiant and convective heat flux control fire spread, and flame angle acts to increase both quantities. As the flame tilts toward the surface, radiant heat flux rises due to an increasing view factor (Baines, 1990). Concurrently, buoyant eddies shed by the flame achieve an increasingly horizontal component of flow (Zhou et al., 2005), enhancing convective heat transfer. Albini (1981) used dimensional arguments to predict that the flame angle is proportional the square root of the Froude number using flame height as the length scale:

$$\tan\theta \sim \left(\frac{U^2}{gH}\right)^{1/2} \sim Fr^{1/2} \tag{2-15}$$

where H is the height of the flame. This relationship was supported by the experiments of Weise and Biging (1996), who studied the behavior of wind-aided spreading fires in wooden stick fuel beds. They also noted that the relationship held when Froude number based on flame length was used, where flame length is given by:

$$L_f = \frac{H}{\cos \theta} \qquad (2\text{-}16)$$

2.8   Experimental methods

Obtaining accurate measurements of fluid dynamic phenomena can be challenging. This is especially true for flames, as the fire environment is extremely harsh on equipment and instrumentation. Active sensors, such as thermocouples, pitot tubes, and heat flux sensors have long been the workhorses of fire research. However, since they are enveloped in flame, they are subject to thermal damage, fouling from soot, and measurement inaccuracies due to sensor heating (Quintiere, 2006). These issues make the use of passive sensors an attractive option. For measuring the velocity fields in and around laboratory fires, optical methods have been widely used. One such method is particle image velocimetry (PIV), in which the flow field is seeded with small particles which are advected with the flow (Adrian, 1991). A thin laser sheet is used to illuminate the particles in a single plane of interest, and two images of the plane are taken in rapid succession. The two images are compared using a cross-correlation algorithm, which gives the instantaneous velocity field between frames. PIV has been successfully used in laboratory scale fires (Tieszen et al., 2002; Sun et al., 2005; Lozano et al., 2008, Lozano et al., 2010), but it is generally not practical to deploy at larger scales, though it has been used on a 10 m x 5 m outdoor vegetation fire with moderate success (Morandini et al., 2012). Other optical methods, such as

laser-Doppler velocimetry (LDV) have also been successfully deployed on small scale fires (Zhou and Gore, 1995). For measuring flame and fuel temperature, infrared cameras have been widely used, both in the laboratory (Khanna et al., 1994; Engstrom et al., 2004; Martínez-de Dios et al., 2006) and in the field (Clark et al., 1999). Thermal cameras have also been used to estimate flame velocity by tracking the motion of isotherms (Zhou et al., 2003). Lastly, one should not undervalue the usefulness of simple visible images, as they are still commonly used to measure flame structure, height, angle, and rate of spread.

In the experiments described in this dissertation, we make use of several nonintrusive methods – optical flow (of which PIV is a subset), infrared, and visible imagery. These methods are advantageous in that they are simple to deploy, are not damaged by heat or smoke, and provide a relatively high sampling frequency (30 Hz or greater). However, since they can be prone to errors associated with image-based measurements, significant care must be taken when interpreting the results.

3.   A SIMPLE FREE CONVECTION MODEL FOR THE POOL FIRE PULSATION PROBLEM[1]

3.1   Introduction

Among the most compelling features of freely-burning fires is the existence of air currents driven solely by high temperature combustion reactions. The study of these so-called "reactive flows" has a great breadth of application, from the suppression of destructive wildfires to the design of advanced propulsion systems. A long observed feature of free-burning horizontally oriented fires (pool fires) is the oscillatory behavior of the flame structure, commonly known as "flickering" or "puffing". Byram and Nelson (1969) described the behavior as *"...an expansion of the flames near the base of the fire (which is) followed by a sudden collapse of these flames toward the center of the fire. A flame bulge then travels upward to the flame tip in an even, wavelike motion. Expansion of the lower part of the flames starts the cycle again"*. This oscillation occurs at a consistent frequency, and its behavior appears to be a function of fire size and ambient air entrainment path only. Numerous experiments over the past several decades have shown remarkable agreement with the relationship $f \sim D^{-1/2}$, where f is the frequency of oscillation and D is the fire diameter (in meters). The relative indifference of this periodic behavior to other fire-related variables (including heat release rate and fuel type) suggests that it is not a result of combustion or flame chemistry, but rather one of free convection fluid mechanics. Experiments support this idea, as similar oscillatory behavior has been observed in non-reacting buoyant plumes (Cetegen and Ahmed, 1993) and simple Rayleigh-Bénard convection experiments (Qiu, 2001).

---

[1] Parts of this section are reprinted from Combustion Science and Technology Vol. 184, Issue 4, Maynard, T. and Princevac, M. "The Application of a Simple Free Convection Model to the Pool Fire Pulsation Problem", Pages 505-516, Copyright (2012) with permission of Taylor & Francis Ltd.

A single pulsation cycle for a 12.5 cm diameter ethyl alcohol pool fire is shown in Figure 3-1. Near the base of the fire, the flame is initially narrow and appears laminar (frame *a*). By laminar appearance, we mean the absence of fine unsteady structures. In frames *b-e*, a "luminous ring" appears at the base and propagates upward into the fire plume, resulting in significant deformation of the flame sheet. The structure is eventually shed and the flame narrows, after which the cycle begins anew (frames *f-g*). For larger fires, Weckman and Sobiesiak (1988) noted that the cycle began with a small ring of high luminosity near the pool's edge, which propagated toward the center and eventually led to large scale eddies.
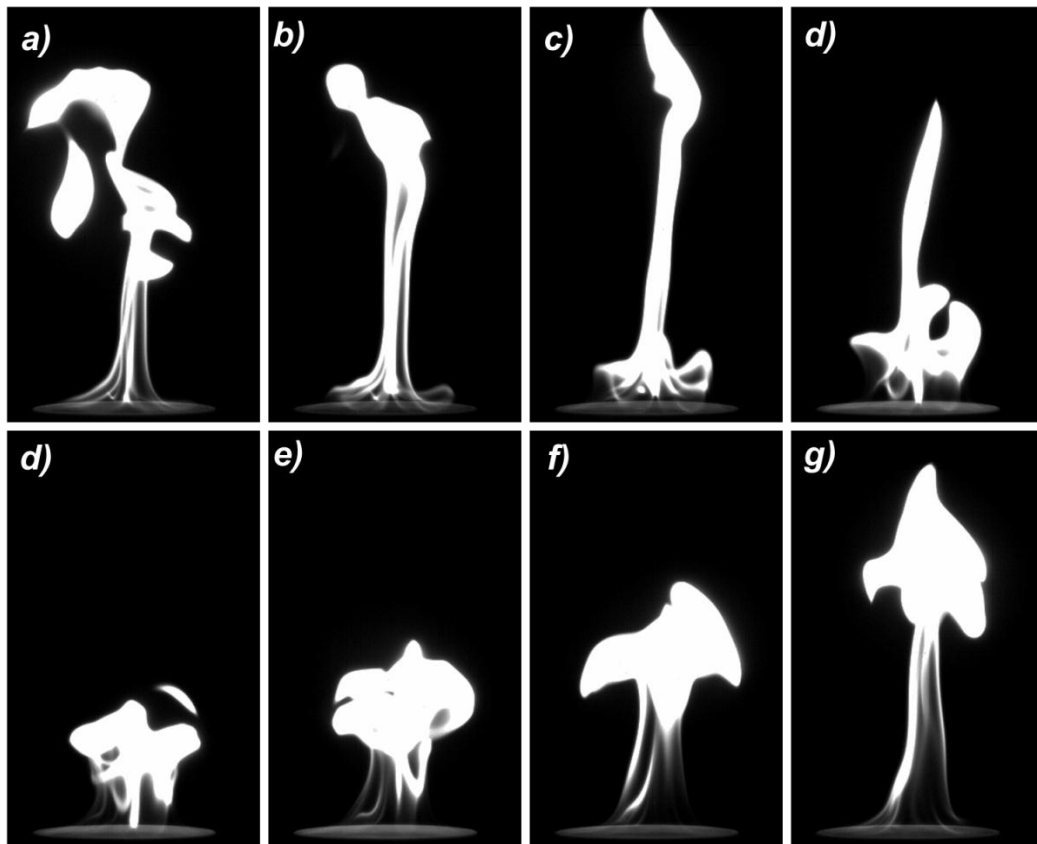
Figure 3-1. Complete pulsation cycle of a 125 mm diameter ethyl alcohol pool fire.

Though many explanations for the pulsation phenomenon have been proposed, there is presently no single accepted theory for its origin. In this section, we propose that the source of pulsation is the development of convective instabilities, or thermals, which form around the rim of the fuel surface. A high speed camera is used to visualize both laminar and turbulent flames, and their pulsation rate is determined by calculating the power spectral density of fluctuations in grayscale image intensity. Two different simple models for thermal growth are proposed, both of which predict the pulsation frequency as a function of diameter ($f \sim D^{-1/2}$), which agrees with published data.

3.2   Background

3.2.1   Theories on the origin of pulsation

While it is quite obvious that pulsation is a phenomenon of fluid dynamics, the source of the instability has long been debated. The first documented study on flame pulsation known to the author was by Chamberlin and Rose (1948), who studied the behavior of pulsating laminar flames from gas burners using eight different fuels and two different burner tips. Changes in fuel type and gas flow rate appeared to have little to no effect on their pulsation rate, which was nominally 10 Hz. Changing to a smaller burner tip, however, did cause a small increase in oscillation frequency. They hypothesized that the periodicity was due to changes of oxygen diffusion rate into the flame, with the longest flame lengths occurring during high rates of diffusion, and vice versa. Byram and Nelson (1969) began to focus more specifically on the fluid mechanics of the problem. They studied the pulsation of large, turbulent flames from circular pools of up to 8 ft. in diameter. From dimensional analysis, they identified two important dimensionless groups:

$$\pi_1 = t \left(\frac{g}{D} \right)^{1/2} \qquad\qquad (3\text{-}1)$$

$$\pi_2 = \frac{I}{(gD)^{1/2} \rho c_p T} \qquad\qquad (3\text{-}2)$$

where t is the pulsation period, D is the fire diameter, and I is the rate of convective heat output per unit area. They theorized that well-organized pulsation only occurs over a range of π_2 values. If π_2 is too small, the areal burning rate is not large, and the fire likely consists of multiple flames (a mass fire). Though each of these flames may individually pulse, unified behavior is not discernible. Conversely, they suggested as π_2 becomes large, the lower portion of the flame begins to assume jet-like behavior, and much of the pulsation appears to cease. It is in their discussion of π_2 that "convection cells" are first mentioned, a concept which will be key to our pulsation model. From their experiments, Byram and Nelson (1969) determined that pulsation frequency generally followed:

$$f \propto D^{-1/2} \qquad\qquad (3\text{-}3)$$

where f is the frequency of pulsation, and D is the fire diameter in meters. This relationship has been subsequently demonstrated by other researchers using gas, liquid, and solid fuels over a wide range of geometric scales (Sibulkin and Hansen, 1975; Hertzberg et al., 1978; Evans et al., 1992).

Over the past three decades, most researchers have focused on fluid instability analyses and numerical studies. Cetegen and Ahmed (1993) theorized that as the rising plume of heated gas decelerates in ambient air, the air entrained at the base of the fire is significantly disturbed by

vertical shear, which leads to the formation of large vortices. Weckman and Sobesiak (1988) hypothesized that strong buoyant accelerations cause the development of vortices around the fire perimeter, which then disturb the existing flame sheet, which lead to various modes of instability. Yuan et al. (1994) used buoyant helium plumes as an analog to support the idea that buoyant acceleration at the plume base directly leads to a Kelvin Helmholtz-type instability. The experiments of Tieszen et al. (2002) clearly illustrate that the visual effect of pulsation is caused by the passage of large turbulent structures from the base of the flame to its top. In recent years, direct numeric simulation (DNS) studies (Luo, 2004) have popularized the theory that rotation caused by the misalignment of the density and pressure gradients (*baroclinic* vorticity) is the primary mechanism of fire pulsation. As mentioned in the previous section, since baroclinicity is the only term in the vorticity equation that creates vorticity, Luo (2004) theorized that pulsation begins as a baroclinic instability at the base of the flame.

3.2.2   Pool fire velocity fields

As previously mentioned, McCaffrey (1979) observed that the pool fire velocity field consists of three distinct zones. The *persistent flame* region, which exists directly above the base, is characterized by a stable, luminous flame which surrounds a core of "cold" fuel-rich vapor. The existence of this region is evident at the surface of the pool fire velocity field (axial center) shown in Figure 3-2. The vapor core is believed to exist because the laminar nature of this region limits the entrainment of oxygen (Corlett, 1974). Above the persistent flame zone is the *intermittent* region, where strong flame fluctuations occur and temperature begins to decrease with height. Finally, in the *plume* region, buoyancy production ceases and temperature continues to decrease with elevation.
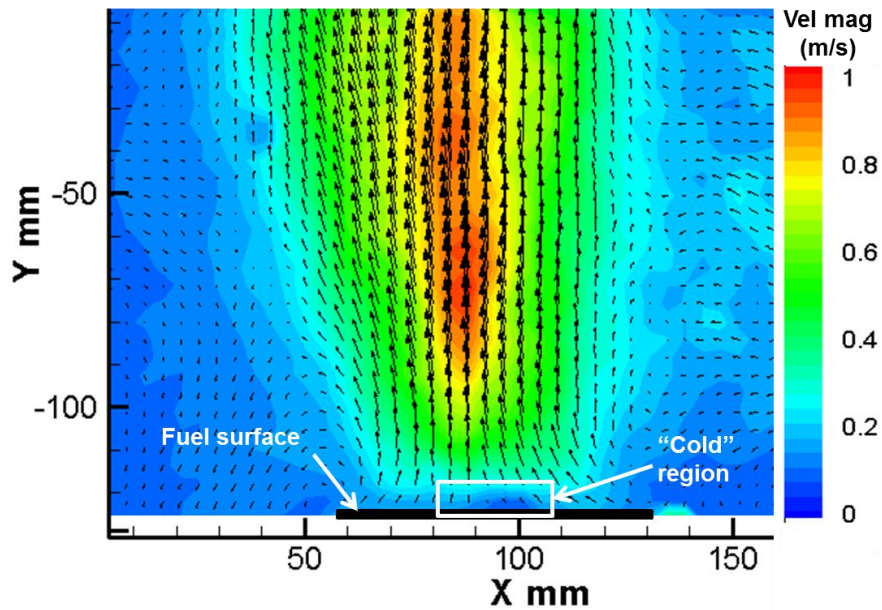
Figure 3-2: Time-averaged velocity field for a 70 mm ethyl alcohol pool fire obtained by the author using particle image velocimetry (PIV). Note the presence of the central region of low velocity near the base.

The primary source of vertical motion in pool fires is buoyancy, which is produced by high temperature combustion reactions throughout the fire plume. Inflow, or entrainment, is a result of both buoyancy and turbulent mixing. Previous experiments (Sun et al., 2003) demonstrate that the peak velocities occur at a significant distance above the fuel surface. Very near the surface, buoyancy flux and entrainment are minimal (Figure 3-2). It is within this initial "quiescent" portion of the persistent flame region that large scale pulsations appear to originate.

3.2.3 Thermal convection

Howard (1966) developed a theory of natural convection over a heated horizontal plate based on the thermals. In essence, he assumed that during initial heating of the surface, a molecular boundary layer grows over the plate (conductive phase). This is immediately followed

by a short separation phase during which the fluid parcel thermal is liberated from the surface (convective phase). After the thermal leaves, the original conditions are restored, and a new cycle begins. Since it is assumed the conductive phase is much longer than the separation phase, the traditional error function solution of the heat conduction equation is averaged over the conductive time scale. The key result is that the molecular boundary layer thickness grows as:

$$\delta = \left(\alpha t\right)^{1/2} \tag{3-4}$$

In a pool fire, the origin of the flame's vertical motion is the fuel surface, where fuel vapor is generated and ascends into the plume. One of the primary mechanisms of fuel vaporization in pool fires is radiant feedback from the fire plume itself (Hertzberg, 1973). Since air is largely transparent to incident radiation, radiant heating of the fuel surface likely creates a temperature gradient between the fuel and the air in the quiescent region directly above. This condition can be considered analogous to a horizontal heated plate, with the fuel surface acting as the heat source. If this surface is at a higher temperature than the gases above, the situation is statically unstable. It is hypothesized that this instability leads to the large scale pulsation observed in pool fires.

3.3   Laboratory experiments

Flames are a unique class of fluid flows, since their luminous appearance provides "free" flow visualization, at least for a portion of the flow field. This is helpful, since, as mentioned in the background section, accurate quantitative measurements of fire-induced velocity fields are difficult to obtain. For fire pulsation, simple flame imagery has captured many of the salient features of the phenomenon, including the expansion and contraction of the turbulent flame (Weckman and Sobesiak, 1988), the pulsation of laminar diffusion flames (Yuan et al., 1994), and the formation of large scale structures (Cetegen and Ahmed, 1993). Malalasekera et al.

(1996) used high speed videography to analyze the structure of pulsating pool fires. They noted that though the visible flame is only a limited approximation of the true velocity field, they found that the pulsation frequencies obtained were comparable to those measured using a pressure probe near the base of the flame.

In our study, the objective of laboratory experiments was twofold; first, we aimed to see if thermal-type instabilities were luminous and evident on the pool surface, and second, we wanted to develop a simple method to quantify pulsation rate based only on a series of images.

3.3.1   Experimental Setup and Measurement Techniques

High speed videography was used to visualize the behavior of six separate pool fires, which were conducted using reservoirs with diameters of 30, 40, 70, 75, 105, and 125 millimeters. The fuel used was ethyl alcohol (190 proof), and fuel reservoirs were filled to the maximum level possible prior to ignition. As noted by Cetegen and Ahmed (1993), pulsation appears to be insensitive to fuel type, so luminosity and smoke production were the only considerations in fuel selection. Of the fuels tested, ethyl alcohol produced the most luminous flame with minimal smoke.

Images with a resolution of 640 x 480 pixels were captured at rate of 125 Hz, using a Troubleshooter (Fastec Imaging Corporation) high speed camera. The camera was placed directly in front of the fire at a distance which allowed the entire visible flame to be captured. A butane lighter was used for ignition and fires were allowed to burn for 30 seconds prior to capturing. The laboratory environment was controlled to ensure flames were not disturbed by ambient flows. Fuel reservoirs were placed on a flat table and were isolated from objects to allow for unobstructed entrainment. For each fire diameter, a total of five captures (consisting of 875 frames each) were recorded. Between captures, the reservoir fuel level was replenished. The

small decrease in fuel level during the burning period was assumed to have a minimal effect on overall flame behavior.

3.3.2   Image processing

Typical applications of high-speed imagery in the study of fire pulsation have primarily focused on qualitative or simple quantitative analysis (by determining the number of frames between pulsations). More recently, Wu et al. (2011) developed a method for quantifying pulsation frequency based on the moment function of the imagery. In our study, the behavior of grayscale pixel intensity was analyzed to determine if a correlation exists between simple pixel intensity fluctuations and the visible pulsation of flames.

To process images, video captures were separated into their individual frames, with a total of 875 unique images (7 seconds) for each case. For each frame, the grayscale intensity of each pixel was converted to an 8-bit integer, with zero representing "total absence" (completely black) and 255 representing "total presence" (completely white). For each frame, the sum of pixel intensities was calculated:

$$\sum_{x=1}^{n}\sum_{y=1}^{m} I(x, y) \tag{3-5}$$

where I is the grayscale intensity and n and m are the number of pixels in the x and y directions, respectively.

To obtain pulsation frequency from the image series, the power spectral density (PSD) of the image intensity signal was calculated. In statistical signal processing, the PSD is a metric which describes the distribution of signal power in the frequency domain. The power of a signal is defined as (O'Shea et al., 2011):

$$P = \frac{1}{T}\int_0^T |x(t)|^2 dt \qquad (3\text{-}6)$$

where x is the signal and T is the period. Parseval's theorem states that the integral of the square of a function is equal to the integral of its Fourier transform. Thus, the power of a signal can be obtained from its representation in the frequency domain:

$$P = \sum_{k=-\infty}^{\infty} |X_k|^2 \qquad (3\text{-}7)$$

where X_k is the Fourier transform of the signal. In our case, the image signal is finite (125 frames per second), so the discrete Fourier transform (DFT) is used:

$$X_k = \sum_{n=0}^{N-1} x_n \exp\left(\frac{-2\pi i k n}{N}\right) \qquad (3\text{-}8)$$

The power spectral density is the representation of P as a function of frequency, and it allows the identification of periodicity in a signal. In a plot of PSD, the power of the signal will be large at frequencies which coincide with the signal's periodicity. Signals with strong periodicity have spikes of large amplitude at the dominant frequency, while less uniform signals distribute their energy over a larger spectrum of frequencies.

3.3.3 Experimental results

3.3.3.1 Visual observations

Since Reynolds number could not be reliably determined using the imaging techniques described above, the stability classification of flames (laminar, transitional, or turbulent) was

determined subjectively, based on the appearance of fine eddy-like structures (or lack thereof) within the flame.

For the two smallest fires (30 and 40 mm), the flame was laminar in appearance. Dramatic changes in flame structure were not evident, but the flame did exhibit a periodic undulating motion. At the peak of the pulsation cycle, the upper part of the flame separated from the lower portion and rapidly left the frame.
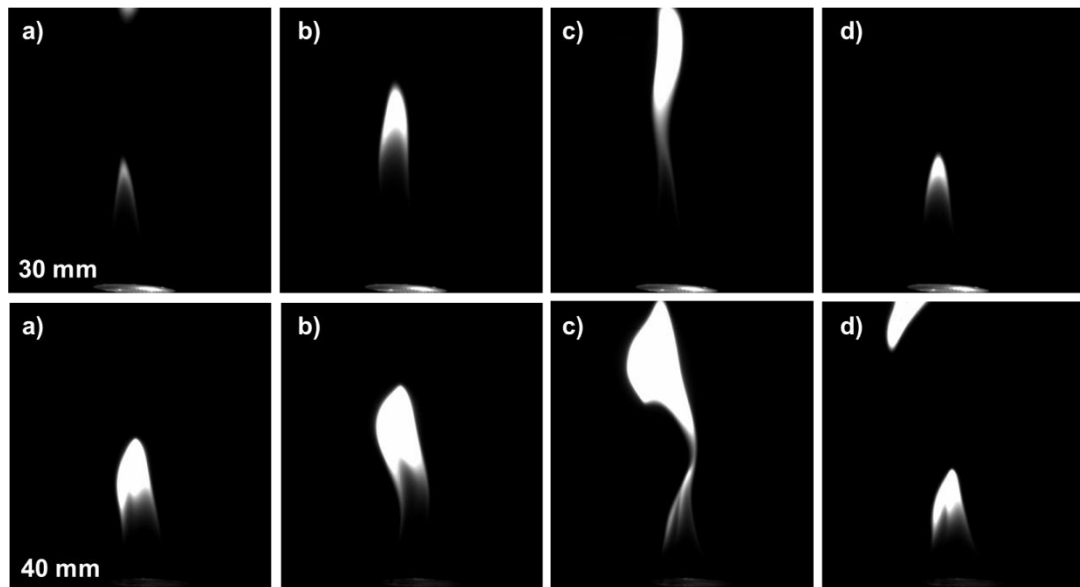
Figure 3-3: Pulsation cycle of 30mm (upper) and 40mm (lower) flames. Time between frames is 25ms.

As the fire diameter increased to 70 mm, the early transition to turbulence (fine, unsteady eddy-like structures) was evident in the upper regions of the flames (Figure 3-4). A definite pulsing behavior became apparent mid-way up the flame. However, disturbances at the fuel surface were not visible. The 75 mm flame was similar, except even finer structures were visible in the flame (Figure 3-5).
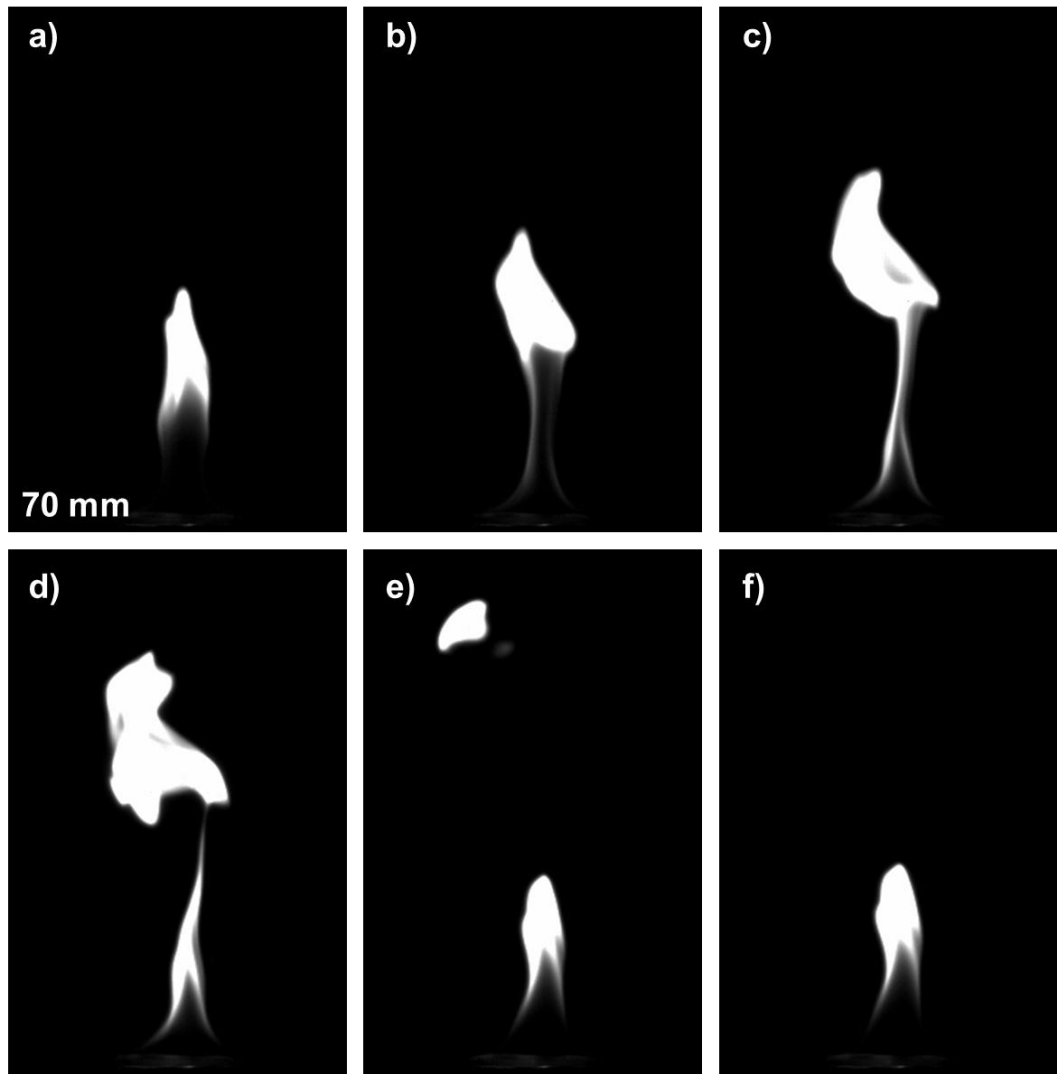
Figure 3-4: Pulsation cycle of 70 mm flame. Time between frames is 25ms.
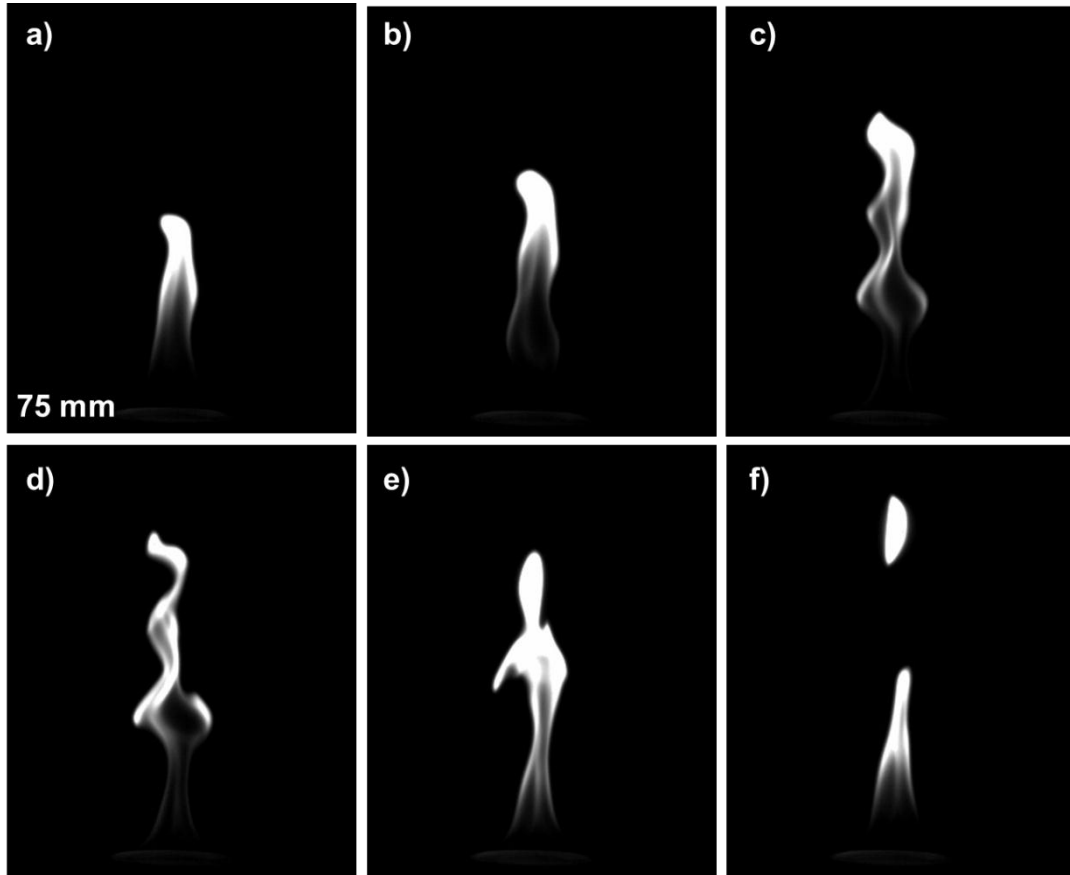
Figure 3-5: Pulsation cycle of 75 mm flame. Time between frames is 25ms.

Images from the 105 mm flame are shown in Figure 3-6. The flame appeared fully turbulent (a range of unsteady eddy-like structures was apparent) in the upper region of the flame, but at low elevations the flame still appeared to be laminar. Disturbances appeared to originate from the base of the flame, but the luminosity was insufficient to determine if this was the case.
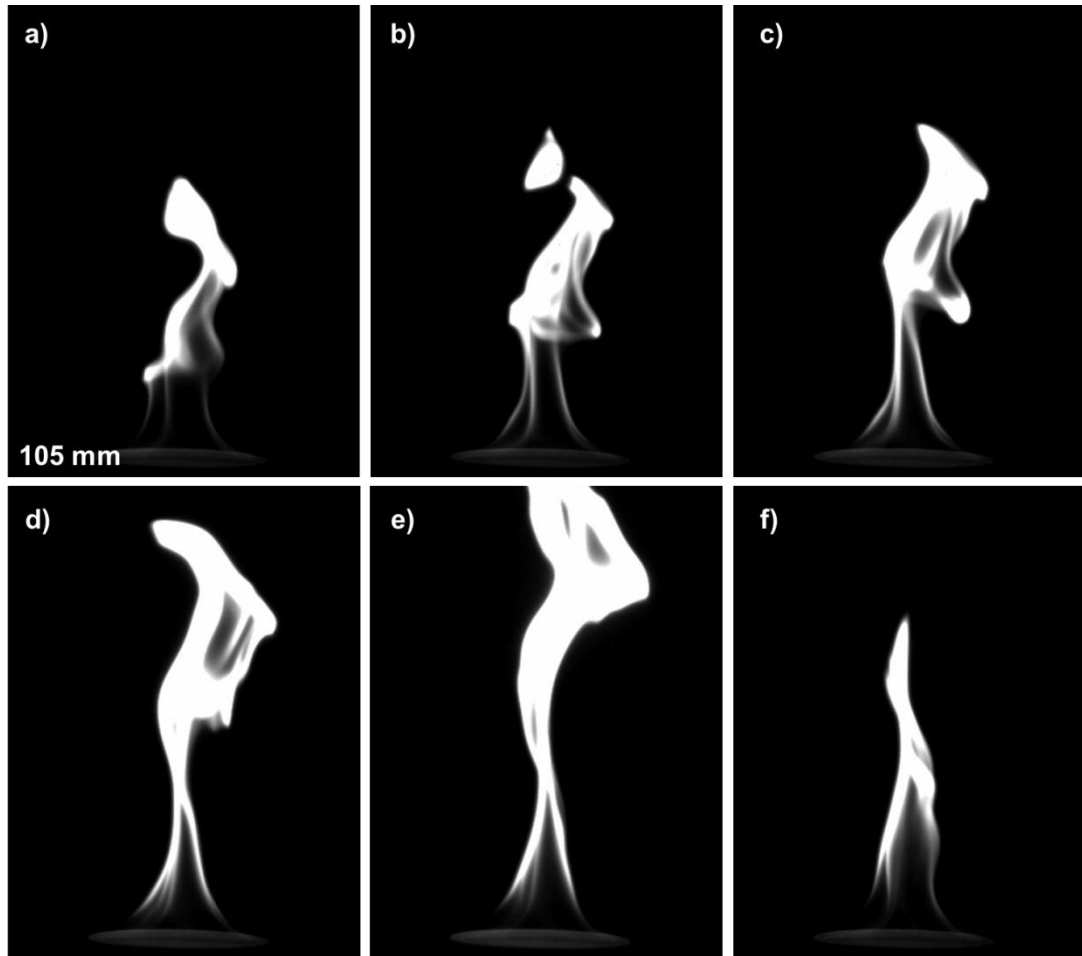
Figure 3-6: Pulsation cycle of 105 mm flame. Time between frames is 25ms.

For the 125 mm flame, pulsations were clearly visible and began with the development of multiple, visible luminous structures at the base of the flame. These structures often appeared as a continuous ring around the entire rim of the flame, but sometimes only appeared in a single location. In Figure 3-7 (frames *b* and *c*), a luminous structure appears at the base of the flame. After rising vertically, it is quickly absorbed inward towards the flame core. This is immediately

followed by the formation of a large scale vortex that propagates upward through the fire plume and eventually burns out.
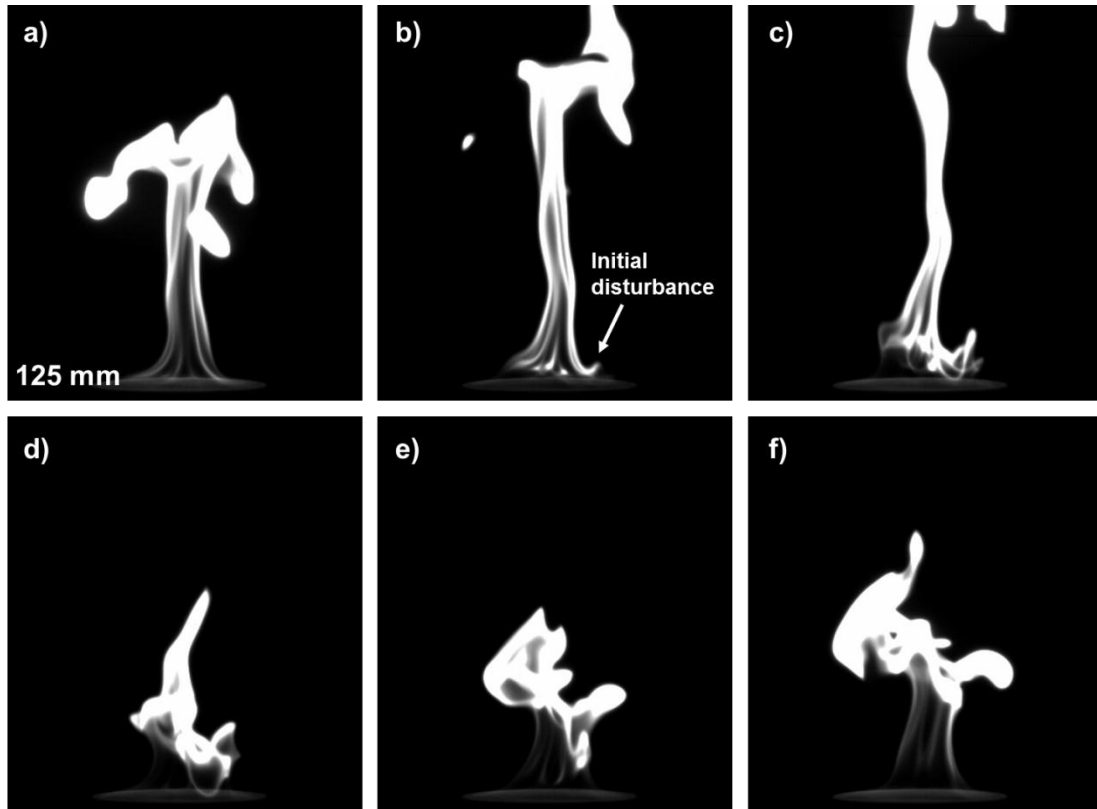
Figure 3-7: Pulsation cycle of 125 mm flame. Time between frames is 25ms.

Given the interesting characteristics of the disturbances at the base of the 125 mm flame, a second experiment was run for this case where the video camera was angled slightly toward the pool surface. The same camera and frame rate (125 Hz) were used. As shown in Figure 3-8, small structures were seen to form on the pool surface (frame *b*), which appeared to amalgamate and lead to a larger scale disturbance in the upper part of the flame, resulting in a sudden large

increase in luminosity, which is apparent in frame *h*. Though we cannot say conclusively that this is evidence of Rayleigh-Bénard -type convection, these images appear to support this notion.
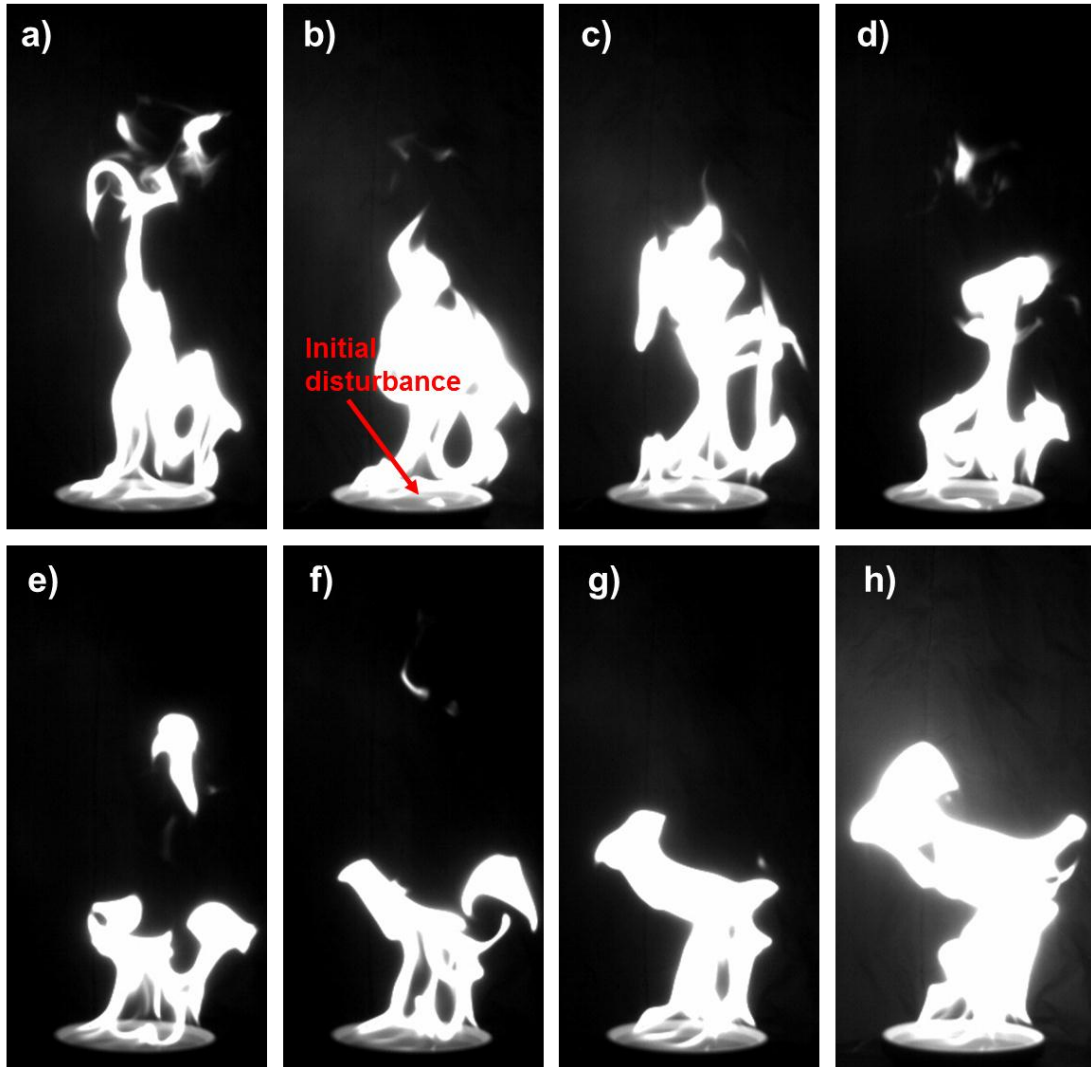
Figure 3-8: Pulsation cycle of 125 mm flame with camera tilted toward pool surface. Time between frames is 80ms. Note the formation of small disturbances on the surface of the fuel and the sudden increase in luminosity in frame *h*.

3.3.3.2 Pulsation frequency

In analyzing the high speed imagery presented above, it was observed that the peak of the pulsation cycle coincided with an increase in visible light. This was verified by analyzing the temporal behavior of the image intensity. As shown in Figure 3-9, for most flames, the pulsation cycle coincided with large changes in image intensity.
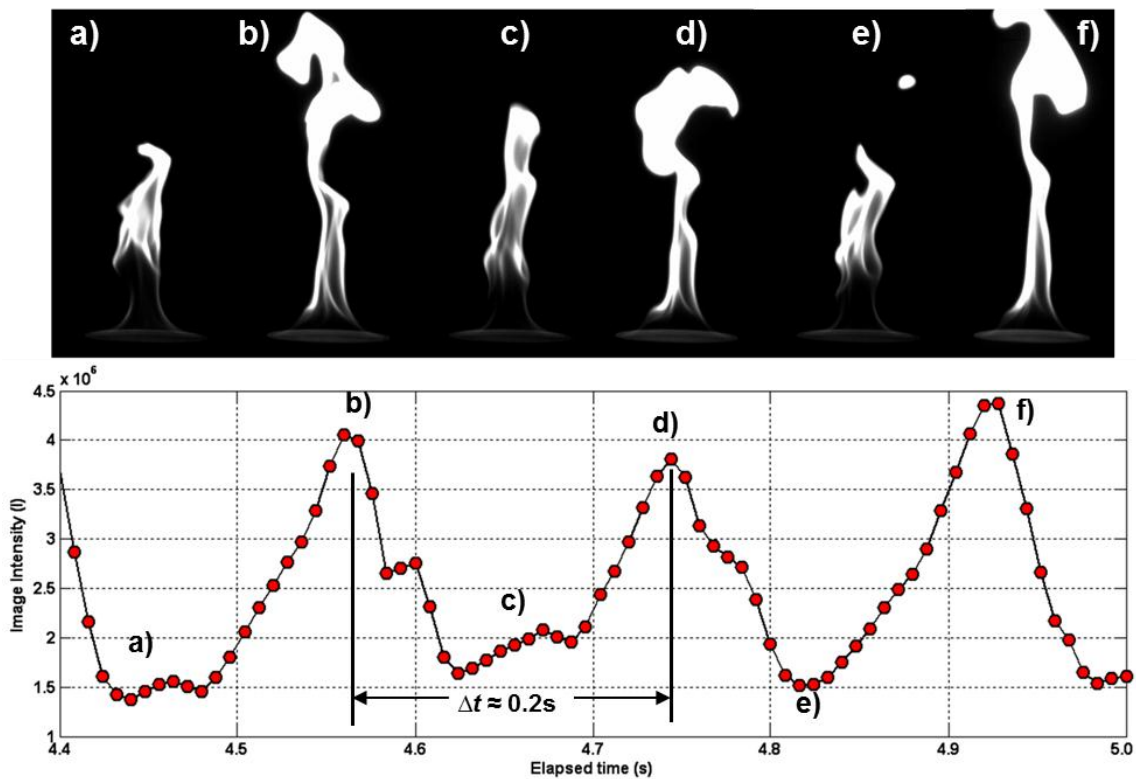
Figure 3-9: Fluctuation of RGB components for the 105 mm ethyl alcohol flame.

The power spectral density of the 30 mm flame is shown in Figure 3-10. Clearly, the signal's energy is being distributed at or very near a frequency 10 Hz – the additional peaks are harmonics of this fundamental frequency.
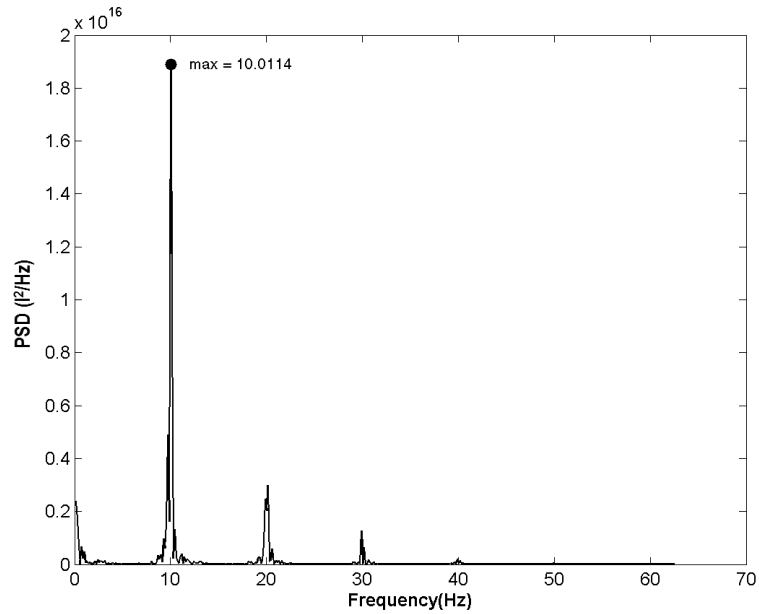
Figure 3-10: PSD of image intensity for 30 mm fuel bed diameter showing dominant frequency at 10 Hz.

The PSD of the 40 mm flame (Figure 3-11) appears similar to the 30 mm flame, except the frequency is lower by nearly 1 Hz, and more noise is present in the signal. The source of this noise is likely related to the transition to turbulence, since eddies can affect the image intensity in a somewhat random manner. For the remaining fires, the trend of decreasing frequency and increasing noise continues (Figures 3-12 through 3-15).
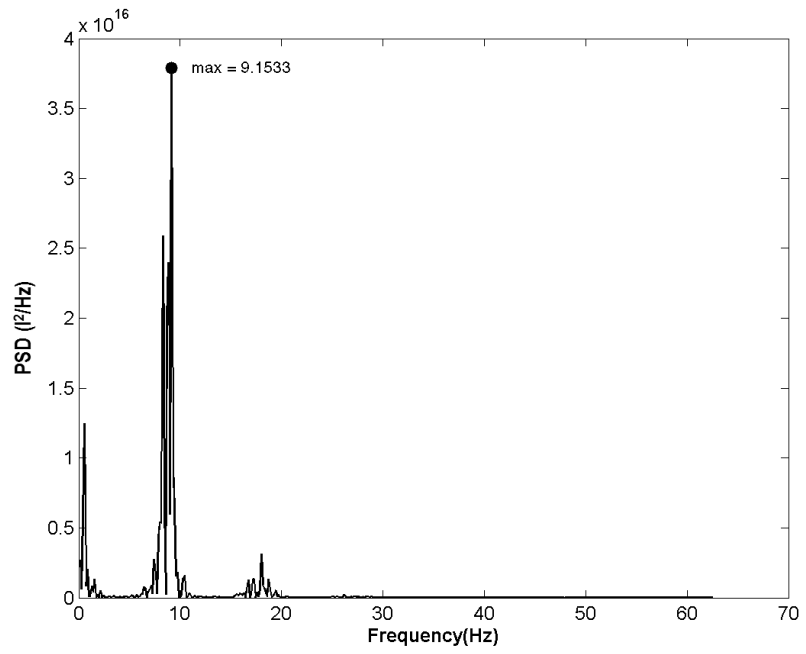
Figure 3-11: PSD of image intensity for 40 mm fuel bed diameter.
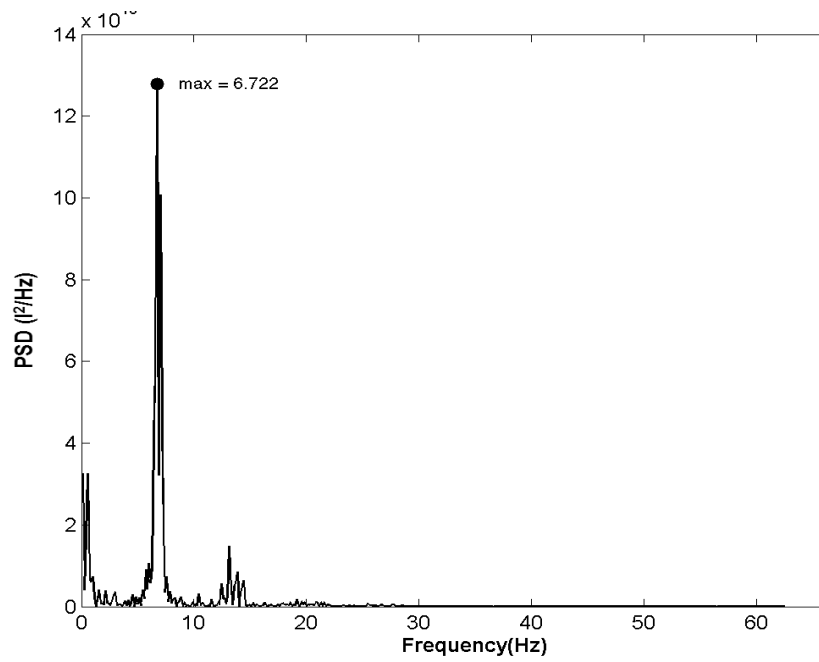
Figure 3-12: PSD of image intensity for 70 mm fuel bed diameter.
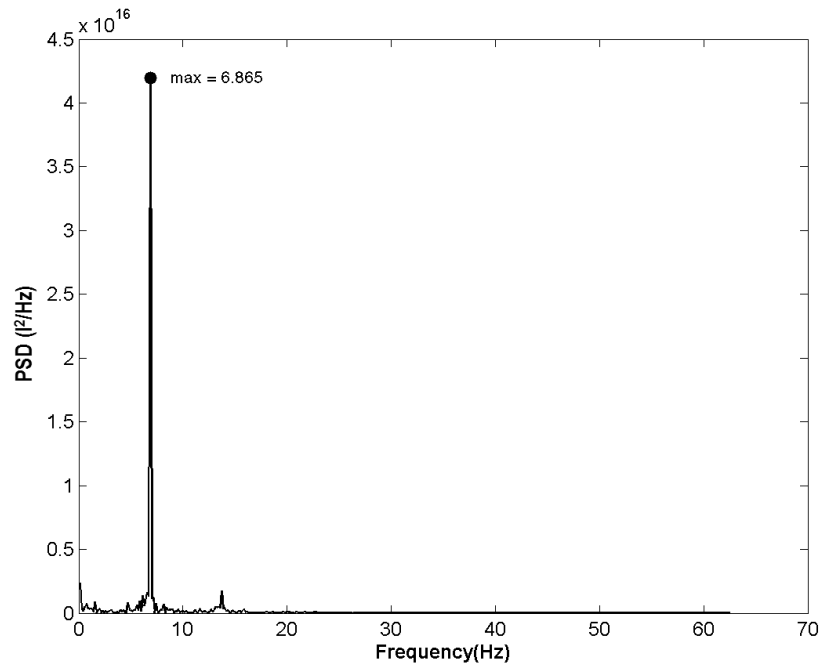
Figure 3-13: PSD of image intensity for 75 mm fuel bed diameter.
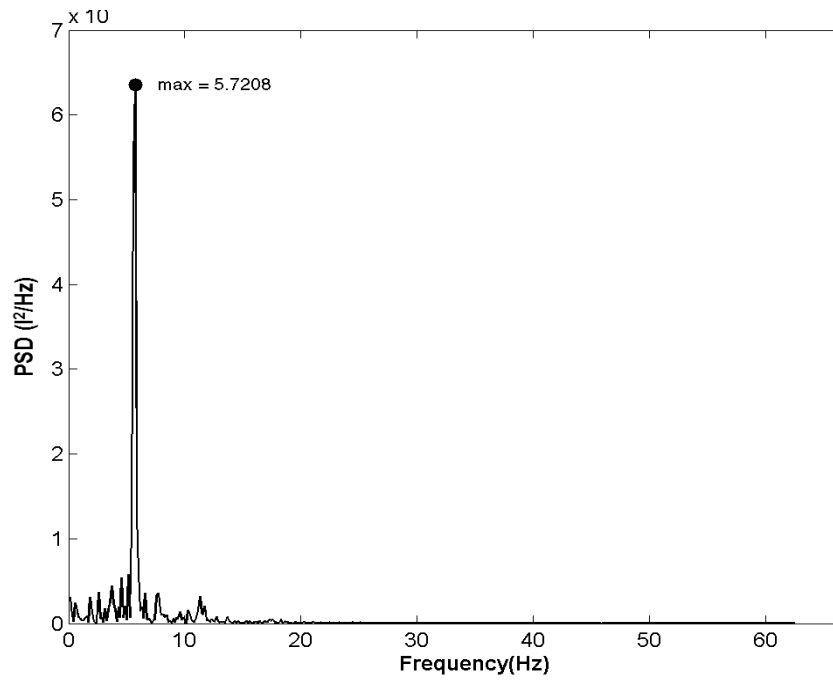
Figure 3-14: PSD of image intensity for 105 mm fuel bed diameter.

45
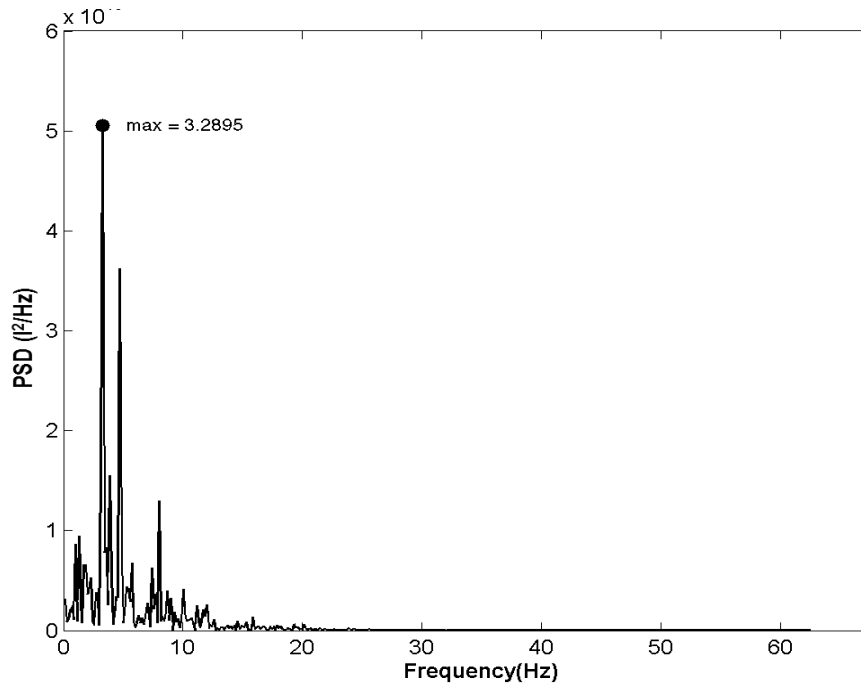
Figure 3-15: PSD of image intensity for 125 mm fuel bed diameter.

Pulsation frequency versus fire diameter is shown in Figure 3-16. Overall, the data were in good agreement with the empirical relationship ($f \sim D^{-1/2}$). The larger experimental error for the 30 and 125 mm flames are likely due to effects of flame luminosity. The 30 mm flame produces a relatively small amount of light when compared to the larger fires, making the detection of "hot" pixels less definite. Conversely, the structure of the 125 mm fire is much less uniform, and localized areas of combustion can cause rapid fluctuations in overall image intensity.
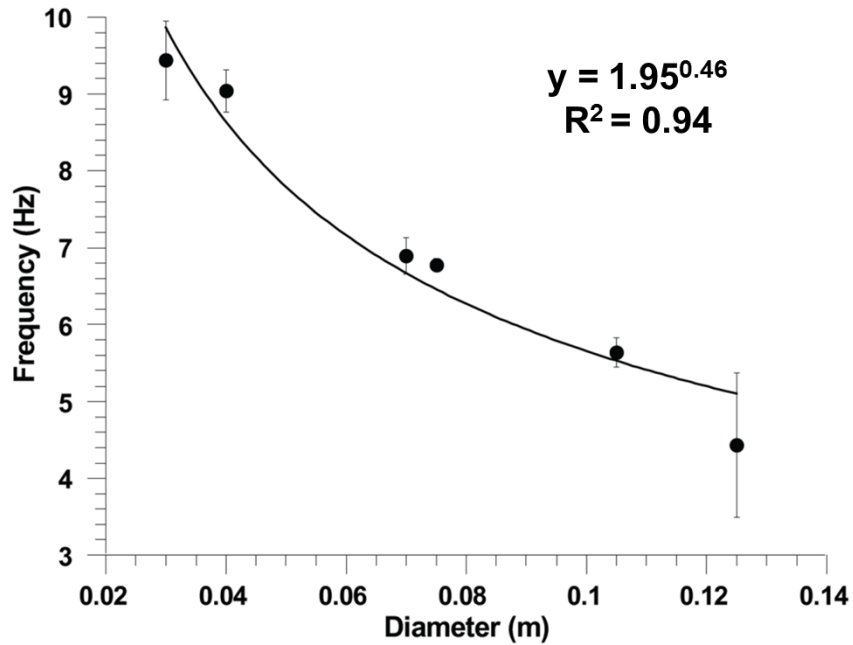
Figure 3-16: Frequency versus diameter (from PSD of image intensity signal). Error bars represent one standard deviation of the mean.

3.4   Conceptual model

In the experiments presented above, the appearance of discrete luminous structures and isolated "blobs" of low density supports the idea that thermals may form in the pool fire environment. The development of thermals has been widely studied in atmospheric science, but comparatively little research exists for high Rayleigh number conditions, specifically those present in reacting flows. In order to consider the pool fire as an analog to the simple heated plate, one must first address the critical differences between the two. A typical heated plate experiment uses electrical power to increase the plate's surface temperature, and the amount of heat flux at the surface of the plate is easily determined. At the initiation of heating, small convective instabilities begin to appear. As instabilities grow, they approach critical Rayleigh number,

separate, and eventually produce large scale motion. For the heated plate, all convective motion is driven by this process. Relating this mechanism of instability to a pool fire is not straightforward. Though a heat source exists at the surface, its characteristics are not easily defined. The heat flux at the surface of the pool fire is complex, and consists of convective, conductive, and radiative heat fluxes both *into* and *out of* the pool surface (Hertzberg, 1973). In addition, energy production continues throughout the plume due to combustion reactions, which may occur far above the fuel surface (Zhou et al., 2003). This differs from the heated plate, which provides homogeneous heating in a single horizontal plane.

3.4.1   Where can thermals form?

For a semi-infinite horizontal plate with uniform heating at the surface, the vertical temperature profile is everywhere unstable. There is no preferred location for instabilities to form, and thermals are distributed evenly across the surface. Near the surface of a pool fire, however, the amount of heat released is non-uniform. The constant fluctuation of the flame leads to an ever-changing radiation view factor at the surface.

Around the rim of the pool, however, the temperature profile becomes intermittently unstable, a condition ripe for the formation of convective instabilities. In addition, thermal growth rate is proportional to the rate at which air can be entrained, which will be greatest around the edge of the flame. Therefore, it is expected that thermals will form most rapidly around the rim of the pool fire.

3.4.2   Single or multiple thermals?

Observations of thermal blob convection indicate that the vertical and horizontal length scales of thermals are comparable (Princevac and Fernando, 2007; Sparrow et al., 1970).

Rearranging Eq. 3-4 and substituting the critical Rayleigh number (10^3) gives a length scale of ~1 cm for the thermal. Thus, it is expected that multiple thermals will form across the surface of all but the smallest pool fires.

When observed in real-time, the structures which signal the beginning of a pulsation cycle typically appear as a uniform ring surrounding the flame. However, as shown in Figure 1, the instability is often lead by the appearance of a structure in a single location. This initial disturbance is usually followed by a vortex-like structure which appears to surround the entire fire. It is theorized that the initial structure is a single thermal which has separated from the surface. This departing thermal leads to enhanced entrainment at the surface, which perturbs the remaining thermals and causes them to leave the surface as a "cluster". This process is illustrated in Figure 3-17.

a) Flame radiates heat to fuel surface – temperature is unstably stratified around the rim

b) Thermals begin to form around rim

c) Single thermal reaches critical Rayleigh number and breaks away from surface – its wake triggers "cluster" of remaining thermals to release

d) Cluster of thermals rise into flame, breaking down vapor core and leading to increase in combustion activity and turbulent mixing

Figure 3-17: Proposed mechanism for fire pulsation based on the development of thermals

3.5   Theoretical model

3.5.1   Mass conservation model – turbulent flames

Observations of heated horizontal surfaces show that a single thermal will separate from the surface when the Rayleigh number, based on its own volume, reaches a critical value ($Ra \approx$ 1000). However, as discussed previously, for fires larger than ~1 cm, multiple thermals should develop across the surface. Because thermal growth is dependent on entrainment rate, peripheral thermals will grow more rapidly than those near the center. Since the proposed mechanism for pulsation involves a group of thermals (a "cluster") releasing from the surface, here we consider the heating of the entire volume directly above the pool fire. The growth of a cluster of thermals can be described from the conservation of mass:

$$\frac{dV}{dt} = u_e \frac{V}{D} \tag{3-9}$$

where u_e is the rate of entrainment into the thermal growth region, V is the volume of the cluster, and D is the diameter of the fire. The product V/D represents the area through which the cluster of thermals entrains. Separating and integrating over a single growth period, we obtain:

$$\ln\left(\frac{V_C}{V_0}\right) = \frac{u_e}{D} t_C \tag{3-10}$$

where the subscript c represents conditions at the critical Rayleigh number. Note that if the initial volume in Eq. (3-9) is taken as zero, no solution exists. For now, we will assume the initial volume of the thermals is some small fraction of the critical volume. This assumption is reasonable since in high Rayleigh number thermal convection, thermal blobs do not appear to

experience a "clean break" from the surface; most of the blob leaves, but some portion of the thermal boundary layer remains and contributes to the growth of subsequent thermals:

$$V_0 = cV_C \quad c \ll 1 \tag{3-11}$$

Substituting Eq. (3-10) into Eq. (3-9) yields the growth timescale for the thermal region:

$$t_C = \frac{D}{u_e} \ln\left(\frac{1}{c}\right) \tag{3-12}$$

Inverting Eq. (3-13) gives the frequency of thermal generation:

$$f = \frac{u_e}{D}(-\ln(c)) \tag{3-13}$$

The entrainment velocity can be estimated by applying the *entrainment assumption* from classical plume theory, which assumes the entrainment rate is proportional to the vertical velocity of the plume (Morton, Taylor, and Turner; 1956):

$$u_e = \varepsilon w \tag{3-14}$$

where ε is an entrainment coefficient, and w is the mean vertical velocity of the fire. This assumption has been applied to fires by Thomas et al. (1961). Corlett (1974) estimated the vertical velocity of fire plumes as the velocity due to buoyancy to be:

$$w = (gbl)^{1/2} \tag{3-15}$$

where l is the vertical acceleration length scale and b is the average density difference:

$$b = \frac{\Delta\rho}{\rho} \tag{3-16}$$

Finally, assuming l is of magnitude D and substituting Eq's (3-14) and (3-15) into Eq. (3-13), we obtain the frequency of thermal generation:

$$f = \frac{A}{\sqrt{D}}$$

(3-17)

where A is a dimensional constant:

$$A = \frac{\varepsilon\sqrt{g\bar{b}}}{-\ln(c)}$$

(3-18)

Using the entrainment coefficient determined by Thomas et al. (1961) ($\varepsilon = 0.16$) and the buoyancy number estimated by Corlett (1974) ($b \approx 3$) gives $A \approx 0.4$, which is less than the coefficient estimated for pulsating fires from the literature (1.5), and our fit from Figure 3-17 (1.95). However, this simple model only considers a cluster of thermals leaving the surface instantaneously. In actuality, the cluster is first triggered by a single thermal emanating from the fuel surface. This will result in the "global" instability of the pool fire appearing later, resulting in a longer pulsation period.

3.5.2   Energy balance model – laminar flames

A different result, also a function of diameter, can be obtained by using an energy balance in the thermal boundary layer, and considering both the generation and entrainment of a single thermal. Princevac and Fernando (2007) used the results of Howard (1966) in conjunction with scaling analysis to determine a criterion for thermal blob development in upslope (anabatic) atmospheric flows. While the details of upslope flows are immaterial here, the method of analysis proves useful for the general case of a fire.

3.5.2.1 Thermal growth

A schematic of a growing thermal is shown in Figure 3-18. It is assumed that combustion provides a uniform heat flux to the fuel surface, which in turn heats the quiescent air directly above, which is approximated as a cylindrical volume.
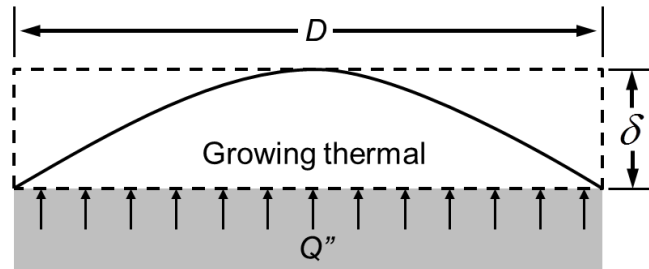
Figure 3-18: Schematic of the development of a single thermal.

Following Princevac and Fernando (2007), an energy balance in the boundary layer yields:

$$Q''t_T \approx c_p \rho_0 \Delta T \delta_c \tag{3-19}$$

where Q'' is the heat flux at the base of the thermal, ΔT is the difference between the thermal and ambient air, t_T is the time scale for blob generation, and δ_c is the value of δ at separation. This can be expressed as a balance of buoyancy flux:

$$q_0 t_T \approx g \alpha \Delta T \delta_c \tag{3-20}$$

where α is the thermal expansion coefficient, and the buoyancy flux is given by:

$$q_0 = \frac{Q'' g \alpha}{\rho_0 c_p} \tag{3-21}$$

Combining Eq's (2-13), (3-3), and (3-21), the frequency of blob separation is given by:

$$f_T = 2(C\sqrt{\pi}D)^{-1}$$

(3-22)

where $f_T = 1/t_T$ and C is given by:

$$C = \left(\frac{Ra_C \nu \rho_0 c_p}{Q g \alpha}\right)^{1/2}$$

(3-23)

where Q is the heating rate. For most experimental fires, the value of C is of order one. Note that Eq. (3-22) is dependent on the inverse of fire diameter, whereas the previous experiments, including ours, are dependent on the inverse square root. Thus, for smaller fires, Eq. (3-22) over-predicts pulsation frequency, but under predicts for larger fires.

The size of thermal blobs also must be considered when applying this theory to pool fires. Experimental visualizations of thermals (Sparrow et al., 1970) and Rayleigh-Benard convection theory (Koschmieder, 1993) predict cells of aspect ratio ~ 1 at the critical Rayleigh number. Here the blob aspect ratio will also be considered as unity (blob length scale $l \sim \delta$).

3.5.2.1 Entrainment of thermal

After the thermal blob is released from the surface, it undergoes buoyant acceleration while simultaneously being drawn toward the plume center and upwards with the mean flow, following the general path illustrated in Fig 3-18.

55
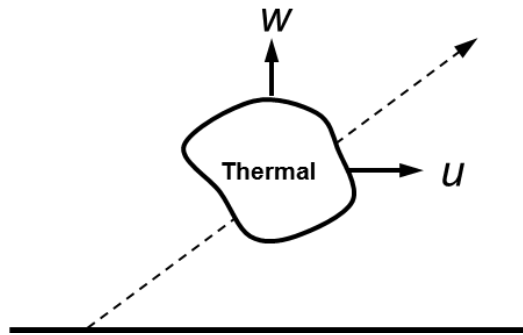
Figure 3-19: Motion of a rising thermal.

The timescale for the blob to be transported into the center of the flame will be a function of the horizontal velocity, which, from the entrainment assumption (Eq. 3-15), is a function of vertical velocity. The characteristic vertical velocity can be determined by considering the buoyancy force per unit mass:

$$\frac{F_B}{m} = g' = g\frac{\Delta\rho}{\rho} \tag{3-24}$$

Buoyancy will cause a vertical acceleration of the parcel:

$$\frac{F_B}{m} = \frac{dw}{dt} \tag{3-25}$$

Substituting (3-25) into (3-24):

$$\frac{dw}{dt} = g\frac{\Delta\rho}{\rho} \quad \text{where} \quad dt = \frac{dz}{w} \tag{3-26}$$

$$wdw = g\frac{\Delta\rho}{\rho}dz \qquad (3\text{-}27)$$

Integrating yields:

$$w = \sqrt{2gbz} \qquad (3\text{-}28)$$

which for $z \sim l$ is equal to Eq. (3-15). Using the entrainment assumption, we can determine an order of magnitude estimate for the blob entrainment timescale:

$$dr = udt \qquad (3\text{-}29)$$

where r is the horizontal length scale from the edge of the pool to the center.

Substituting the entrainment assumption and integrating Eq. (3-29) over one transit period (blob traveling from plate edge to center), we obtain the following expression for the entrainment timescale:

$$t_e = \frac{1}{2\varepsilon}\left(\frac{D}{gb}\right)^{1/2} \qquad (3\text{-}30)$$

where it has again been assumed that $l \sim D$. The frequency follows:

$$f_e = c_e D^{-1/2} 2\varepsilon\left(\frac{gb}{D}\right)^{1/2} \qquad (3\text{-}31)$$

where

$$c_e = 2\varepsilon(gb)^{1/2} \qquad (3\text{-}32)$$

Using $b \approx 3$ as in the previous model, an entrainment coefficient of 0.13 gives the value of c_e that matches the best fit coefficient of our pulsation experiments (1.95). This value is relatively close to the entrainment coefficients for different fire types measured or deduced by several researchers, including Rouse et al. (1952) ($\varepsilon = 0.16$), Yih (1952), ($\varepsilon = 0.15$) and Cetegen et al. (1984) ($\varepsilon = 0.21$).

3.6   Conclusions

A series of experiments exploring the pulsation mechanism of pool fires has been presented. High speed imaging was used to visualize the behavior of small pool fires of varying diameter, and a simple method for determining pulsation frequency based on image intensity was introduced. The image analysis methods introduced were able to accurately determine the pulsation rate of experimental fires. Observations of experiments support the idea that the pulsation cycle may begin with the development of discrete buoyant structures at the surface of the pool. Using experimental results, a new theory of fire pulsation was developed, based on the growth and release of "clusters" of thermals at the fuel surface. Though simple, this model predicts the same dependency of pulsation rate on fire diameter that has been empirically shown in the literature.

4. THE FLUID MECHANICS OF INTERACTING LINE FIRES

4.1 Introduction

As two or more freely burning fires converge, their behavior can change, sometimes significantly (Figure 4-1). Flame length, flame angle, heat release rate, and propagation rate (for spreading fires) have all been observed to increase during flame merging (Johansen, 1984; Finney and McAllister, 2011). Aside from being an intriguing physical problem, fire interactions can prove challenging for firefighters, who are often required to adjust tactics to maintain control of the fire. Fire interactions are used frequently to control the intensity of a prescribed fire in order to achieve natural resource management objectives (e.g. Martin and Dell, 1978; Green, 1981; Wade et al., 1989).

Figure 4-1: Merging of a ring of fire burning in longleaf pine understory (*Pinus palustris* Mill). Note the significant change in fire behavior as the flame fronts converge.

The physical interaction of two flames is a complex process which has been examined both theoretically and with numerical physical models (Morvan et al., 2011). As with single

flames, radiant heat transfer plays an important role. As flames converge, the radiant energy emitted by each flame heats the neighboring fire and intervening fuels (for spreading fires), leading to accelerated burning rates and fire spread. Liu et al. (2009) showed that the burning rate of pool fire arrays increased as their separation distance decreased. This effect occurred until a critical separation was reached, below which the burning rate began to decrease. They explained the initial rise in combustion rate as a result of an increased radiation view factor (enhancement of heat feedback to burning fuels), while the eventual decline was due to restriction of airflow into each fire.

While much of the work on merging fires has focused on radiant heat transfer, entrainment and convection also appear to play a significant role in interactions. As two flames converge, their independent entrainment fields interact, resulting in an inward tilting of the flames (Sugawa and Takahashi, 1993). Flame tilt affects fire behavior by increasing the amount of radiant heat transfer (view factor) to the surface (Byram et al., 1966) and by increasing the horizontal component of convective heat flux forward of the flame (Baines, 1990). Baldwin et al. (1964) theorized that flame tilt is a product of the flow restriction between flames, which causes a pressure drop that competes with buoyancy. A similar mechanism has also been proposed for non-combusting buoyant plumes at laboratory scale (Pera and Gebhart, 1975).

In this section, we develop a model to explain flame tilting as a result of momentum imbalance across the flame front. The model uses the conservation of linear momentum, coupled with potential flow theory, to describe the behavior of the flow field surrounding two fires as a function of separation distance. This model is compared with experiments to determine the velocity field outside of adjacent alcohol pool fires using cross-correlation optical flow analysis.

The model and experimental results are discussed in the context of potential effects on overall fire behavior, and an analogy between merging flames and wind-driven single flames is suggested.

4.2   Background

4.2.1   Interactions in wildland fires

During wildland fires, interactions may occur naturally due to the convergence of spot fires and multiple flame fronts, or they may be induced to produce desired fire behavior (Figure 4-2). In prescribed fires, flame merging is often desired as part of a predetermined burn plan. Two common prescribed fire ignition techniques are strip-head firing and spot firing. In strip-head firing (Figure 4-2a), crews ignite lines of fire increasingly upwind of a control line, either by hand (using a drip torch), or by a helicopter equipped with a helitorch, a device which dispenses a steady stream of thickened, burning fuel (Masters et al., 1986). The individual strips are allowed to merge together, and both fire intensity and flame length are directly dependent on the distance between ignition lines (Wade et al., 1989). In spot firing (Figure 4-2b), point source ignitions are placed strategically throughout the burn area, either by drip torch, flare gun, or by an aircraft equipped with a plastic sphere dispenser (PSD) machine, which dispenses time-delay ignition devices (Byrne and Just, 1982). In general, when compared to strip-head fires, spot firing produces lower intensity fires which are more easily managed (Rothermel, 1984), though too many spot fires in a small area can be problematic (Wade et al., 1989). Spot firing is often desirable for resource benefit fires, as it can produce a natural mosaic pattern that closely mimics the burn patterns produced by lightning fires (Baker, 2006).
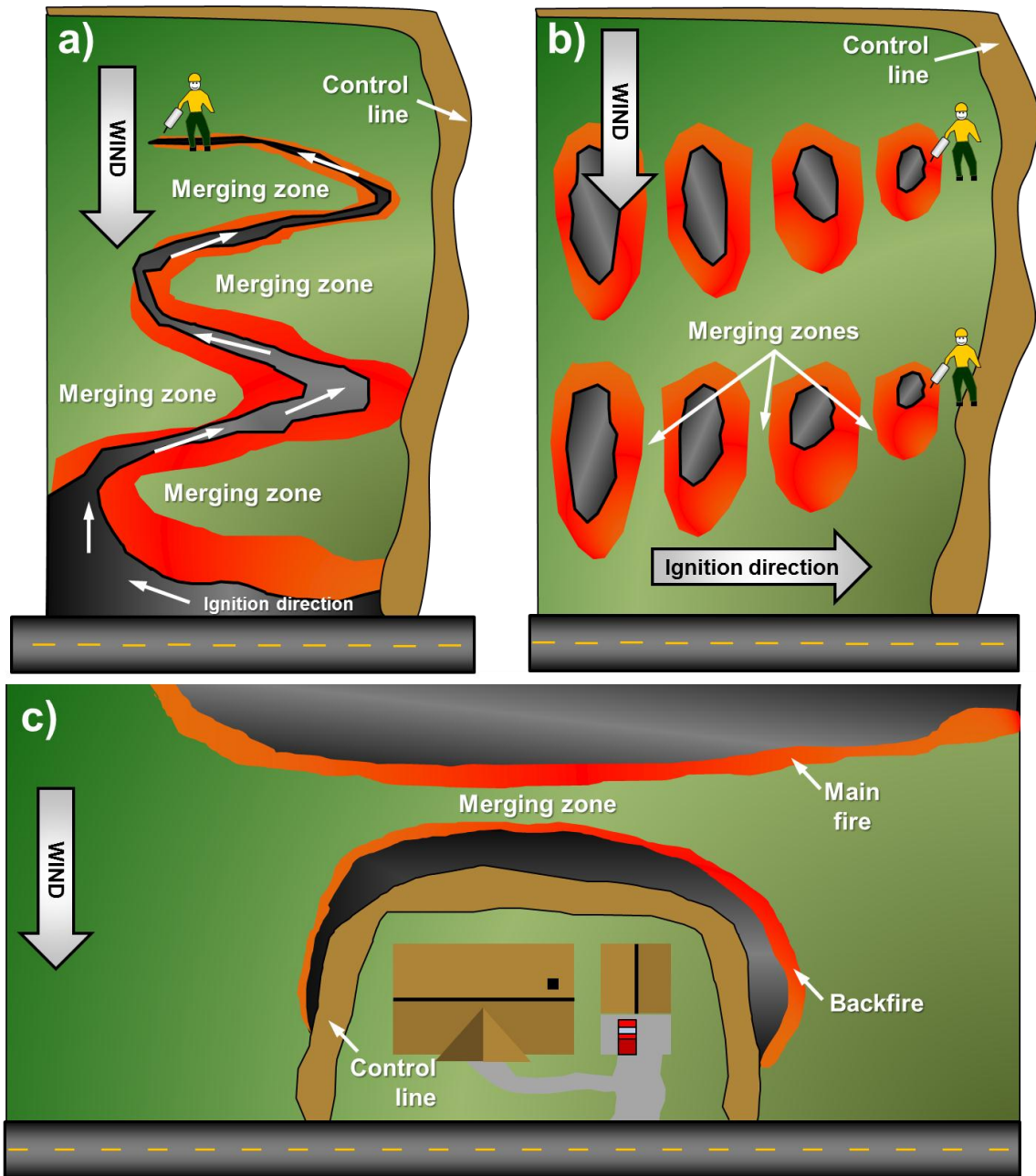
Figure 4-2: Examples of induced fire merging – a) Strip-head firing, b) Spot firing (adapted from Wade et al., 1989), c) Backfiring to protect a structure from a wildfire.

In wildfire suppression, tactics utilizing fire interaction are often a key component of the fire management strategy. Burning out and backfiring are two practices of intentionally burning fuels ahead of the main flame front in an attempt to slow or stop its progression (Figure 4-2c), which results in the primary and secondary flame fronts merging. Burnout operations are typically used as part of a direct attack strategy (containment actions occur close to the main fire) to reinforce containment lines, while backfiring is itself a method of indirect attack (containment actions occur away from the main fire). Backfiring is often used as a defensive tactic to protect an immediately threatened control line, structure, or compromised firefighters by removing fuels ahead of the flame front. (National Wildfire Coordinating Group, 1996).

The physical effects associated with fire merging can be problematic in both prescribed and suppression fires. For resource benefit fires, it is often desired to consume the understory fuels (leaf litter, duff) while minimizing damage to trees and plants. The increased flame lengths and intensities associated with fire interaction can lead to undesired tree and plant mortality (Johansen, 1984). In addition, the ability of a wildland fire to propel embers over long distances (which can serve as new ignition sources) is directly related to its intensity (Albini, 1983).

4.2.2   Interactions in structure fires and the wildland-urban interface

Flame interactions are also prevalent in urban area fires. Countryman (1964) cites numerous conflagrations in the early 20th century, including the bombings of Dresden and Hamburg, Germany during World War II, as prime examples of destructive fire behavior. These cities were principally damaged not by the bombs themselves, but by the resulting groups of fires ("mass fires"), which induced extreme winds and burning rates. In wildland areas with significant residential development, the wildland-urban interface (WUI), fire interactions present a twofold dilemma. First, the close proximity to communities restricts the use of prescribed fire for fuels

management and other resource objectives. When prescribed burning is used, the management plans may limit the available ignition techniques, many of which rely on flame merging for complete fuel consumption (Wade et al., 1989). Second, during wildfire events, burning structures may interact with surrounding vegetation fires, leading to unexpected fire behavior (Rehm and Mell, 2009).

4.2.3   Flame tilting

As illustrated in Figure 4-2, merging often occurs between relatively straight flame fronts, referred to herein as line fires. Line fires are common in prescribed and wildland fires. Strip head and chevron firing (igniting "V" shaped strips that spread perpendicular to the wind) techniques result in relatively long, straight fires at the time of merging. Flames in wildfires can be kilometers wide and often form a semi-linear front as they propagate through the available fuel. Even point source ignitions (spot fires) typically evolve into quasi-line fires before merging, though the lines are not necessarily straight. Therefore, in developing a model for flame tilt, we use line fires as the basis for our investigation.

For line fires, Thomas et al. (1965) proposed that the tilting of adjacent diffusion flames is caused by the convergence of streamlines entering the space between flames, leading to a pressure drop which competes with buoyancy:

$$P = B \sin \theta \qquad (4\text{-}1)$$

where P is the pressure force, B is the buoyancy force, and θ is the angle of flame from vertical. The pressure drop was calculated from Bernoulli's equation, assuming the area between fires is triangular. They used this model to estimate flame length as a function of separation distance, line length, and flame zone depth (width of flame). However, their model relied heavily on

assumptions about the magnitude of entrainment velocity, which may have contributed to the significant disagreement between their model and experiments.

It should also be mentioned that a model based on static pressure drop fails to predict flame tilt at the center of each flame, since that is the location where flow streamlines from each side meet, causing flow stagnation (Figure 4-3). In reality, we do not expect zero fluid motion in this region, but we argue the pressure here should be very close to ambient. As will be discussed in the experiments section, our observations show that the central region is relatively quiescent, but flame tilt is still strongly evident.
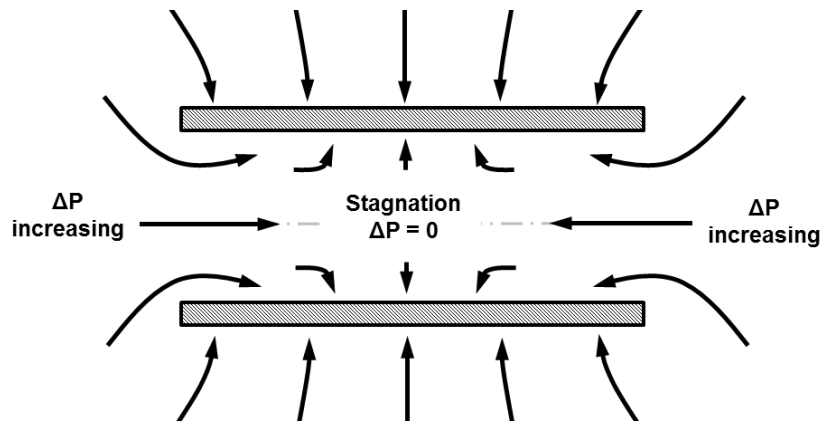
Figure 4-3: Conceptual schematic of flow streamlines around two adjacent line fires. Pressure drop increases as streamlines converge, but disappears near the center due to flow stagnation.

As discussed by Smith, Morton and Leslie (1975), classical plume models which assume that entrainment is due only to the turbulent diffusion of momentum as the plume expands (e.g. Morton, Taylor, and Turner; 1956) are not completely appropriate for characterizing the induction of air into large fires. Unlike isothermal buoyant plumes, the combustion process releases a tremendous amount of heat and requires significant amounts of oxygen for sustenance. Turbulent

entrainment alone cannot provide a sufficient volume of air, leading to the existence of a horizontal inflow over the fire perimeter, called the *fire wind*. They note that this is *far-field* entrainment, where the dynamic pressure field is the medium which communicates the effect of buoyancy to the surrounding fluid.

4.3   Theoretical model

4.3.1   Conservation of linear momentum

Fire plumes are strongly buoyant, resulting in rapid vertical acceleration of air within and above the flame which is the visible base of the plume. Continuity requires this ascending air mass to be replaced by a horizontal inflow. For very long line fires, the inflow can only come from the sides of the flames. As two fires converge, flow on the inside edge of each flame (nearest the neighboring flame) is restricted, resulting in asymmetric entrainment. This leads to an imbalance of forces acting on the fire plume, causing it to tilt in the direction of least velocity.
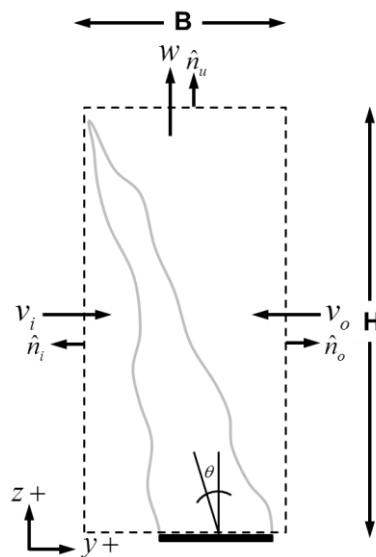
Figure 4-4: Control volume for momentum balance

A two-dimensional slice of a line fire is shown in Figure 4-4. For this control volume, the plume angle can be estimated as:

$$\theta = \tan^{-1}\left(\frac{F_Y}{F_Z}\right) \tag{4-2}$$

where F_Y and F_Z represent the sum of horizontal and vertical forces acting on the control volume, respectively. These forces can be determined using the conservation of linear momentum:

$$F_Y = \frac{\partial}{\partial t}\left[\int_V \rho_o v_o dV + \int_V \rho_i v_i dV\right] + \int_A \rho_o v_o(\hat{n}_o \cdot v_o)dA + \int_A \rho_i u_i(\hat{n}_i \cdot v_i)dA \tag{4-3}$$

$$F_Z = \frac{\partial}{\partial t}\left[\int_V \rho_p w_o dV\right] + \int_A \rho_p w(\hat{n}_u \cdot w)dA \tag{4-4}$$

where v and w are the components of horizontal and vertical velocity, respectively, ρ is the fluid density, and subscripts o, i, and p represent the outer, inner, and interior regions of the plume, respectively. We assume that all inflows and outflows are steady implying that the fire has achieved quasi-steady state, and that combusting fuel vapor enters the control volume with negligible momentum. Using the sign convention shown in Figure 4-4, Eq's (4-3) and (4-4) can be simplified and expressed as force per unit length of flame front:

$$F_Y' = \rho_o H(v_o^2 - v_i^2) \tag{4-5}$$

$$F_Z' = \rho_P B w^2 \tag{4-6}$$

where H is the height of the flame and B is the width of the control volume. Flame angle is then given by:

$$\theta = \tan^{-1}\left(\gamma \frac{v_o^2 - v_i^2}{w^2} \right) \qquad (4\text{-}7)$$

where

$$\gamma = \frac{\rho_o H}{\rho_P B} \qquad (4\text{-}8)$$

A similar model for flame angle was proposed by Welker and Sliepcevich (1966), except they considered a single circular flame with uniform entrainment but an externally imposed wind.

4.3.2   Potential flow approximation

Note that Eq. (4-6) requires the velocities to be known. Since the horizontal inflow is driven by buoyancy, we expect these velocities to be related to the vertical velocity of the plume. As a first approximation, we propose that the horizontal flow field surrounding the fires is analogous to the potential flow field generated by two adjacent line sinks of fluid. This concept is not new, as Baldwin (1968) mentioned using potential flow in the study of merging flames by modeling individual fires as point sinks of fluid. The idea was employed by Weihs and Small (1987), who studied the interaction of fire plumes by modeling each fire as a vertical distribution of point sinks (in the flaming region) and point sources (in the upper "thermal plume" region). Additionally, the existence of sink-like inflow near fires is supported by Smith, Morton and Leslie (1975), who studied natural convection above strongly heated line sources. More recently, Kaye and Linden (2003) used potential flow to approximate the entrainment field surrounding

adjacent axisymmetric plumes. Since a line sink can be approximated as a series of closely spaced point sinks, this is a natural extension of this concept.

An incompressible potential flow field is one which satisfies Laplace's equation:

$$\nabla^2 \varphi = 0 \qquad\qquad\qquad (4\text{-}9)$$

where φ is the velocity potential, a scalar function. The two-dimensional velocity field can be obtained from the velocity potential:

$$u = \frac{\partial \varphi}{\partial x} \qquad v = \frac{\partial \varphi}{\partial y} \qquad\qquad (4\text{-}10)$$

Since solutions to Laplace's equation can be linearly combined, the solutions of multiple flow features (sources, sinks, uniform flows, etc) can be added to construct the aggregate velocity field (Meyer, 1971). Of course, potential flow is not without its limitations. To satisfy Laplace's equation, the velocity field must be both incompressible and irrotational. Incompressibility is a reasonable assumption - though the combustion process itself is one of rapid expansion, the flow field surrounding the fire is of minimal velocity. Irrotationality, however, is more difficult to justify. The flow field surrounding fires often exhibits rotation at multiple scales. This is evident by the well-organized convection columns observed above large fires, and by the existence of fire whirls, highly rotational vertical columns of combusting gas. However, large convection columns only appear to play a significant role for very large fires or groups of fires (Finney and McAllister, 2011) which are beyond the scope of this study. Moreover, fire whirls and other vortices are highly transient, so it may be argued that potential flow represents an average velocity field which is periodically perturbed by these local events.

This complex potential for a distributed line sink, which consists of an infinite number of closely-spaced point sinks distributed over a defined length, is given by Paraschivoiu (2003):

$$F(z) = \frac{-k}{2\pi a}\left[z \ln z - (z - \ell)\ln(z - \ell)\right]$$

(4-11)

where z is the complex number $x + iy$, ℓ is the length of the line sink, and k is the strength of the sink. The derivative of Eq. (4-11) yields the complex velocity:

$$W(z) = \frac{dF}{dz} = \frac{-k}{2\pi\ell}\ln\frac{z}{z - \ell}$$

(4-12)

where $W = u - iv$, and u and v are the components of velocity parallel and normal to the line sink, respectively. The complex velocity for two neighboring line sinks is:

$$W(z) = \frac{dF_1}{dz} + \frac{dF_2}{dz} = \frac{-k}{2\pi\ell}\left[\ln\left(\frac{z_1}{z_1 - \ell}\right) + \ln\left(\frac{z_2}{z_2 - \ell}\right)\right]$$

(4-13)

where subscripts 1 and 2 reference the line sinks shown in Figure 4-5.
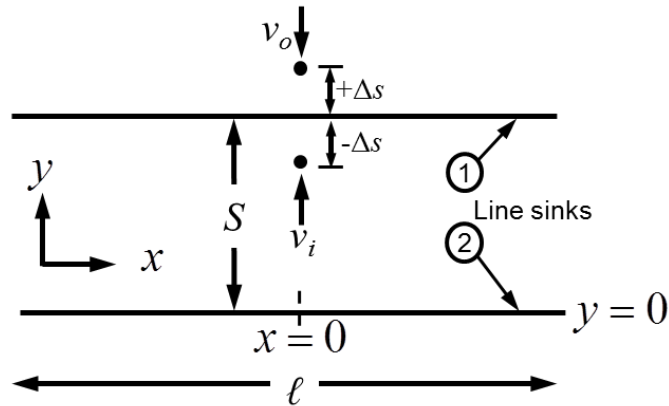
Figure 4-5: Schematic for potential flow of two adjacent line sinks

The velocity difference across the upper line sink is given as:

$$\frac{\Delta v}{q} = \frac{\Delta v}{w} = \text{Im}\left[\frac{1}{2\pi} \left\{ \begin{array}{l} \ln\left(\dfrac{x+i(S+\Delta s)}{x-\ell+i(S+\Delta s)-\ell}\right) + \ln\left(\dfrac{x+i(\Delta s)}{x-\ell+i(\Delta s)}\right) - \\ \ln\left(\dfrac{x+i(S-\Delta s)}{x-\ell+i(S-\Delta s)-\ell}\right) - \ln\left(\dfrac{x+i(-\Delta s)}{x-\ell+i(-\Delta s)}\right) \end{array} \right\} \right] \tag{4-14}$$

where $q = k/\ell$ is the strength of the sink per unit length, which has units of velocity. Physically, q represents the amount of fluid terminating in the sink per unit length per unit time. In a fire, buoyancy causes fluid to rise with velocity w. This rising fluid acts as a sink since it has to be replaced through the horizontal inflow. Thus, for fires, we make the assumption that q is equivalent to the vertical velocity of the fire plume, w.

The effect of separation distance on the potential flow field for two distributed line sinks is shown in Figures 4-6 and 4-7. Each line sink draws in fluid from all directions at a constant rate. As the separation distance between lines decreases, the magnitude of the inner velocity component normal to the line sink is reduced. To satisfy continuity, this decrease is balanced by an increase in flow velocity on the outside of the sink (Figure 4-7). Since the magnitude of the inflow velocity is proportional to the source strength, the velocity difference across each line sink normalized to vertical velocity is a function of S/ℓ only.
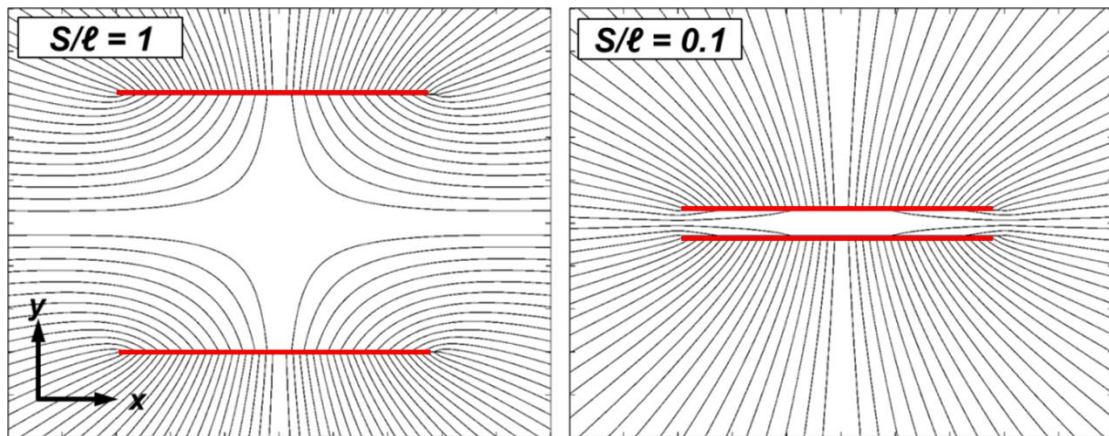
Figure 4-6: Streamlines for two converging line sinks

Qualitatively, the velocity difference can be explained by considering the path of fluid parcels as they enter the region between sinks. As shown in Figure 4-6, streamlines entering the central region are nearly parallel to the sinks, and parcels enter the region with almost no y-component of velocity. Once the parcel is between the sinks it will start accelerating towards the nearest one. As the separation distance decreases, so does the length scale of parcel acceleration, which ultimately limits the inner velocity. Additionally, the neighboring fire imposes a horizontal pressure gradient force which opposes parcel acceleration, further reducing velocity.
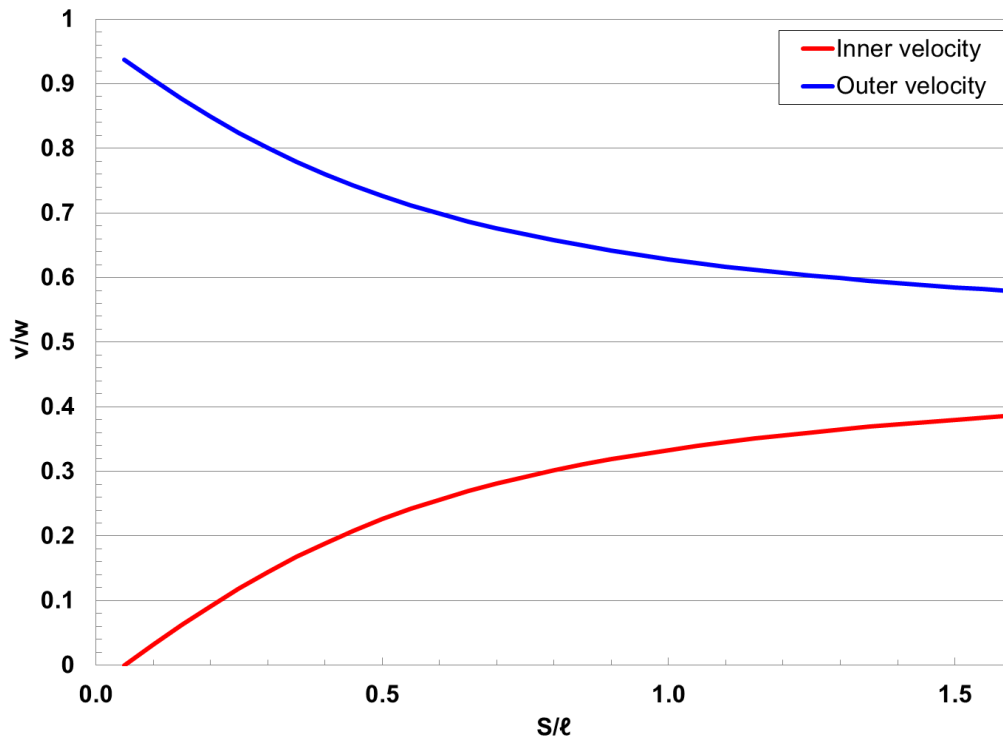
Figure 4-7: Potential flow model - effect of separation distance on inner and outer velocities normal to the line sink at $x = 0$, normalized to vertical velocity.

4.4   Laboratory experiments (flame tilting)

4.4.1   Experimental setup

To investigate the validity of the proposed model for merging flames, experiments were performed to measure the velocity field surrounding stationary line fires. A schematic of the experiment is shown in Figure 4-8. Two rectangular steel pans ($\ell = 150$ cm, $D = 7$ cm), each containing equal volumes of liquid fuel (isopropyl alcohol, 91% by volume) were placed next to each other at six different separation distances, from S/ℓ of 0.1 to 1.5. For line fires, Yuan and

Cox (1996) give a functional relationship between flame length and heat release rate per unit length:

$$L = 0.034 Q_L^{2/3} \qquad (4\text{-}15)$$

where L is the flame length (m), and Q_L is the heat release rate per unit length (kW/m). For the flame lengths observed in our experiments, Eq. (4-15) yields a heat release rate per unit length of approximately 50 kW/m, which is in the low range of intensity for vegetation fires in surface fuels (see summary by Alexander and Cruz, 2012).

For each separation distance, the behavior of the leftmost fire was captured by a video camera with a frame rate of 30 frames per second (standard frame rate for a consumer-grade video camera), with the fire placed directly in the center of the frame. The frame was spatially calibrated to determine the linear dimension per pixel at the center of the fire. To visualize the surrounding flow field, colored smoke cartridges (ammonium chloride/potassium chlorate) were placed on both sides of the fire (Figure 4-9). Smoke from the cartridges was discharged horizontally (into the image plane) to minimize initial momentum. The high contrast smoke from cartridges made easy to identify fluid structures as they were drawn into the fire plumes. Each fire was ignited simultaneously and allowed to burn for at least 10 seconds prior to capture. Video was captured for approximately 60 seconds during the steady burning period. Six test burns with only single flames (no adjacent flame) were used to determine the average flame height. For each separation distance, the experiment was replicated three times to estimate error.
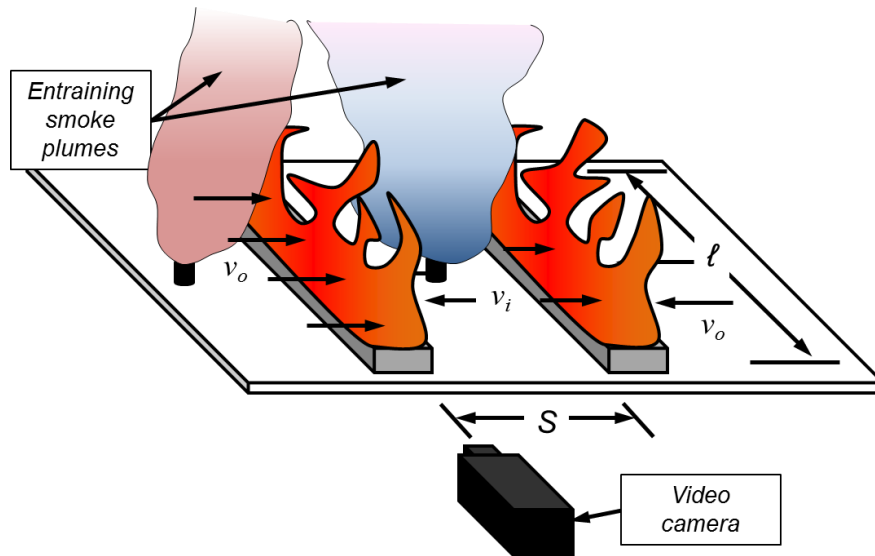
Figure 4-8: Schematic of pool fire experiments

Figure 4-9: Use of smoke cartridges for flow field visualization. Exaggerated flame angle on right is

fictitious, due to perspective distortion (figure is cropped; camera is actually centered on left fire).

4.4.2   Analysis

To obtain the best possible insight into merging fire entrainment, a method of nonintrusive

quantitative visualization capable of determining the entire velocity field over a relatively large

region was desired. One common technique for this is Particle Image Velocimetry (PIV). In PIV, the velocity field is "seeded" by reflective particles which are assumed to follow the flow. A pulsed laser is used to illuminate the particles in a thin plane, and two images are then captured in rapid succession. The images are compared to determine particle displacement using a cross-correlation algorithm, yielding the velocity field (Adrian, 1991). PIV has successfully been deployed on small and medium-sized pool fires (Zhou and Gore, 1995; Tieszen et al., 2002), as well as for fires in vegetative fuel beds (Lozano et al., 2010). However, for the scale of the present experiments, PIV has several distinct limitations. The spatial resolution of PIV is directly related to the size, density, and homogeneity of seeding particles. In our case, the region of interest spans several meters (both horizontally and vertically), which presents severe difficulties in obtaining adequate particle density and exceeds the size of plane produced by the focused lasers. Since our goal was to determine the bulk motion of the entrainment field over a large region, we determined that PIV would not be the ideal option. Instead, we chose to pursue a more general "optical flow" analysis, of which PIV may be considered a specialized type.

The optical flow field is the velocity field which results from the motion of an object within an image frame. Though numerous classes of optical flow methods exist, the two most common approaches involve the gradient-based analysis of a conserved image signal (e.g. Horn and Schunck, 1981) and the cross-correlation of image features (Adrian, 1991). Cross correlation has been used to obtain the time-averaged velocity field for plumes with high visible contrast consisting of discrete fluid structures which rotate, translate, and deform as they rise, namely ocean hydrothermal vents (Crone et al., 2007). These plumes are analogous to the smoke used for flow visualization in our experiments. In our case, the smoke originates from a point source (the cartridge), but rapidly assimilates to the local flow field. In cross correlation optical flow, the image cross-correlation coefficient is defined as:

$$C_{fg}(m,n) = \sum_i \sum_j f(i,j) \times g(i+m, j+n) \qquad \text{(4-16)}$$

where $f(i,j)$ and $g(i,j)$ are the image intensity distributions in the first and second images, respectively, and m and n are the pixel offsets between each image. Essentially, the cross-correlation function attempts to match the progression of image features from frame to frame. Images are parsed into interrogation regions which are compared between frames of known Δt. The displacement vector is then calculated by finding the displacement of the correlation peak between frames – i.e., the locations where the regions best match each other. A similar technique using thermal images from IR cameras was used by Zhou et al. (2003) to estimate flow fields within a flame.

4.4.3 Experimental methods

4.4.3.1 Velocity field

For each experiment, three separate intervals, each with a duration of five seconds (150 frames), were analyzed. Image analysis was performed using OpenPIV (Taylor et al., 2010), an open-source cross-correlation algorithm designed for use with PIV imagery. For each capture, three separate regions, outer, inner and upper, (Figure 4-10) were analyzed to determine the relevant velocity fields. The inner and outer regions extended laterally from the location of the respective smoke cartridge (25 cm from the reservoir) to the approximate flame edge, and vertically to the approximate flame tip. The upper plume region was located directly above the flame tip and spanned several flame widths. Each region was approximately 200 x 200 pixels. An interrogation window of 32 x 32 pixels and an overlap of 8 x 8 pixels were used for the cross-correlation analysis.

The mean velocity fields were obtained by taking the average of the instantaneous fields over the capture duration (five seconds). For the horizontal inflow (outer and inner), the mean velocity value was determined by taking the average value of the horizontal velocity profile from the base of the flame to its tip, directly next to the flame. Vertical velocity was determined by taking the maximum value of the vertical velocity in a horizontal plane at the top of the intermittent flame zone, as defined by McCaffrey (1979).

4.4.3.2 Flame height and angle

Mean flame height and angle were determined by analyzing the spatially calibrated video frames. Since the flame's brightness was much greater than the smoke and background, an algorithm was used to identify the location of the flame boundary in each frame by searching for continuous regions of maximum pixel intensity. Similar methods have been used to determine statistical properties of flame geometry and luminous intensity (Audoin et al., 1995; Maynard and Princevac, 2012). However, this method was not amenable to determining flame angle, since the flame shape is irregular, making it difficult to detect a horizontal midpoint at the flame tip. Instead, flame angle was determined by manual measuring the angle of five sampled frames per capture via an image processing program. The length of the flame (L_f) was calculated from the flame height and angle (Albini, 1981):

$$L_f = \frac{H}{\cos \theta} \tag{4-17}$$

where H is the maximum height of visible flame above the surface.

Figure 4-10: Outer (left), inner (middle) and upper (right) plume instantaneous velocity fields from

OpenPIV processing

4.4.4   Error estimation

One cannot expect the optical flow method discussed here to provide the same accuracy as methods which measure motion in a single plane, such as PIV. As the seeding smoke plumes rise from their source, the plume expands radially, and its visible flow features gradually move toward the camera. We can estimate the error in performing cross-correlation analysis on a video image of the smoke plumes. Consider the motion of a visible structure in the smoke plume, as illustrated in Figure 4-11.
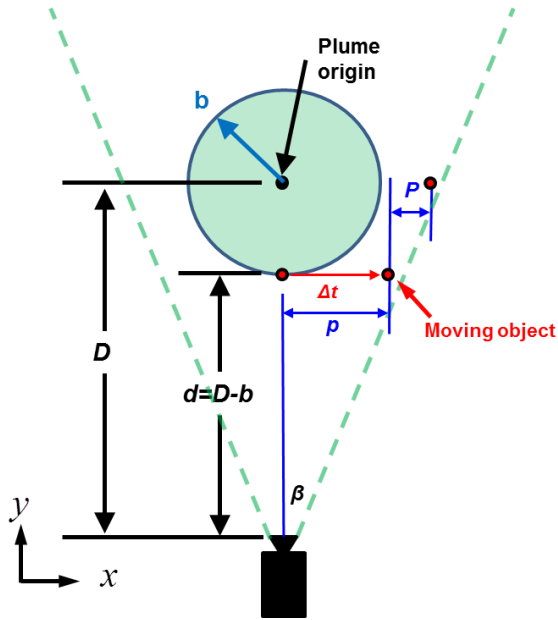
Figure 4-11: Imaging of a point source plume (top view)

In our analysis, we assume all motion occurs at distance D, but most the visible motion is actually on the outer radius of the plume, at distance d. We assume the smoke cartridge acts as a continuous, turbulent point source. In this case, the plume radius scales linearly with height (Batchelor, 1954):

$$b = \alpha z \qquad (4\text{-}18)$$

where α is the entrainment constant and z is height above the origin. An object with velocity u at distance D will appear to move slower than the same object with the same velocity viewed at the closer distance d.

If in time t, an object at distance d moves by amount p in the x direction (Figure 4-11), its u component of velocity is given by:

$$u_d = \frac{p}{t}$$ (4-19)

The apparent distance traveled in the D plane is increased by amount P:

$$u_D = \frac{p+P}{t}$$ (4-20)

where

$$P = (D-d)\tan\beta = b\tan\beta$$ (4-21)

where β is the half-angle of view between the lens and object. p is similarly determined:

$$p = d\tan\beta$$ (4-22)

The relative error can then be estimated:

$$E = \frac{u_D - u_d}{u_d} = \frac{P}{p} = \frac{\alpha z}{D - \alpha z}$$ (4-23)

where D is the distance from the lens to the smoke cartridge. For the experimental setup described here, Eq. (4-23) estimates errors of 2-5% depending on measurement height.

4.4.5   Results

4.4.5.1 Velocity field

Sample velocity profiles are shown in Figures 4-12 through 4-14 for decreasing values of S/H_S, where H_S is the average height of the single flame from the test burns. For the largest separation distance ($S/H_S = 6.6$, Figure 4-12), the magnitudes of inflow velocity on both sides are similar, but the direction of the inner flow is more vertical. As the flames are moved closer ($S/H_S = 3.3$, Figure 4-13), the magnitude of velocity on the inner side decreases, and the inner flow becomes more vertical, though it still retains coherent horizontal motion into the flame. As the

flames are brought close together ($S/H_S = 1.9$, Figure 4-14), the flow on the inner side loses nearly all of its horizontal motion. It should be reiterated that motion in the x plane (into and out of the frame) was not measured, and we expect that as flames are drawn closer, flow into the channel between them becomes significant. However, this flow should not have a substantial effect on flame tilt, as it is parallel to the flames.
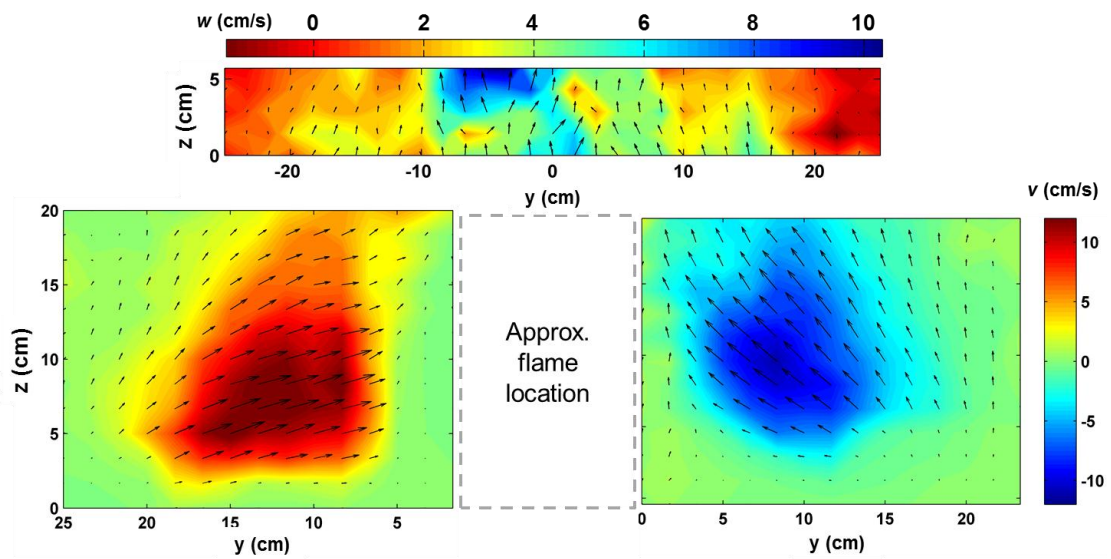
Figure 4-12: Outer, inner, and vertical velocity fields for $S/H_S = 6.6$. Velocity fields are shown in their approximate locations relative to the flame.
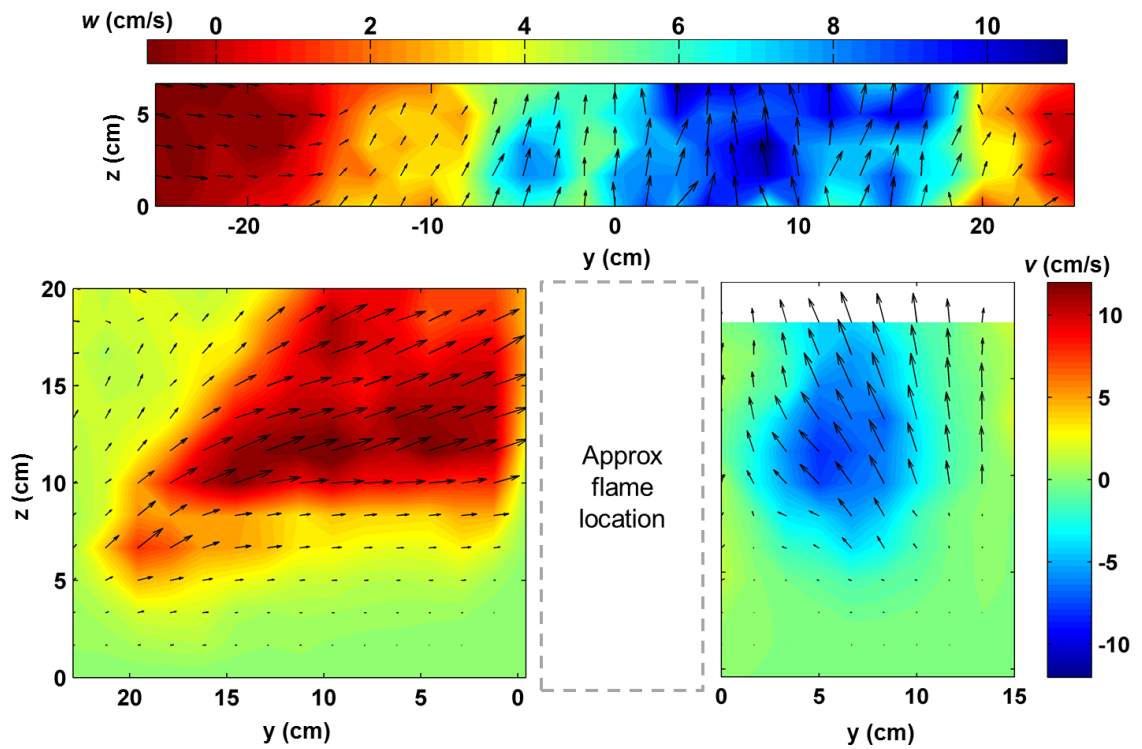
Figure 4-13: Outer, inner, and vertical velocity fields for $S/H_S = 3.3$. Velocity fields are shown in their approximate locations relative to the flame. The inward shift of the upper (vertical) velocity is due to the flame tilting.
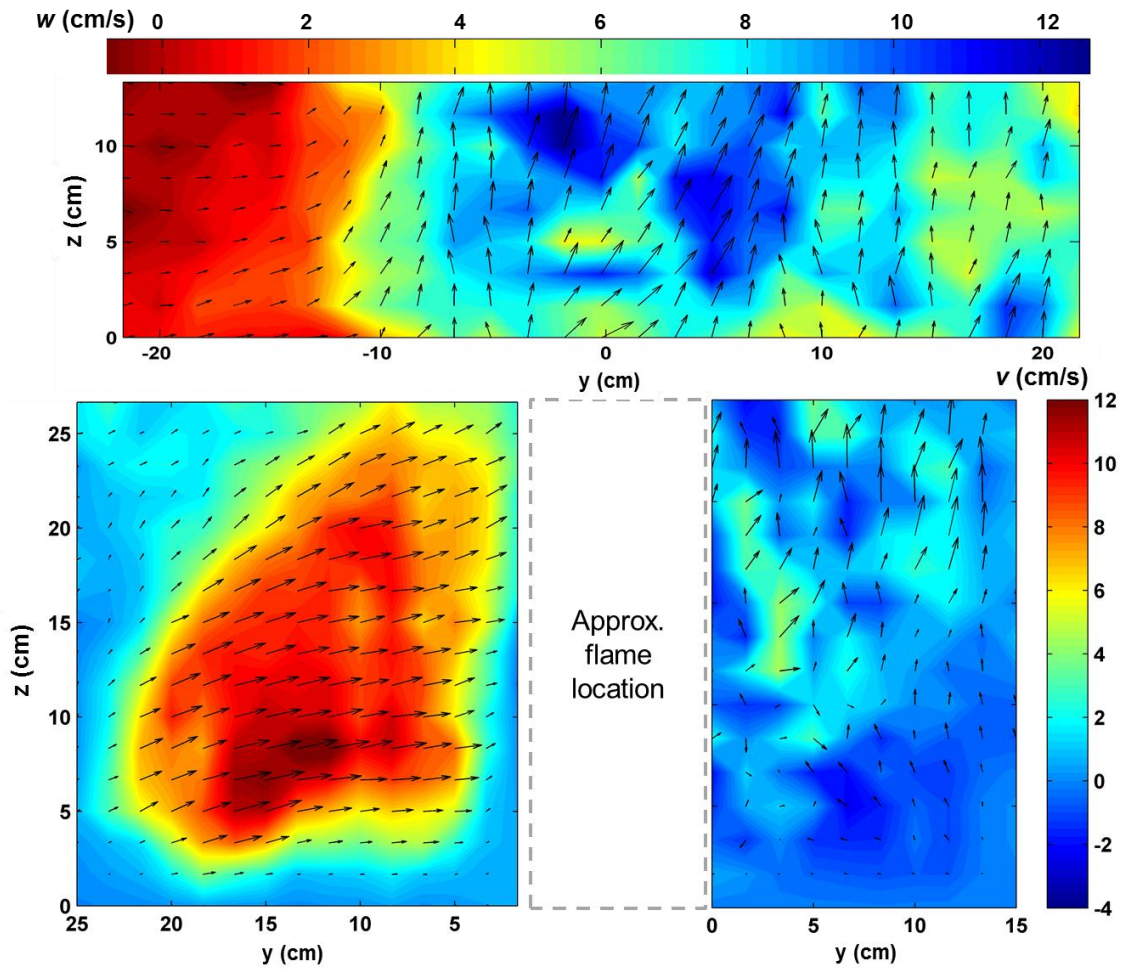
Figure 4-14: Outer, inner, and vertical velocity fields for $S/H_S = 1.9$. Velocity fields are shown in their approximate locations relative to the flame. Note that the presence of the neighboring flame is noticeable in the upper (vertical) velocity field.

4.4.5.2 Vertical profiles of velocity

Vertical profiles of velocity for $S/H_S = 3.25$ are shown in Figure 4-15. Profiles for other separation distances appear similar, though the magnitudes are different. For the outer flow region, horizontal velocity increases with height, but decreases near the top of the flame. This is

logical, since the bulk of the heat release (which drives the flow) occurs in the middle of the flame. The inner flow region shows most horizontal entrainment occurs close to the base of the flame. At S/H_S = 3.25, the flame is tilted approximately 15 degrees from vertical, which may contribute to the sudden decrease in horizontal velocity at z = 10 cm.
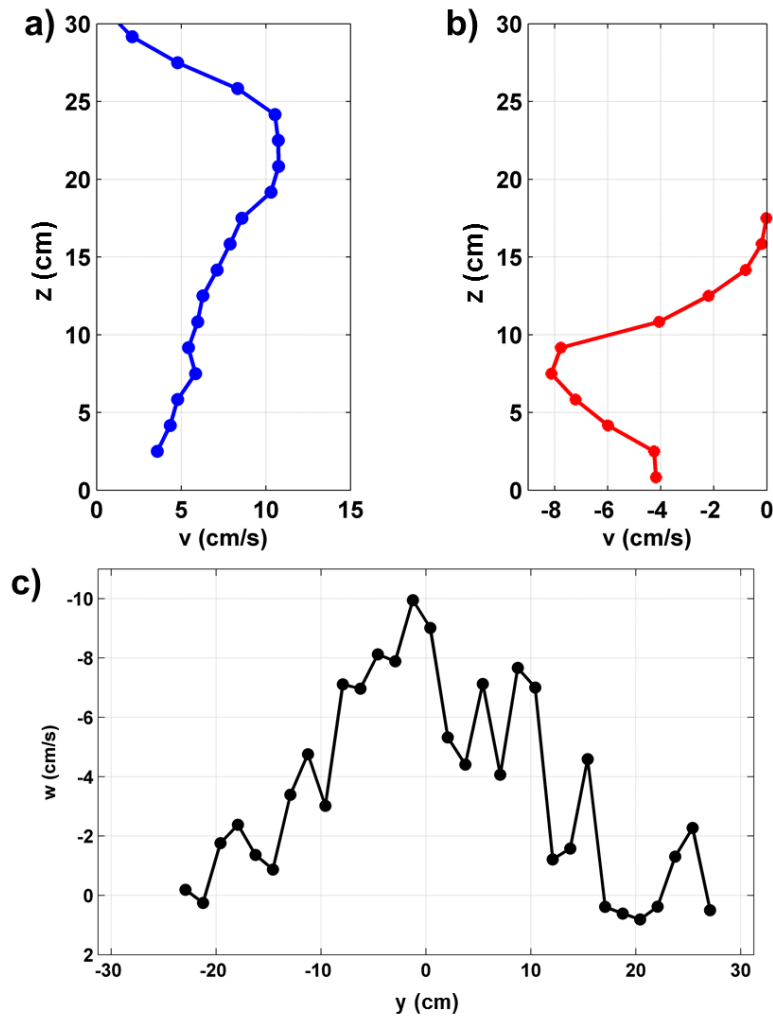
Figure 4-15: a) Vertical profile of outer inflow velocity adjacent to the flame b) Vertical profile of inner inflow velocity adjacent to the flame c) Horizontal profile of vertical velocity above the flame. All profiles represent the quantity time-averaged over a period of five seconds.

4.4.5.3 Mean velocity

For the outer plume, mean horizontal inflow velocities of 5-10 cm/s were present for all experiments, which is comparable to the values measured by Zhou and Gore (1995) using laser Doppler velocimetry around a 7.1 cm toluene pool fire. As expected, the mean velocity on the inner side of the flame was lower, and decreased with decreasing separation distance, while the outer velocity increased slightly (Figure 4-16). For the smallest separation distance ($S/H_S = 0.3$), flames were almost completely merged. For this case, inner velocity could not be measured, but was assumed to be zero. Immediately evident is the existence of a velocity differential at even the largest separation ($S/H_S = 5$), which suggests that fire interactions can begin to occur at even larger distances. Overall, the data agree reasonably with the behavior predicted by the potential flow model, except at the smallest separation distance ($S/H_S = 0.3$). At this distance, the flames are fully merged at a short distance above the surface, and the inner edge of the flame can no longer entrain in the y direction above the merging height. Comparison of vertical and inflow velocities for the merged plume becomes more complicated, since they are both dependent on the degree of merging. Two fully merged plumes of equal strength have twice the buoyancy flux of each plume (Briggs, 1975), but this is not necessarily manifest by the vertical velocity, since destructive interference between plumes may cause it to decrease (Macdonald et al., 2002).
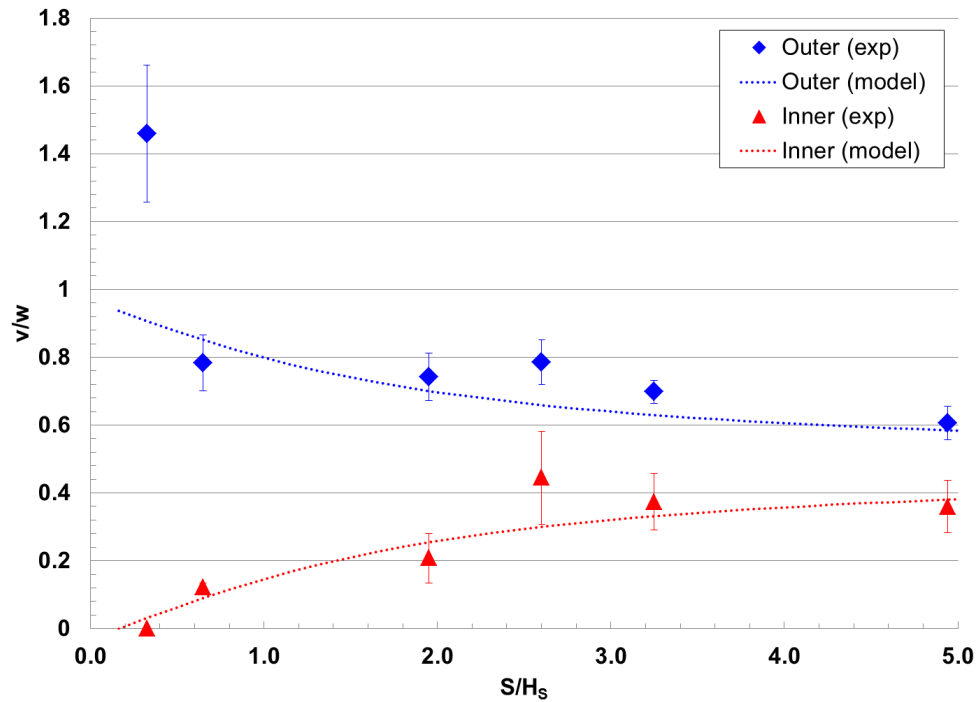
Figure 4-16: Mean outer and inner velocities normalized to vertical velocity. Error bars represent one standard deviation of the mean.

4.4.5.4 Vertical velocity

Vertical velocity increased slightly with decreasing separation distance, until $S/H_S < 2$, below which it decreased rapidly (Figure 4-17). This is likely an effect of burning rate, which is proportional to the heat release rate (HRR) of the fire (Drysdale, 2011). For line plumes, vertical velocity scales with buoyancy flux, and thus HRR, to the 1/3 power. As discussed by Liu et al. (2009), as proximate pool fires approach each other, augmented radiant feedback accelerates burning. However, as separation distance becomes very small, entrainment becomes restricted and burning rate decreases. Our measurements of vertical velocity appear to agree with this notion, though burning rate was not explicitly measured.
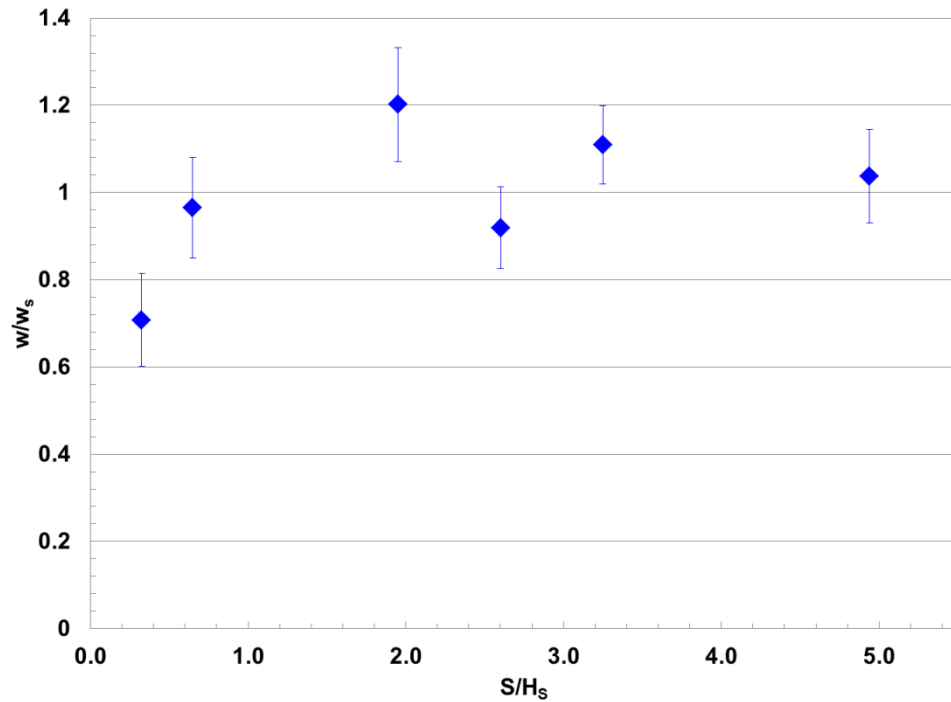
Figure 4-17: Vertical velocity normalized to single flame vertical velocity. Error bars represent one

standard deviation of the mean.

4.4.5.5 Flame angle

Flame angle is shown in Figure 4-18. The measured value was calculated using Eq. (4-6) with $\gamma = 1$. It should be noted that γ can be greater than unity, since both the density ratio (ρ_o / ρ_p) and H/B are greater than one. However, since vertical velocity was taken above the height of visible flame, the density ratio (ρ_o / ρ_p) is much closer to unity than if it were measured in the flaming region. Additionally, the ratio H/B decreases with flame angle (see Figure 4-4).

Overall, both the observed and measured values (Eq. 4-6) agree reasonably with each other and with the angle predicted by potential flow for most of the experimental range, but

diverge from the model as the flames begin to merge. This is to be expected, since at small separation distances, the flames are forced to merge with the neighboring buoyant plume, gradually straightening until they eventually return to the vertical as a fully merged, single plume.
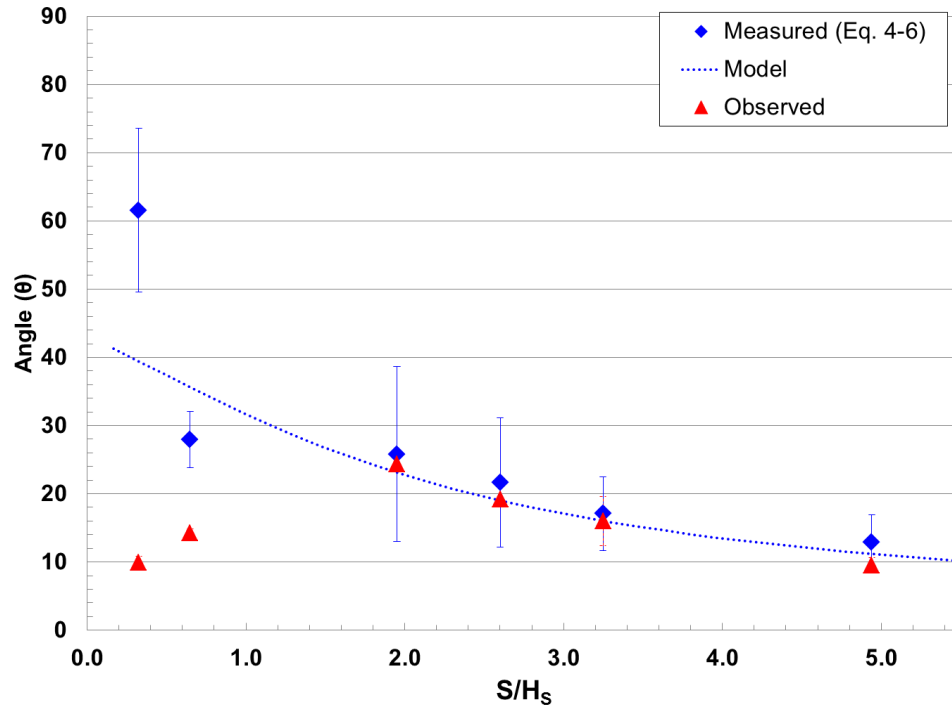
Figure 4-18: Flame angle. Measured value calculated from Eq. (4-6) with $\gamma = 1$. Flames begin to merge below $S/H_S = 2$. Error bars represent one standard deviation of the mean. Large uncertainty in measured value is due to the summation of relative uncertainty of the squares of three measured values.

4.4.5.6 Flame length

In general, flame length was not significantly affected by interaction (Figure 4-19). This differs from the results obtained by other researchers using gas burners, who observed increases in flame height as fires converged (Sugawa and Takahaski, 1993; Fukuda et al., 2004). However,

in their studies, the burning rate was kept constant. For freely burning liquid fires, burning rate is not controlled. For line fires, flame length is related to heat release rate (Eq. 4-14), which is proportional to the burning rate. As mentioned above, from our measurements of vertical velocity, it was inferred that burning decreased as the flames began to merge. Thus, the potential increase in flame length due to merging effects was masked by the reduced burning rate. This issue is worthy of further study, since flame lengths are observed to increase in merging vegetation fires, where burning rate is inherently coupled with fire behavior.
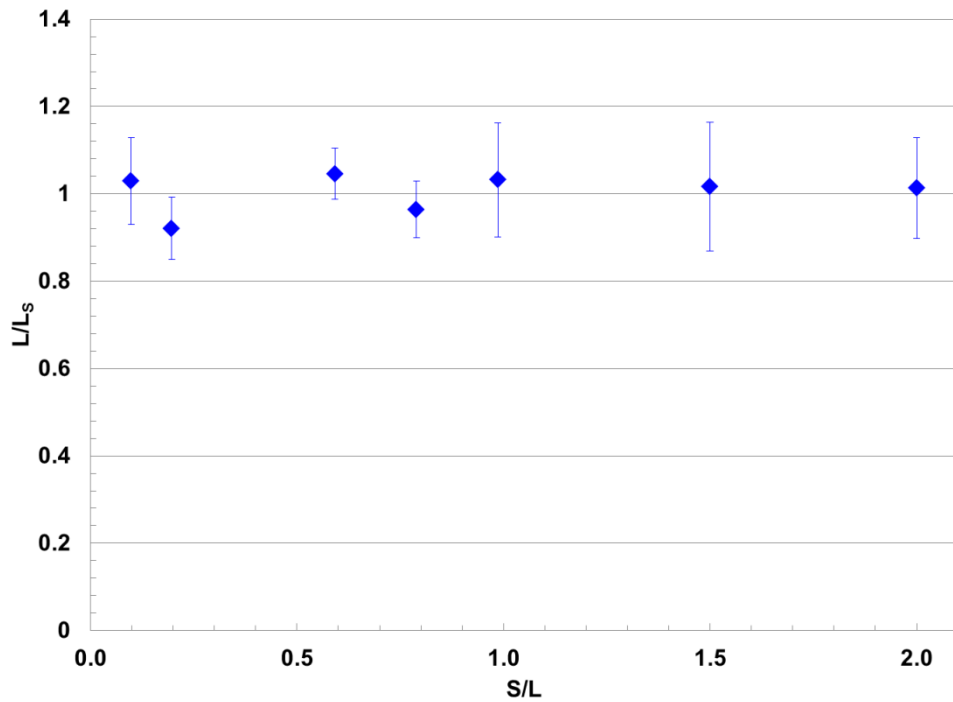
Figure 4-19: Flame length, normalized to single flame. Error bars represent one standard deviation of the mean.

4.5   Discussion

4.5.1   Do interacting flames become "windblown" flames?

Many of the effects observed during fire merging are similar to those which occur with single flames burning under the influence of an ambient wind, including increased flame angle and rate of spread (Brown and Davis, 1959; Albini, 1981). As mentioned in the introduction, wind can have a marked effect on fire behavior.

The model and experiments discussed in this paper suggest that converging line fires are subject to non-uniform entrainment as a result of their position relative to each other. This leads to the development of a velocity difference normal to each flame front, causing the flame angle to depart from vertical. Of interest is whether this velocity difference has the same effect as an ambient wind of equal magnitude, which could suggest that merging flames may transition to "wind-driven" fire behavior as their separation distance reaches a critical value.

At present, there is no universally accepted definition for what constitutes a wind-driven fire. Byram (1959) made one of the earliest attempts to classify fire behavior relative to the influence of ambient wind. He introduced the *convection number*:

$$N_C = \frac{2gI}{\rho_a c_p T_a u_a^{\,3}}$$

(4-24)

where I is the fireline intensity (energy released per unit length of fire front), ρ_a is the density of ambient air, c_p is the specific heat of air at constant pressure, T_a is the ambient air temperature, and u_a is the ambient wind velocity. The convection number represents the rate at which thermal energy is converted to kinetic energy in the convection column ("power of the fire") relative to the horizontal flux of kinetic energy from the mean flow ("power of the wind"). Based on

91

analysis of several large fires, Rothermel (1991b) used a convection number of unity to differentiate between plume (buoyancy) dominated and wind-driven fires. The convection number for a line fire can be represented as the inverse of a Froude number based on buoyancy flux (Albini, 1981; Nelson in Weise and Biging, 1996, Nelson et al. 2012):

$$F_R = \frac{u_a^3}{b_F} = 2N_C^{-1} \tag{4-25}$$

where b_F is the buoyancy flux per unit length of source:

$$b_F = \frac{gI}{\rho_a c_p T_a} = \frac{u_a^3 N_c}{2} \tag{4-26}$$

Nelson et al. (2012) derived Eq. (4-53) by relating line fire plumes with those from ocean outfall diffusers, which were studied by Roberts (1979). Based on his analysis and experiments, he proposed three distinct regimes for line plumes subject to a mean flow. For small Froude numbers ($F_R < 0.2$), the plume is dominated by buoyancy and the flow is strongly vertical. For large Froude numbers ($F_R > 1$), there is an excess of inflow, forcing the plume to stay attached to the surface and propagate downstream. The intermediate regime ($0.2 < F_R < 1$) represents a transition between the two extremes. Nelson et al. (2012) applied this criterion to line fires. Using Eq. (4-25), they proposed that $N_C > 10$ implies that wind has a minimal effect on the fire plume, while $N_C < 2$ implies a strong wind influence.

Rouse, Baines, and Humphreys (1953) studied interacting turbulent line plumes and showed that the vertical velocity scaled with the buoyancy flux per unit length as:

$$w = b_F^{1/3} \tag{4-27}$$

Substitution of this vertical velocity into Eq. (4-25) suggests the convection number for line fires scales as a function of inflow and vertical velocities only:

$$N_C \approx \left(\frac{w}{u_a} \right)^3 \tag{4-28}$$

An identical result can be obtained by substituting the characteristic buoyant velocity for a fire, defined by Nelson (2003):

$$w_B = \left(\frac{2gI_B}{\rho_a c_p T_a} \right)^{\frac{1}{3}} \tag{4-29}$$

into the first equality of Eq. (4-26). If we assume the asymmetric entrainment caused by fire convergence to have the same effect as an ambient wind of equal magnitude, then the convection number can be represented a function of *S/H*:

$$N_C = \left(\frac{w}{v_o - v_i} \right)^3 = f\left(\frac{S}{H} \right) \tag{4-30}$$

Using Eq. (4-28), the convection number from our experiments is plotted in Figure 4-20. Using the above-mentioned criteria, the transition to wind-driven fire behavior in our experiments begins at $S/H_S \sim 1$. It must be mentioned that the convection number was developed as a metric to study the behavior of convection columns above large fires. As such, it was originally derived

using a complex coupled atmosphere/thermodynamic model (Nelson, 1993; Nelson, 2003), effects which are not considered in our analysis. However, its representation as a function of buoyancy flux clearly illustrates its local importance on the behavior of wind-driven flames, as indicated by the experiments of Nelson and Adkins (1986) and Weise and Biging (1996).
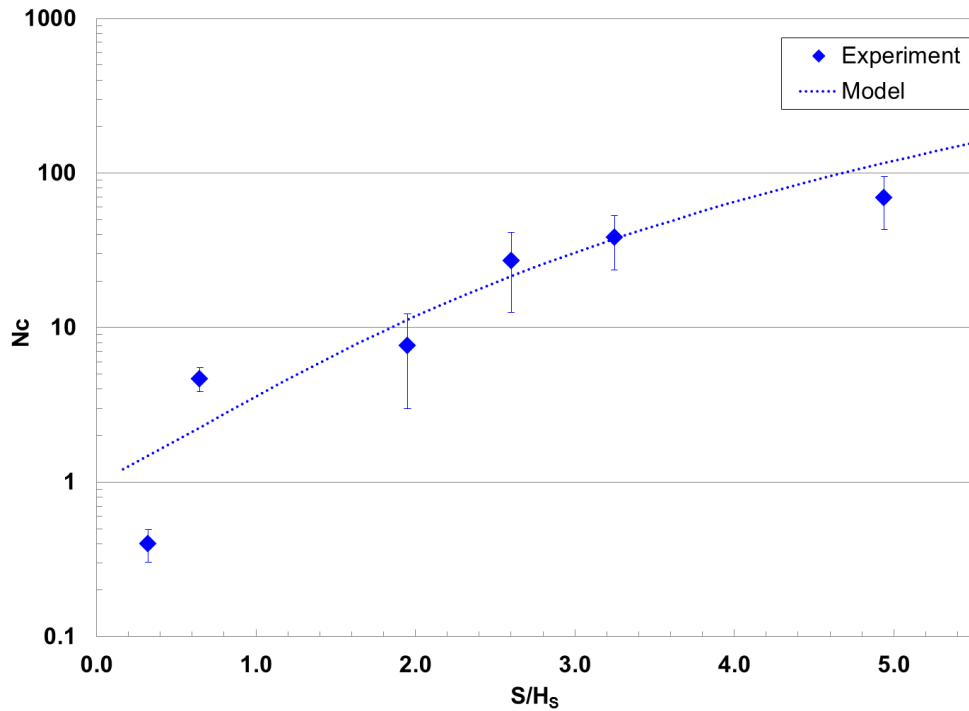
Figure 4-20: Convection number. Error bars represent one standard deviation of the mean.

4.6   Conclusion

The effects associated with flame interaction are important for both the physical understanding and practical control of fire. In this section, the fluid mechanics of merging line fires was explored, specifically the effects of asymmetric entrainment on flame angle. A simple model was proposed to explain flame tilt as a result of linear momentum balance, where the

velocity components outside of the flame are determined using potential flow. To validate the model, experiments were performed using rectangular alcohol pool fires. The entrainment field was seeded with colored smoke, and velocity of smoke structures was measured using a cross-correlation optical flow analysis. From our experiments, the following conclusions can be made:

1. The proposed mechanism for the tilting of interacting flames is an imbalance of horizontal momentum across the flame front. This is caused by flow restriction on the inner edge of the flame due to the combined effects of reduced acceleration length and the opposing dynamic pressure gradient generated by the neighboring fire.

2. Potential flow appears to be a reasonable assumption for the entrainment field surrounding interacting fires. Despite the simplicity of the proposed model, the measured velocities compared favorably with the predicted values.

3. Cross-correlation optical flow analysis is a useful method for estimating the flow field surrounding fires. However, care must be taken when obtaining and interpreting results, since this method is inherently less accurate than planar measurement techniques, such as particle image velocimetry (PIV).

4. The asymmetric entrainment associated with flame merging causes flames to tilt as if exposed to an ambient wind. This may explain why interacting fires often exhibit behavior similar to windblown flames.

To be of practical use for fire managers, field measurements would be useful to see how results hold for larger, spreading fires. Of particular interest is whether the analogy to windblown fires is manifest at field scale, as this could allow simple improvements to existing fire models to account for merging fire behavior. Factors such as fuel composition, ambient wind, and ignition technique likely have a direct impact on the behavior of merging flame fronts in the field.

5.   INTERACTING LINE FIRES - HEAT TRANSFER AND FIELD OBSERVATIONS

5.1   Introduction

As discussed in Section 2, the importance of radiant heat transfer to fire spread is still uncertain, and the proposed explanation for the tilting of stationary flames in Section 4 did not directly address heating. Though the focus of this dissertation is primarily fluid mechanics, in this section we discuss radiant and convective heat transfer in detail, since they undoubtedly bear at least *some* importance to the merging fire problem. As two fires approach each other, radiant heat produced by each flame is transferred to the burning interface of the opposite flame, and to the intervening fuels, accelerating preheating.

In this section, the effect of an adjacent flame on heat transfer and fire spread is discussed in the context of existing fire spread theories and experimental data, and modifications to the existing model of De Mestre et al. (1989) are proposed. Though comprehensive laboratory experiments to validate these modifications were not performed, we discuss the potential effects in terms of existing published data. We also discuss the effect of heat transfer and flow field interactions in qualitative observations of several prescribed burns in Columbia, SC in November, 2011.

5.2   Background

5.1   Heat transfer and fire spread

The problem of fire spread has been approached using statistical (Albini and Rand, 1964), deterministic (Anderson et al., 1982), and physical approaches (Fons. 1946; Frandsen, 1971; De Mestre et al., 1989), and by using models which combine these methods with empirical

data (Rothermel, 1972). Here, we focus only on physical models, as they provide the broadest foundation for understanding the mechanism of fire spread.

Most physical fire spread models have used the concept of "ignition temperature", which assumes that a fuel element ignites upon reaching a specified temperature (Fons, 1946; Albini, 1985; De Mestre et al., 1989; Weber, 1991). This approach is advantageous in that it avoids explicitly dealing with the physicochemical processes of combustion, and it reduces the problem of fire spread to one of heat transfer only. However, even this simplification presents significant difficulties, as estimating the individual heat transfer terms is not trivial. Although numerous well-developed analytical models exist to approximate the contribution from radiant energy, constant fluctuations in flame geometry, intensity, and inhomogeneity in fuel loading make accurate estimation difficult. The convection terms present an even greater challenge, as the motions of gases within and around the flame vary greatly both in character and scale. Local phenomena such as eddies and fire whirls may increase or decrease heat transfer to adjacent fuels (Pagni and Peterson, 1973), while large scale effects such as wind and "plume domination" can lead to chaotic fire behavior (Byram, 1954; Rothermel, 1991). In terms of fuels, the physical characteristics of most wildland fuels have been well studied in laboratory experiments. However, precise estimation in the field still has still proven elusive.

5.2   The model of De Mestre et al. (1989)

Here, we introduce the model of De Mestre et al. (1989), since it will serve as the foundation for our two-fire heat transfer model. They applied the conservation of energy principle to a single line fire of known dimension burning in a horizontally-oriented, homogeneous vegetative fuel bed consisting of thermally thin fuel elements. Radiation was assumed to be the primary mechanism of heat transfer – natural convection is only included later as an energy loss

term. To simplify the model, they assumed the flame front to be purely vertical and propagating at a steady rate with constant radiative properties. A schematic of the coordinate system is shown in Figure 5-1.
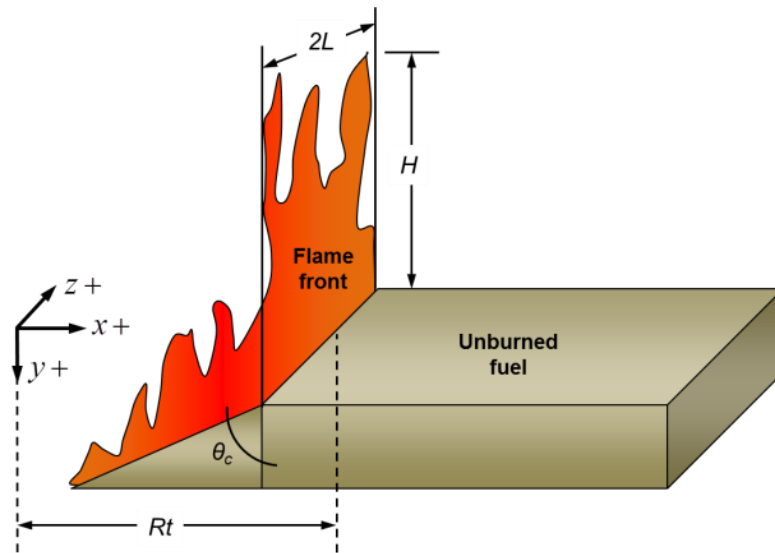
Figure 5-1: Coordinate system for fire spread model (adapted from De Mestre et al., 1989)

5.2.1   Model formulation

De Mestre et al.'s (1989) model originates from a simple conservation of energy relation, where it is assumed some portion of the thermal energy produced by the flame and combusting fuel bed is absorbed by the adjacent fuel. Ignoring heat loss (for now), this can be represented as:

$$Q_a + Q_c = \frac{\partial Q_f}{\partial t} \tag{5-1}$$

where

Q_a is the heat absorbed from flame by an elemental volume of fuel, per unit volume

Q_c is the heat absorbed from within the combusting fuel bed by an elemental volume of fuel, per unit volume

Q_f is the internal thermal energy of elemental volume of fuel, per unit volume

Assuming the fire has achieved a steady rate of propagation, we can make the transformation:

$$R = \frac{dx}{dt} \tag{5-2}$$

where R is the steady state rate of spread (m/s). Substituting (5-2) into (5-1) yields:

$$Q_a(X) + Q_c(X) = -R\frac{dQ_f}{dX} \tag{5-3}$$

where $X = x - Rt$ is the position of the flame front relative to the origin. In this reference frame, the flame is stationary and the fuel moves toward it at rate R. The rate of spread R is negative because, in this frame of reference, the fuel moves towards the flame in the $-X$ direction. This model assumes that the fuel moves towards the flame front at a steady rate of spread from $X \rightarrow \infty$ (ambient temperature) to $X = 0$ (ignition temperature). Note that, at present, convective heat transfer is completely absent in this energy balance.

De Mestre et al. (1989) noted that a traditional radiation view factor is not appropriate to determine heat absorbed from the flame into the fuel bed, since the fuel is semi-transparent, with thermal radiation being absorbed, reflected, and reradiated within the fuel bed. To address this, they assumed that the amount of thermal radiation absorbed is proportional to the absorptivity of the fuel, defined as:

$$\alpha = \frac{s_f \rho_b}{4\rho_f} \tag{5-4}$$

where α is the absorptivity, s_f is the surface to volume ratio of a fuel element, ρ_f is its density, and ρ_b is the bulk density of the fuel bed. The amount of radiant power per unit volume delivered to the surface of the fuel bed ahead of the flame is then given by:

$$Q_f(X) = \alpha \sigma \varepsilon_{fl} T_{fl}^{4} W(X) \tag{5-5}$$

where ε_{fl} and T_{fl} are the emissivity and temperature of the flame, respectively and σ is the Stefan-Boltzmann constant. The term $W(X)$ is the "modified" radiation view factor, which has been manipulated from its usual definition to account for absorption of thermal radiation:

$$W(X) = \frac{2}{\pi} \arctan\left\{ \frac{HL}{X(L^2 + H^2 + X^2)^{\frac{1}{2}}} \right\} \tag{5-6}$$

near the centerline of the fire ($z = 0$) (From this point forward, we refer to this as the "absorption view factor" to prevent confusion with the traditional form). The absorption view factor for the combustion zone follows similarly, but with a more complex form due to its geometry:

$$U(X) = \frac{X \cos \theta_c}{\pi} \int\limits_{z=-L}^{L} \int\limits_{y=0}^{\delta} \xi^{-3} e^{-\alpha \xi} \, dy \, dz \tag{5-7}$$

where

$$\xi^2 = (X + y \tan \theta_c)^2 + y^2 + z^2 \tag{5-8}$$

and θ_c is the angle of the burning interface.

Eq. (5-3) then becomes:

$$I_F W(X) + I_c U(X) = -R \frac{dQ_f}{dX} \tag{5-9}$$

where $I_F = \alpha \varepsilon_f \sigma T_f^{\ 4}$ and $I_c = \alpha \varepsilon_c \sigma T_c^{\ 4}$,and where T_f and T_c are the temperatures of the flame and burning fuel bed interface, respectively. The right hand side of Eq. (5-9) represents the change in the fuel's internal energy. This requires an appropriate model for a vegetative fuel. De Mestre et al. (1989) used a two-phase model which considers the effect of moisture and the latent heat of evaporation:

$$dQ_f = \begin{cases} \overline{\rho c} dT_s & T_s \leq 373K \\ \rho_b c_f dT_s & T_s > 373K \end{cases} \tag{5-10}$$

where

$$\overline{\rho c}(373 - T_a) = \rho_b c_f (373 - T_a) + M \rho_b c_w (373 - T_a) + M \rho_b l \tag{5-11}$$

where M is the fractional moisture content of the fuel, c_w is the specific heat of water, and l is the latent heat of vaporization of water at 373K.

Including convective and radiative heat loss, Eq. (5-11) becomes:

$$-R \frac{dQ_f}{dX} = I_G V(X) + I_H U(X) - \alpha \sigma (T_s^{\ 4} - T_a^{\ 4}) - 4h\alpha (T_s - T_a) \tag{5-12}$$

where $I_G = I_F - \alpha \varepsilon_f \sigma T_a^{\ 4}$ and $I_H = I_c - \alpha \varepsilon_c \sigma T_a^{\ 4}$, and h is a convection coefficient. Boundary conditions are:

$$T_s = T_i \text{ @ } X = 0; T_s \to T_a \text{ as } X \to \infty \qquad (5\text{-}13)$$

Since Q_f is a function of fuel temperature, Eq. (5-12) can be solved for R using iterative methods. In physical terms, R represents the amount of radiant energy produced by the flame and burning fuel bed which is absorbed by the fuel over the region $X = 0$ to ∞, relative to the amount of energy required to raise the fuel from ambient to ignition temperature.

5.2.2 Experimental results – the importance of convection

De Mestre et al. (1989) tested their model by measuring the rate of spread and temperature profile of laboratory scale fires in pine needle fuel beds (*Pinus ponderosa* Laws). Rate of spread was observed visually, while the temperature profile was measured using thermocouples affixed to a fuel element ahead of the flame front. Using the observed rate of spread, the theoretical temperature profile was calculated using Eq. (5-12). In general, it over-predicted the actual fuel surface temperature profile by a significant margin. The prescribed boundary condition at $X = 0$ ensured the model would yield $T_f = T_i$ here, but it did not forecast the measured rapid rise in surface temperature (over 100 K) within 1-2 centimeters of the flame front. This was attributed to either 1) an underestimation of burning bed (combustion zone) radiation, or 2) an unknown short range convective heating effect. The latter seems to be the most likely, as intermittent "flame-bathing" of fuel elements appears to directly precede their ignition, as discussed in Section 2 (Finney et al., 2010, Albini; 1967). One consequence of this was mentioned by Baines (1990), who noted that the gradient term of Eq. (5-12) becomes much smaller than the flame radiation term within a few centimeters ahead of the flame front, meaning the fuel bed is essentially in thermal equilibrium (heat input is balanced by convective and

radiative losses). This allows the surface temperature profile outside this range to be determined algebraically:

$$I_G W_L(X) + \alpha\sigma(T_s^4 - T_a^4) - 4h\alpha(T_s - T_a) = 0 \qquad (5\text{-}14)$$

Although De Mestre et al.'s (1989) model likely does not explain the complete mechanism for flame spread, it still serves as a valuable basis for examining the effect of radiation in merging flames, and could serve as a foundation for future physical models which incorporate both radiation and convection. Thus, we have chosen to use it as a platform for discussion.

5.3 Theory – radiant and convective heat exchange in merging flames

To estimate the impact of an adjacent flame front on the fire's rate of spread, we first consider the likely mechanisms which could affect fire propagation. In terms of radiation heat transfer, we expect the addition of a neighboring flame to have two primary effects:

1. As the adjacent flame moves closer to the primary flame, more of it is "seen" by the intervening fuel (as described by the absorption view factor), so the amount of radiant energy absorbed by the fuel bed (relative to that of a single flame) increases as flames converge.

2. Because the intervening fuel now receives a continuous heat flux from two converging sources, we expect that the thermal energy required to bring the fuel to ignition will become progressively smaller. This differs from the single flame case, where the flame always moves towards new, unheated fuel which exists initially at ambient temperature.

Physical intuition leads one to expect that both of these factors will cause the rate of spread to increase in some way, since we are *increasing* the amount of radiant energy added to

the fuel bed, while simultaneously *decreasing* the amount of energy required to bring the fuel to ignition.

In terms of convective heat transfer, we have no basis on which to make such a definitive assessment. If we simply assume that convective heat transfer is important only for close-range heating, then we cannot logically conclude that the addition of a neighboring flame would affect this process much until the separation distance is very small, at which point complete coalescence is imminent anyway. However, as shown in Section 4, the entrainment fields of fires interact at larger distances, which could affect convective heat transfer to/from the burning interfaces and intervening fuel bed.

In this section, we begin by modifying De Mestre et al.'s (1989) model by including the effect of flame angle, since, as discussed in Section 4, converging flames tilt towards. Next, modify the governing equations to include a second flame front, and we follow this by a discussion of convective heat transfer and propose a simple model to determine rate of spread.

5.3.1 The effect of flame angle and flame length

The absorption view factor terms above were derived for vertical flames of constant height, an assumption which conflicts with the observed behavior of merging flames. As fire fronts converge, both the flame angle (from vertical) and flame height can increase. These both affect the flame view factor, since it is directly related to the surface area and orientation of the radiating surface relative to the fuel bed.

De Mestre et al. (1989) derived Eq. (5-6) using the view factor between for two elemental areas, but modified to account for absorption within the fuel bed, resulting in the following expression:

$$W(X,z) = \int_{-w}^{w}\int_{0}^{H} \frac{\cos\theta_1}{\pi r^2} \, dy \, dz \tag{5-15}$$

where W is the view factor, r is the distance between the flame and the area absorbing radiation, and θ_1 is the angle between r and the vector normal to the flame. To simplify the integration, Eq. (5-15) can be easily modified for the case of a vertical flame burning on an inclined surface (Figure 5-2):
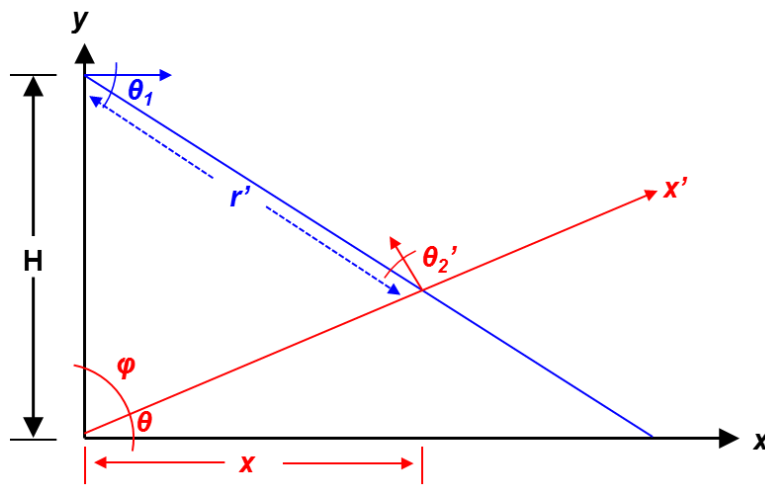
Figure 5-2: Coordinate transformation for tilted flame view factor calculation

By inspection of Figure 5-2, the cosine term in Eq. (5-14) can be represented as:

$$\cos\theta_1 = \frac{x}{r'} = \frac{x'\sin\varphi}{r'} \tag{5-16}$$

where x' represents the upslope distance, φ is the angle between the flame and the surface, and r' is the distance between the origin (flame) and the point where the radiation line intersects the surface:

$$r' = \sqrt{(x'\sin\varphi)^2 + (y - x'\cos\varphi)^2 + z^2} \qquad (5\text{-}17)$$

and Eq 5-15 becomes:

$$W'(X, z, \theta) = \int_{-w}^{w} \int_{0}^{H} \frac{x'\sin\varphi}{\pi r'^{3/2}} \, dy \, dz \qquad (5\text{-}18)$$

The form of Eq. (5-18) also allows direct comparison with other forms of the absorption view factor derived for upslope flames. For the same configuration, Weber (1989) gives a simplified form of view factor for a flame of infinite width:

$$W_{\theta}(X, \theta) = \frac{2}{\pi} \arctan\left\{ \frac{H\cos\theta}{X' - H\sin\theta} \right\} \qquad (5\text{-}19)$$

which yields a result identical to Eq. (5-18) for a very wide flame. Since the radiation view factor between two surfaces is dependent only on the orientation between them, and not the orientation relative to any specific datum, Eq. (5-18) can be directly applied to the case of an angled flame burning on a horizontal fuel bed.

Eq. (5-17) is plotted in Figure 5-3 for several values of φ. The maximum value of the absorption view factor now approaches 2, compared to a maximum of 1 for Eq. (5-14). This was noted by Baines (1990), who stated that flame angle has the potential to double the effect of flame radiation.
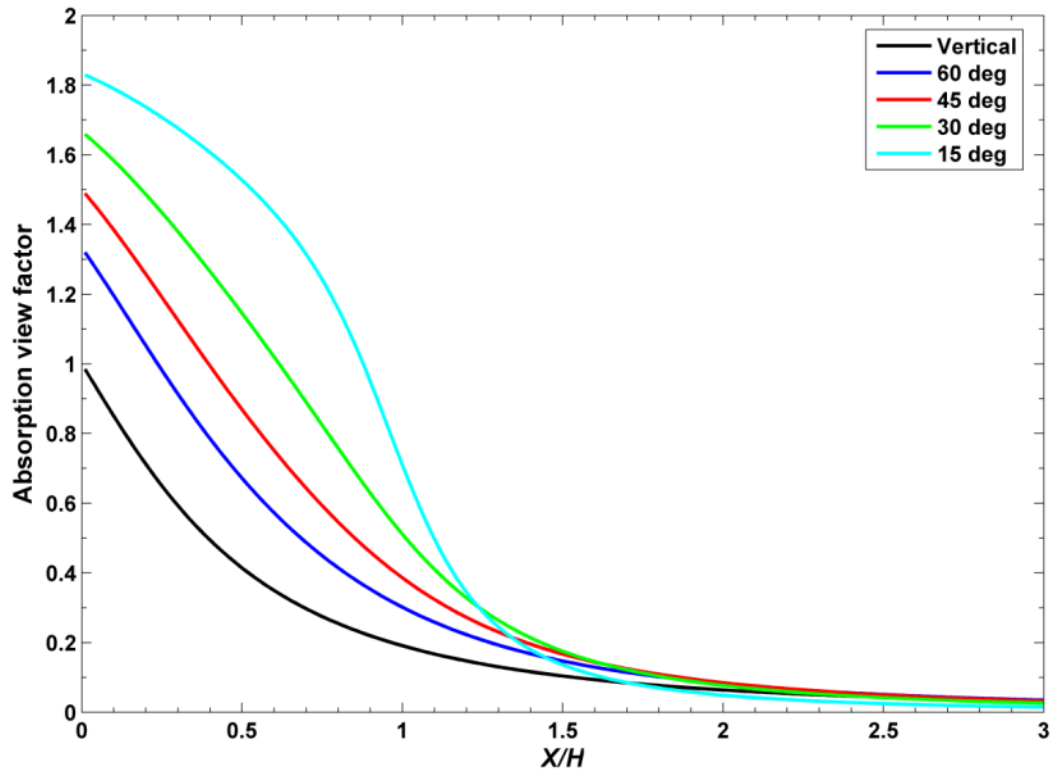
Figure 5-3: Effect of flame angle (from vertical) on absorption view factor

5.3.2   Addition of an adjacent flame front to De Mestre et al.'s (1989) model

Before attempting to estimate how spread rate is affected by an adjacent flame, we first consider how the addition of a second fire placed at distance S affects the instantaneous rate of radiant heat transfer to the intervening fuel bed. Ignoring losses and assuming both flames emit the same amount of radiant energy, the total heating rate due to heat flux from both flames (and their combustion interfaces) is given as:

$$\frac{dQ_T}{dt} = I_G\left[W_L(X) + W_R(X)\right] + I_H\left[U_L(X) + U_R(X)\right] \tag{5-20}$$

where the subscript T represents the total amount of internal energy within the fuel bed, and the subscripts L and R represent the individual flames. $W_R(X)$ and $U_R(X)$ are similar to Eqs. (5-6) and (5-7), except they are shifted by the separation distance between flames (S):

$$W_R(X) = \frac{2}{\pi} \arctan\left\{ \frac{HL}{(S-X)(L^2 + H^2 + (S-X)^2)^{1/2}} \right\} \tag{5-21}$$

$$U_R(X) = \frac{(S-X)\cos\theta_c}{\pi} \int_{z=-L}^{L} \int_{y=0}^{\delta} \xi_R^{-3} e^{-\alpha\xi} dydz \tag{5-22}$$

where

$$\xi_R^{\;2} = \left[(S-X) + y\tan\theta_c\right]^2 + y^2 + z^2 \tag{5-23}$$

To compare the heating rate for two adjacent flames versus a single flame, we define the relative heating rate:

$$Q' = \frac{dQ_T / dt}{dQ_s / dt} \tag{5-24}$$

where the subscript s denotes the single fire case. If we assume a homogeneous fuel bed, the relative increase in thermal energy absorbed per unit time is given as:

$$Q'(S) = \frac{I_F \left[W_L(X) + W_R(X)\right] + I_H \left[U_L(X) + U_R(X)\right]}{I_F \left[W_L(X)\right] + I_H \left[W_L(X)\right]} \tag{5-25}$$

The relative heating rate of a surface fuel element at $X/H = 0.01$ (close to the left flame) is shown in Figure 5-4, using flame geometry and fuel conditions of De Mestre et al. (1989). As the separation distance approaches zero, the relative heating rate doubles, as expected. Conversely, as S approaches infinity, the relative heating rate approaches that of the single fire. Although Eq. (5-25) serves as useful physical insight, in practice it is unrealistic since losses are not considered. If losses were included, we expect that the relative rate of heating would not increase so rapidly at small S/H.
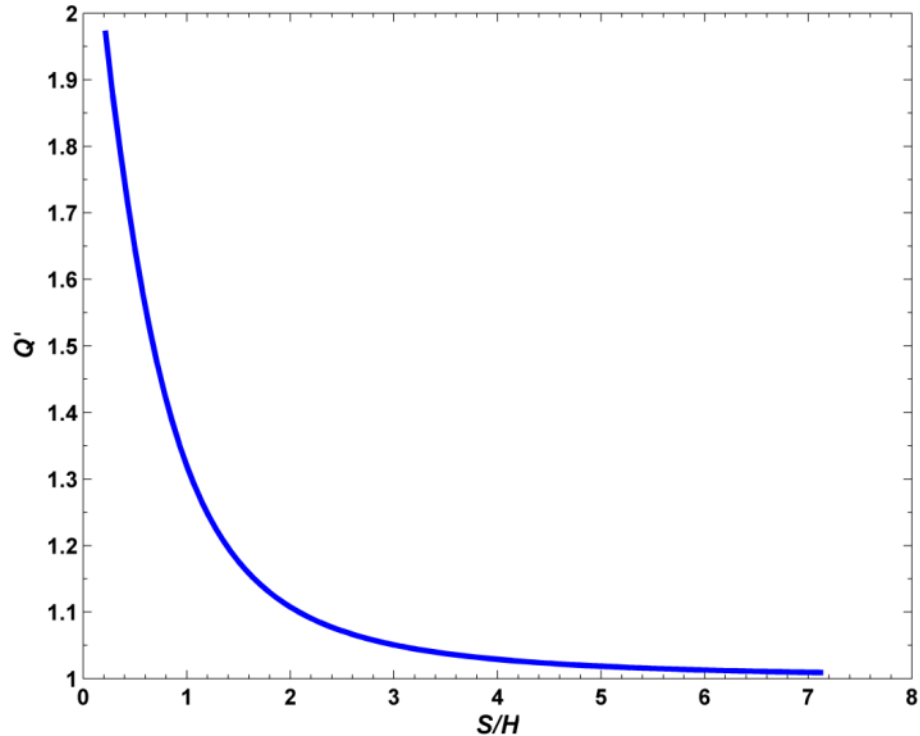
Figure 5-4: Relative heating rate of a fuel element at $X/H = 0.01$ for two fires versus a single flame.

In terms of rate of spread, we can define an equation analogous to Eq. (5-12) for a flame which is influenced by a neighboring flame:

$$-R\frac{\overline{\rho c}dT_S}{dX} = I_G[W_L(X) + W_R(X)] + I_H[U_L(X) + U_R(X)]$$
$$-\alpha\sigma(T_s^{\ 4} - T_a^{\ 4}) - 4h\alpha(T_s - T_a)$$

(5-26)

where $\overline{\rho c}$ represents the average volumetric heat capacity over the entire fuel bed. Actually solving this equation is not trivial; unlike Eq's. (5-12) and (5-13), two boundary conditions are required (each flame should have $T_s = T_i$ at its burning interface). Since Eq. (5-26) is a first order ordinary differential equation, it cannot be simply solved to simultaneously satisfy both boundary conditions. Though not shown here, given several assumptions, the governing equation can be manipulated to yield a solution. However, these assumptions are quite restrictive, and we recognize that, as mentioned throughout this dissertation, the assumption that radiation completely governs the rate of spread is likely invalid anyway. Radiation is important, however, in determining the fuel surface temperature, which should affect convection to some extent.

5.3.3 The role of convection

As mentioned previously, the role of convection as a mechanism of fire spread cannot be ignored. Though the actual physics behind this process are not well understood, we can make some assumptions about its influence relative to the two-fire problem. We acknowledge that thermal radiation preheats the fuel bed, but we assume that the short-range, intermittent flame contact described by Finney et al. (2010) is the final process which brings the fuel to ignition temperature. It is not entirely clear how an adjacent flame front would affect this behavior. If convection is locally governed (i.e. not largely affected by the presence of the neighboring flame), then the characteristics of the short-range convective heating effect should not change appreciably with flame separation distance. However, it can be logically argued that a greater initial fuel surface temperature (due to augmented radiant preheating) will reduce the amount of

time required for the convective effect to bring a given fuel particle to ignition temperature. Thus, in a given time period, we theorize that the overall effect of augmented preheating is to increase the distance over which the flame front can advance.

As a first approximation, we use a lumped capacitance model to determine the time required to bring a fuel particle at given temperature to ignition. The applicability of lumped capacitance here is somewhat debatable, since a given fuel element may not be completely enveloped in convective gas; it is likely touching other fuel elements. However, it serves as a useful preliminary estimate. To be valid, lumped capacitance requires the temperature to be homogeneously distributed throughout the object being heated. The qualifying condition for this is a Biot number of less than 0.1:

$$Bi = \frac{hL}{k} < 0.1 \qquad (5\text{-}27)$$

where L is a characteristic length, typically the ratio of volume to surface of the object. For the experiments of De Mestre et al. (1989), the fuel particles (pine needles) had an average volume to surface ratio of 1.75×10^{-4} m. Stocksted (1974) gives a thermal conductivity for a ponderosa pine needle as 0.07 W/m, meaning the heat transfer coefficient must be of order 10 or smaller to satisfy Eq. (5-27). Convection coefficients for fuel elements depend on particle size and orientation of flame spread, and tend to increase as particle diameter decreases and can become on the order of 10^2 for fine fuels (Cohen and Finney, 2010), but few measurements are available. However, Beer (1990) and De Mestre et al. (1989) showed that theoretical analysis of a cylinder with the dimensions of a ponderosa pine needle has a heat transfer coefficient of approximately 44 W/m^{2}-K, which gives $Bi = 0.1$. Thus, our assumption that the average pine needle is thermally thin is justified, if just barely. The time for a material to reach a specified temperature using lumped capacitance is given as (Bergman et al., 2011):

$$t = \frac{\rho V c_p}{h A_S} \ln\left[\frac{T_0 - T_\infty}{T_f - T_\infty}\right] \tag{5-28}$$

where ρ is the density of the material, V is the volume of the object, A_S is the surface area, and subscripts 0, f, and ∞ represent the initial, final, and ambient temperatures, respectively.

Since the rate of spread is defined as the propagation rate of the flame interface, for an identical fuel bed, the relative rate of spread between the two-fire and single fire case is then:

$$R' = \ln\left[\frac{(T_S(\gamma)_S - T_\infty)}{(T_i - T_\infty)}\right] \times \ln\left[\frac{(T_i - T_\infty)}{(T_S(\gamma)_D - T_\infty)}\right] \tag{5-29}$$

where $T_S(\gamma)$ is the fuel surface temperature at the convection zone boundary, and subscript D represents the two fire case. The temperatures at the convection zone boundary are determined using Baines' (1990) thermal equilibrium assumption, given by Eq. (5-13) for the single fire. For the two-fire case, the corresponding equation is:

$$I_G[W_L(X) + W_R(X)] + I_H[U_L(X) + U_R(X)] - \alpha\sigma(T_s^4 - T_a^4) - 4h\alpha(T_s - T_a) = 0 \tag{5-30}$$

The result of Eq. (5-30), using the flame geometry and fuel bed properties of De Mestre et al. (1989) for varying hypothetical convection zone depths is shown in Figure 5-5. For these flames, the theoretical relative rate of spread remains largely unaffected until $S/H \approx 5$, below which it begins to increase rapidly, exceeding up to four times the single fire ROS. The validity of the assumptions used to derive Eq. (5-30) deserves to be challenged, since they depend on several complex factors, including the amount of energy contained in the flame deflections, their length scale, and their periodicity.
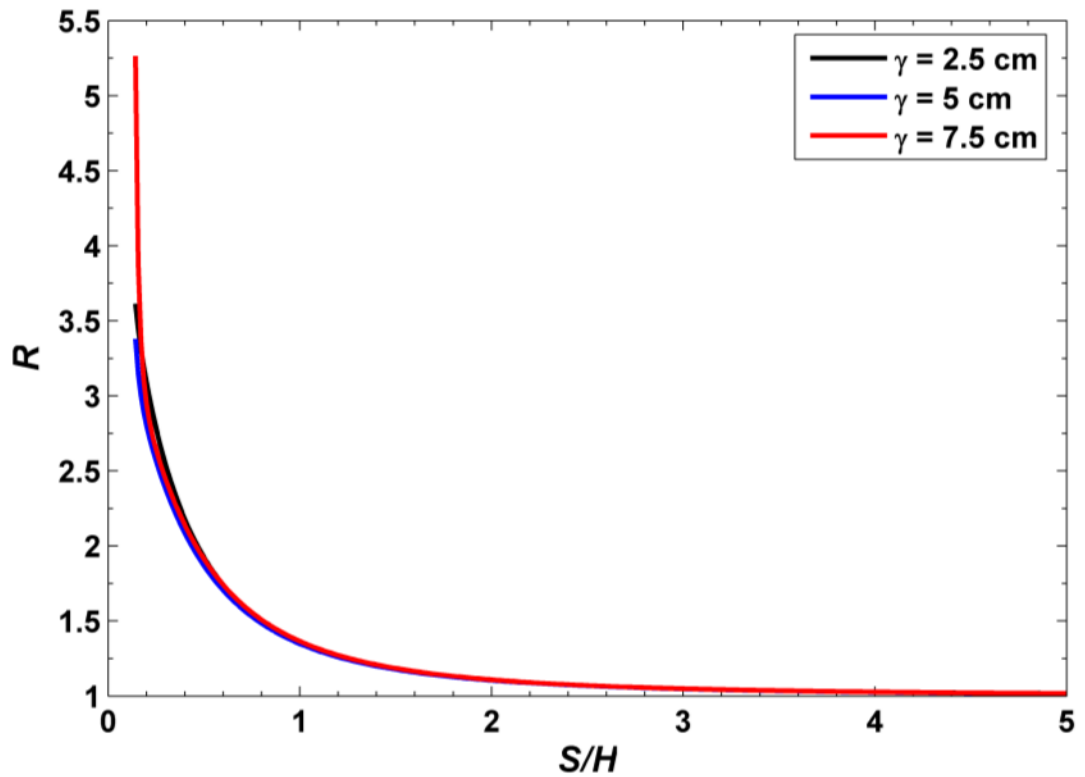
Figure 5-5: Relative change in rate of spread for two fires using Eq. (5-28) and the data of De Mestre et al.

(1989).

5.3.4 The need for laboratory experiments

Clearly, the issue of heat transfer in merging fires is worthy of experimental investigation. Unfortunately, just measuring rate of spread to validate Eq. (5-28) does not provide much physical insight into the problem. Rate of spread is a tempting quantity since it is easy to measure, but it depends on many factors which have been assumed constant in this model, including fuel type, fuel moisture, fuel loading, flame geometry, and ambient conditions. Some researchers have used engineered fuel beds, for example cardboard (Adam et al., 2013) and bamboo (Lozano et al., 2008) to reduce fuel-related uncertainty, but constant fluctuations in flame

geometry still create problems. As highlighted by Finney et al. (2012), the convective structures which heat fuels ahead of the flame are highly transient and three dimensional in nature. Without the ability to reliably measure factors such as convection zone depth and the character of convective fluctuations, we cannot be sure that the actual principles are not being masked by experimental error.

5.4   Field observations

Merging fire behavior was observed during several burns at Fort Jackson in Columbia, South Carolina in November, 2011.

5.4.1   Site description

Fort Jackson is a United States Army installation located in the central part of South Carolina (Figure 5-6), and is primarily used for combat and basic training. Much of the base consists of undeveloped forest, used for training activities as well as wildlife preservation and timber harvesting. The restoration of the longleaf pine (Pinus palustris) ecosystem, once a major component of the southeastern United States, is a primary focus of the base's forest management plan (United States Army, 2007), as well as much of the United States in general. The base contains over 15,000 acres of longleaf pine, and prescribed fire is frequently used to support its management.

Figure 5-6: Location of Ft. Jackson, outside of Columbia, SC. Image courtesy of Google Earth.

Three separate prescribed burns were observed over a period of three days. Site #1 (Figure 5-7) was a flat, 153 acre block consisting primarily of longleaf pine and hardwoods, with a moderate understory of longleaf needles. Site #2 (Figure 5-8) was an 89 acre block, which was flat with the exception of a moderate grade (6%) on the northeast corner. Fuels were similar to Site #1, except there were a greater number of hardwoods, and the understory was less dense. Site #3 (Figure 5-9) was a flat, 71 acre block with fuels similar to Site #1.
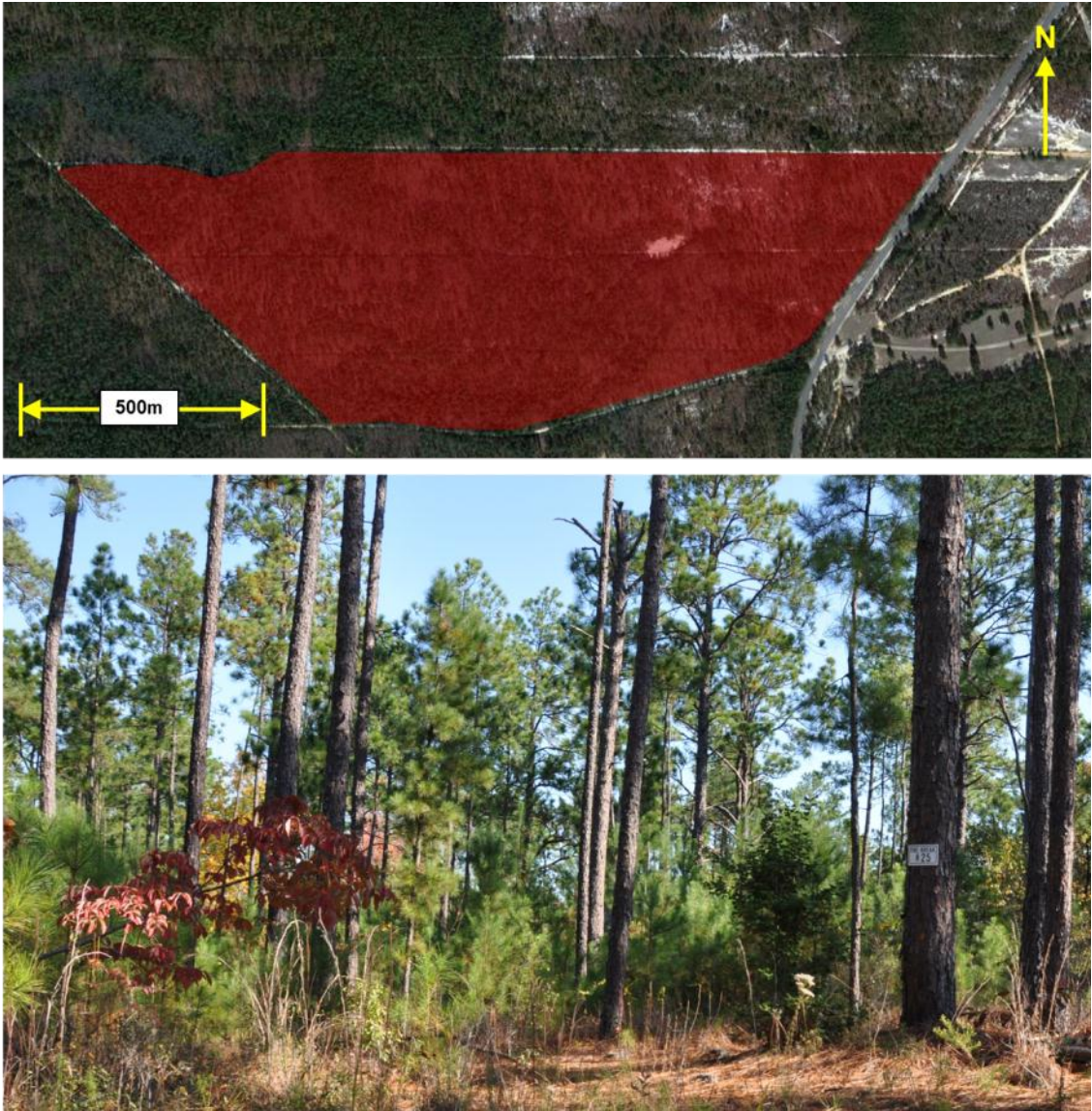
Figure 5-7: Overview of Site #1 (top – courtesy of Google Earth) and representative fuels (bottom)

Figure 5-8: Overview of Site #2 (top – courtesy of Google Earth) and representative fuels (bottom)
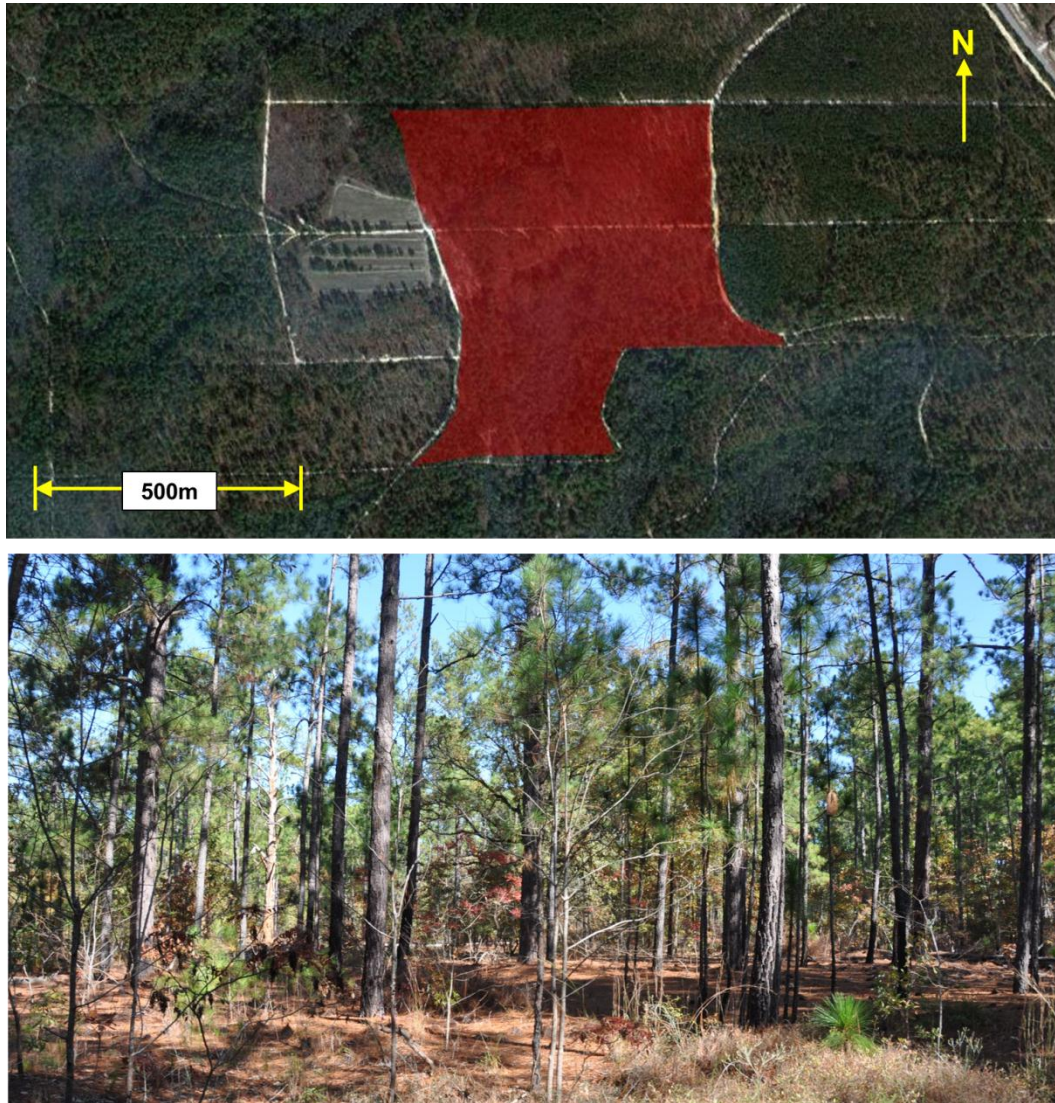
Figure 5-9: Overview of Site #3 (top – courtesy of Google Earth) and representative fuels (bottom)

5.4.2 Weather conditions, ignition techniques, and instrumentation

Weather conditions for all burns were mild, with temperatures of 15-20°C, relative humidity of 40-60%, and winds of 2-5 m/s.

Strip head firing (Figure 4-2a) was the predominant method of ignition, and drip torches (hand and ATV mounted) were used for all burns. In some locations, spot and ring firing were also used to observe merging behavior for these fire configurations. Fire behavior was monitored using still cameras, high definition video, and a handheld infrared camera (FLIR T640).

5.4.3   Fire behavior observations

In general, the intensity of single flame fronts burning in longleaf pine understory was mild, with flame lengths of 1 meter or less. Fire activity increased in areas with dense shrubs, and flame lengths appeared to exceed 3 meters in some of these areas. For merging line fires, flame tilt was quite prevalent, but it was sometimes difficult to determine if tilting was caused strictly by merging, or whether wind was a contributing factor. As shown in Figure 5-10, in many cases, head fires merged with a backing fire. Head fires tilted towards the backing fire (most likely due to wind), while the backing fires sometimes tilted towards the oncoming flame front. However, in Figure 5-10, the backing flame front tilted *away* from the head fire (also evident in the motion of smoke plumes behind the flame front). This is likely due to larger scale effects. In this instance, several acres were vigorously burning behind the backing fire, which may have been the cause of the wind which drove the head fire towards it. This case serves as an important illustration of the difficulty of field measurements – it is often difficult to identify the cause and effect.

119

Figure 5-10: Merging of head and back fires (visible images at top, corresponding infrared image shown at bottom).

Flame height and fire intensity was significantly affected by merging, as shown in Figure 5-11. In this case, there was little to no ambient wind, so each fire initially behaved in a similar manner. As they began to approach each other, changes in fire behavior were noticeable, including inward flame tilt (Figure 5-11b) and rotation (fire whirls, Figure 5-11 c and d). Smoke plumes from burned area behind each flame initially rose lazily, but began to flow strongly into the flame area as convergence began. Though it was not directly measured, rate of spread obviously increased significantly during merging.

Figure 5-11: Convergence of two line fires with minimal ambient wind. Fire intensity increased significantly during merging.

To observe the behavior of merging spot fires, point source fires were ignited by hand in several areas (Figure 5-12). Initially, their rate of outward spread was very slow. As each fire grew, it propagated radially outward. During this radial spread, the ring of flame around each ignition point seemed to interact with itself, tilting inward toward the origin. As the two fires grew closer to each other, they began to exhibit behavior similar to merging line fires, including an increase in flame height and apparent intensity. However, fire behavior was still much less intense than what was observed in merging line fires.

Figure 5-12: Merging of two point source ignitions with minimal ambient wind.

5.4.4   Fuel bed heat transfer – observations

Thermal images recorded during flame convergence were analyzed to determine if the topics discussed earlier in this section, radiant and convective preheating, could be observed. The infrared camera was set to a minimum temperature of 100°C, meaning that any radiating surface above this temperature would be visible. Since it is difficult to determine the actual magnitude of temperature without knowing the exact environmental conditions, distance to target, and emissive properties of the surface, our goal was only to see if any preheating effects were visible. The merging of two spot fires in infrared is shown in Figure 5-13. In this temperature scale, the yellow indicates a temperature of approximately 1200°C, indicating the position of each flame front. Initially, the unburned fuel around each flame is generally not visible, meaning it is relatively cool, except very close to the flame. However, as the flames draw closer, some of the intervening fuel bed becomes visible, indicating that the amount of thermal energy being absorbed by the fuel is greater than the amount being lost. The frequency of embers, pieces of burning material which can serve as new ignition sources, was also observed to increase during the merging process. Though not discussed previously, these may also contribute to the increased rate of spread observed in merging fires, as they can directly ignite intervening fuels.
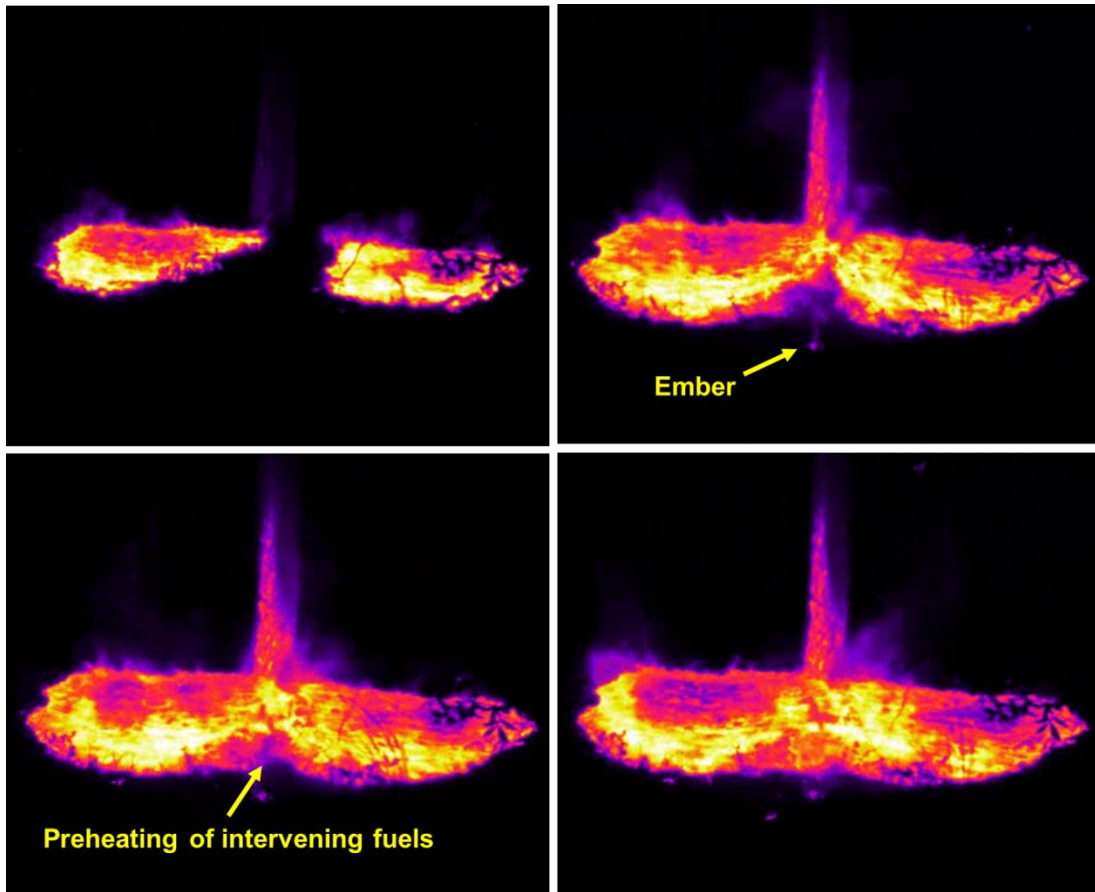
Figure 5-13: Merging of two point source ignitions using a thermal camera.

5.5   Conclusion

In this section, the heat transfer processes behind fire spread were discussed, and a modification to an existing model based on radiant heat transfer was proposed. The new model considers the effect of a neighboring flame front on heat transfer to the intervening fuel bed, as well as the effect of flame angle, which occurs during flame interaction. Since it has been widely observed that radiation heat transfer does not entirely control flame spread, and in fact may be secondary to convection, a new rate of spread model is proposed which assumes convection governs fire spread, but radiation from both flames preheats the intervening fuels.

Additionally, observations from a series of experimental fires at Fort Jackson, SC are presented. The merging fire effects discussed in Sections 4 and 5 were apparent using both visible and thermal infrared imagery.

6.   CONCLUSION

The importance of fire to human civilization cannot be understated. Its effects, both positive and negative, have helped shape our existence in innumerable ways. The desire to understand and control fire has long been a goal of the scientific community, and its study spans many disciplines, ranging from fundamental physics and chemistry to land and emergency management. An understanding of fire behavior is crucial to the ability to both capitalize on its benefits and control its negative effects.

In this dissertation, two physical aspects of fire behavior, flame pulsation and flame interaction, were discussed. Flame pulsation is a distinct characteristic of natural fires, and is characterized by rapid, regular fluctuations of flame structure (flickering). The rate of pulsation does not appear to be dependent on combustion chemistry or fuel type, as it occurs in solid, liquid, and gaseous fuels. Fire interactions, on the other hand, only occur when two or more flame fronts converge. Flame merging often leads to enhanced fire behavior, including increased flame length, flame angle, fire intensity, and rate of spread. This can have significant consequences, both in wildland and structural fires. Flame merging can occur naturally during wildland fires, but is sometimes also induced by fire crews to produce desired fire behavior, often to consume fuels or provide a buffer zone to protect a resource or structure. In structural fires, flame merging can occur when flames from separate burning structures begin to interact. Such scenarios are common during urban conflagrations. In areas where residential and commercial developments exist near wildland areas, the wildland urban interface, wildfires and structure fires can also interact, leading to unexpected fire behavior.

6.1 Fire pulsation

In Section 3, the phenomenon of fire pulsation was explored both experimentally and theoretically. A high speed camera was used to visualize the structure of pulsating ethyl alcohol pool fires with base diameters of 30 to 125 millimeters, covering both laminar and turbulent conditions. To measure pulsation rate from the high speed images, the luminous image intensity between frames was compared using the power spectral density. Pulsation rates were found to compare favorably with those in the literature. To explain the origin of the pulsation mechanism, it was theorized that thermal instabilities at the base of the flame lead to the development of thermals, discrete packets of buoyant fluid which develop at the surface and eventually rise into the surrounding fluid. The proposed theoretical model shows the same dependence on fire diameter as is demonstrated in the literature.

6.2 Fire interactions

In this dissertation, both flame tilting and heat transfer effects in interacting flames were studied. In Section 4, the flame tilting phenomenon was explained as being a result of fluid mechanics. As two flame fronts converge, their entrainment fields interact. As the area between fires becomes smaller, the inflow velocity of intervening air decreases due to the decreased length scale for fluid acceleration and the neighboring fire's dynamic pressure gradient. A simple linear momentum model was used to predict flame angle as a function of the inner and outer fluid velocities outside the flame. To determine velocity, a potential flow model for two superposed line sinks was used. To validate this model, experiments using adjacent stationary line fires with varying separation distances were performed. To visualize the velocity field around the flames, the surrounding area was seeded with passive tracer smoke, and its behavior was captured using high definition video. The motion of the tracer smoke was analyzed using cross-correlation

optical flow analysis, and flame height and angle were determined from the video captures. In general, the inflow velocities and flame angle compared favorably with the values predicted by the model, indicating that momentum imbalance is the cause of flame tilt during fire interactions. Similarities between interacting and windblown flames were discussed, and an analogy between the two cases was proposed.

In Section 5, heat transfer effects in spreading, converging fires were discussed. To determine the effect of flame convergence on the intervening fuel bed, an existing radiation-based fire spread model was modified to account for the addition of a neighboring flame and flame tilting, which occurs during merging. Since it is no longer believed that radiation is the primary mechanism for fire propagation, a simple convection-based model is proposed to explain the augmented rate of spread observed during fire merging.

At the end of Section 5, field observations from prescribed fires at Fort Jackson (Columbia, SC) are discussed in the context of flame tilting and heat transfer. Visible and infrared imagery were used to observe the behavior of flames and the temperature of intervening fuels during the merging of both line and spot fires.

6.3   The need for future study

In terms of being able to predict the overall behavior of both pulsating and merging fires, more work is needed. As highlighted in the discussion of field observations, it is quite difficult to parse out the effects of flame merging when wind, environmental conditions, and fuels are constantly changing. This is especially true for flame tilting, since it causes flames to appear similar to a single windblown flame. The experiments described in Section 4 were performed under controlled conditions with stationary flames. As two spreading flame fronts merge, their behavior rapidly changes, and measuring fire behavior versus separation distance becomes

extraordinarily difficult. One suggestion for future study is to explore the analogy between interacting and windblown flames in more detail. The wind tunnel could be a valuable tool for these experiments, though small wind tunnels could restrict the surrounding airflow, which could be problematic for studying merging fires.

The heat transfer model proposed in Section 5 needs validation, but several difficulties were encountered in attempting experiments to accomplish this. The requirement of measuring fuel temperature is challenging with vegetative fuels. Measuring the temperature of a single fuel element could be useful if its exact position relative to the flame front were known at all times, but this is generally not possible. In addition, most radiant heat transfer models assume the flame to be a quasi-stable radiating surface, which is a poor assumption. The rapid fluctuations in flame geometry cause rapid changes in its radiant emission, and so it is unrealistic to assume these properties remain constant. Clearly, more analysis is needed before realistic working models can be produced.

Pulsation and heat transfer may both have important consequences for both the behavior of merging fires, and even for the propagation of single flames. As mentioned throughout this dissertation, the fundamental mechanism for fire spread in vegetative fuels is still not completely understood. The assumption that radiant heat transfer controls fire spread appears to be incorrect; convection may be of equal or even greater importance. Recent published studies have identified high frequency convective phenomena that appear to directly influence flame spread. Video of carefully controlled experiments in engineered fuel beds appears to show the development of thermal instabilities behind the flames. These instabilities appear to propagate through the flame front, and may contribute to the convective activity ahead of the flame which appears to ignite nearby fuel elements. Future studies focusing on the origin of these instabilities could provide

insight into the spreading fire problem, and may show similarities to the pulsating behavior observed in stationary flames.

REFERENCES

Adam, B.A., Akafuah, N.K., Finney, M.A., Forthofer, J., and Saito, K. (2013), A study of flame spread in engineered cardboard fuelbeds part II: Scaling law approach, presented at the Seventh International Symposium on Scale Modeling (Hirosaki, Japan).

Adrian, R. J. (1991). Particle-imaging techniques for experimental fluid mechanics. Annual review of fluid mechanics, 23(1), 261-304.

Albini, F. A. (1967). A physical model for firespread in brush. In Symposium (International) on Combustion (Vol. 11, No. 1, pp. 553-560). Elsevier.

Albini, F.A. (1981). A model for the wind-blown flame from a line fire. Combustion and Flame 43, 155-174.

Albini, F. A. (1983). Potential spotting distance from wind-driven surface fires. US Department of Agriculture, Forest Service, Intermountain Forest and Range Experiment Station Research Paper INT-309 (Ogden, UT).

Albini, F.A. (1983). Transport of firebrands by line thermals. Combustion Science and Technology 32, 277-288.

Albini, F. A. (1985). A Model for Fire Spread in Wildland Fuels by-Radiation. Combustion Science and Technology, 42(5-6), 229-258.

Albini, F. A., & Rand, S. (1964). Statistical Considerations on the Spread of Fire. Institute for Defense Analyses (Washington, DC).

Alexander, M.E. & Cruz, M.G. (2012). Interdependencies between flame length and fireline intensity in predicting crown fire initiation and crown scorch height. International Journal of Wildland Fire 21(2), 95-113.

Anderson, H.E. (1982). Aids to determining fuel models for estimating fire behavior, USDA Forest Service Intermountain Forest and Range Experiment Station General Technical Report INT-122, Ogden, UT.

Anderson, D. H., Catchpole, E. A., De Mestre, N. J., & Parkes, T. (1982). Modelling the spread of grass fires. Journal of the Australian Mathematical Society, 23, 451-466.

Andrews, P.L. (2007). BehavePlus fire modeling system: Past, present, and future. Proceedings of 7th Symposium on Fire and Forest Meteorology; 23-25 October 2007, Bar Harbor, Maine. Boston, MA: American Meteorological Society. 13 p.

Astrup, P. (1972). Some physiological and pathological effects of moderate carbon monoxide exposure. British Medical Journal, 4(5838), 447.

Audouin L., Kolb G., Torero J.L., Most J.M. (1995). Average centreline temperatures of a buoyant pool fire obtained by image processing of video recordings. Fire Safety Journal 24(2), 167-187.

Badger, S.G. (2012). Catastrophic multiple-death fires in 2011, National Fire Protection Association No. MDS10.

Baines, P. G. (1990). Physical mechanisms for the propagation of surface fires. Mathematical and Computer Modelling, 13(12), 83-94.

Baker, W. L. (2006). Fire and restoration of sagebrush ecosystems. Wildlife Society Bulletin, 34(1), 177-185.

Baldwin, R., Thomas, P.H., Wraight, H.G.G. (1964). The merging of flames from separate fuel beds. *Fire Research Note* 551. Boreham Wood Fire Research Station. (Boreham Wood, Hertfordshire)

Batchelor, G. K. (1954). Heat convection and buoyancy effects in fluids. Quarterly Journal of the Royal Meteorological Society 80.345 339-358.

Bergé, P., and Dubois, M. (1984). Rayleigh-bénard convection. Contemporary Physics, 25(6), 535-582.

Bergman, T. L., Incropera, F. P., Lavine, A. S., & DeWitt, D. P. (2011). Fundamentals of heat and mass transfer. John Wiley & Sons.

Bouhafid, A., Vantelon, J. P., Joulain, P., and Fernandez-Pello, A. C. (1989). On the flame structure at the base of a pool fire. In Symposium (International) on Combustion (Vol. 22, No. 1, pp. 1291-1298). Elsevier.

Bray, K. N. C. (1996). The challenge of turbulent combustion. In Symposium (International) on Combustion (Vol. 26, No. 1, pp. 1-26). Elsevier.

Briggs, G.A. (1975). Plume rise from multiple sources. National Oceanic and Atmospheric Administration, Atmospheric Turbulence and Diffusion Lab No. ATDL-75/17. (Oak Ridge, TN).

Brown, A. A., & Davis, K. P. (1973). Forest fire: control and use. New York: McGraw-Hill.

Brown, J.K., Reinhardt, E.D., Kramer, K.A. (2003). Coarse woody debris: managing benefits and fire hazard in the recovering forest. USDA For. Serv. Gen. Tech. Rep. RMRS-GTR-105.

Buckmaster, J., & Peters, N. (1988). The infinite candle and its stability—a paradigm for flickering diffusion flames. In Symposium (International) on Combustion (Vol. 21, No. 1, pp. 1829-1836). Elsevier.

Budget of the United States Government, Fiscal Year 2009, United States Office of Management and Budget. http://www.whitehouse.gov/omb/budget/fy2009. Accessed April 28th, 2013.

Byram, G.M. (1959). Forest fire behavior. In: K.P. Davis (editor), Forest Fire: Control and Use, McGraw-Hill, New York, 584 pages.

Byram, G.M., Clements, H.B., Bishop, M.E., and Nelson Jr., R.M. (1966). Final report - Project Fire Model: an exploratory study of model fires. USDA Forest Service, Southeastern Forest Experiment Station, Office of Civil Defense Contract OCD-PS-65-40. (Asheville, NC).

Byram, G.M. and Nelson, R.M. (1969). "The Modeling of Pulsating Fires", Fall Meeting of the Western States Section of the Combustion Institute, La Jolla, CA.

Byrne, P.J., and Just, T.E., (1982). Exotic pine plantation prescribed burning using a helicopter, Department of Forestry, Queensland, Technical Paper No. 28 (Queensland, Australia)

Cetegen, B. M., Zukoski, E. E., & Kubota, T. (1984). Entrainment in the near and far field of fire plumes. Combustion Science and Technology, 39(1-6), 305-331.

Cetegen, B.M. and Ahmed, T.A. (1993). Experiments on the periodic instability of buoyant plumes and pool fires. Combust. Flame 93:157–84.

Chamberlin, D. S., & Rose, A. (1948). The flicker of luminous flames. In Proceedings of the symposium on combustion (Vol. 1, pp. 27-32). Elsevier.

Cheung, S. C., & Yeoh, G. H. (2009). A fully-coupled simulation of vortical structures in a large-scale buoyant pool fire. International Journal of Thermal Sciences, 48(12), 2187-2202.

Clark, T. L., Radke, L., Coen, J., & Middleton, D. (1999). Analysis of small-scale convective dynamics in a crown fire using infrared video camera imagery. Journal of Applied Meteorology, 38(10), 1401-1420.

Cohen, J. D., & Finney, M. A. (2010). An examination of fuel particle heating during fire spread. In VI International Conference on Forest Fire Research (pp. 15-17).

Corlett, R.C. (1974). "Velocity distribution in fires", Heat Transfer in Fires, edited by P.L. Blackshear, John Wiley and Sons, New York, pp. 239–255.

Countryman, C.M. (1964). Mass fires and fire behavior, USDA Forest Service, Pacific Southwest Forest and Range Experiment Station, Research Paper RP-PSW-019. (Berkeley, CA).

Cox, G. (1999). Fire research in the 21st century. Fire safety journal, 32(3), 203-219.

Crone, T.J., McDuff, R.E., Wilcock, W.S. (2008). Optical plume velocimetry: a new flow measurement technique for use in seafloor hydrothermal systems. *Experiments in Fluids* 45(5), 899-915.

Davis, R. W., Moore, E. F., Roquemore, W. M., Chen, L. D., Vilimpoc, V., and Goss, L. P. (1991). Preliminary results of a numerical-experimental study of the dynamic structure of a buoyant jet diffusion flame. Combustion and Flame, 83(3), 263-270.

De Mestre, N. J., Catchpole, E. A., Anderson, D. H., & Rothermel, R. C. (1989). Uniform propagation of a planar fire front without wind. Combustion Science and Technology, 65(4-6), 231-244.

Drysdale, D. (2011). An introduction to fire dynamics. (John Wiley & Sons, West Sussex).

Dunn, A. E., González Cabán, A., & Solari, K. (2003). The Old, Grand Prix, and Padua wildfires: How much did these fires really cost? USDA Forest Service, Pacific Southwest Research Station. (Riverside, CA).

Eftim, S. E., Samet, J. M., Janes, H., McDermott, A., & Dominici, F. (2008). Fine particulate matter and mortality: a comparison of the six cities and American Cancer Society cohorts with a medicare cohort. Epidemiology, 19(2), 209-216.

Emanuel, K.A, (1994). Atmospheric Convection, Oxford University press, New York, pp 19:21.

Emmons, H. W. (1964). Fire in the forest. In Fire Research Abstracts and Reviews (Vol. 5, No. 3, pp. 163-178).

Engstrom, J. D., Butler, J. K., Smith, S. G., Baxter, L. L., Fletcher, T. H., & Weise, D. R. (2004). Ignition behavior of live California chaparral leaves. Combustion Science and Technology, 176(9), 1577-1591.

Evans, D. D., Walton, W. D., Baum, H. R., Notarianni, K. A., Lawson, J. R., Tang, H. C., Keydel, K.R., Rehm, R.G., Madrzykowski, D., Zile, R.H., Hoseki, H., and Tennyson, E. J. (1992). In-situ burning of oil spills: Mesoscale experiments. National Institute of Standards and Technology.

Fahy, R.F., LeBlanc, P.R., Molis, J.L. (2012). Firefighter fatalities in the United States – 2011, National Fire Protection Association – Fire Analysis and Research Division FFD10-02.

Fang, J. B., & Steward, F. R. (1969). Flame spread through randomly packed fuel particles. Combustion and Flame, 13(4), 392-398.

Fernandez-Pello, A. C., & Hirano, T. (1983). Controlling mechanisms of flame spread. Combustion Science and Technology, 32(1-4), 1-31.

Finney, M. A. (2004). FARSITE: Fire Area Simulator–model development and evaluation. USDA Forest Service, Rocky Mountain Research Station, Research Paper RMRS-RP-4. (Ogden, UT)

Finney, M. A., Cohen, J. D., Grenfell, I. C., & Yedinak, K. M. (2010). An examination of fire spread thresholds in discontinuous fuel beds. International Journal of Wildland Fire, 19(2), 163-170.

Finney, M. A., Cohen, J. D., McAllister, S. S., & Jolly, W. M. (2012). On the need for a theory of wildland fire spread. International Journal of Wildland Fire 22(1), 25-36

Finney, M.A., Forthofer, J., Grenfell, I.C., Adam, B.A., Akafuah, N.K., and Saito, K. (2013), A study of flame spread in engineered cardboard fuelbeds part I: correlation and observations, presented at the Seventh International Symposium on Scale Modeling (Hirosaki, Japan).

Fischer, S. J., Hardouin-Duparc, B., and Grosshandler, W. L. (1987). The structure and radiation of an ethanol pool fire. Combustion and flame, 70(3), 291-306.

Fons, W. L. (1946). Analysis of fire spread in light forest fuels. Journal of Agricultural Research, 72(3), 93-121.

Fonseca-Azevedo, K., & Herculano-Houzel, S. (2012). Metabolic constraint imposes tradeoff between body size and number of brain neurons in human evolution. Proceedings of the National Academy of Sciences, 109(45), 18571-18576.

Frandsen, W. H. (1971). Fire spread through porous fuels from the conservation of energy. Combustion and Flame, 16(1), 9-16.

Fukuda, Y., Kamikawa, D., Hasemi, Y., Kagiya, K. (2004). Flame characteristics of group fires. Fire Science and Technology 23(2), 164-169.

Gauthier, S., Leduc, A., & Bergeron, Y. (1996). Forest dynamics modelling under natural fire cycles: a tool to define natural mosaic diversity for forest management. Environmental Monitoring and Assessment, 39(1-3), 417-434.

Glitzenstein, J. S., Platt, W. J., & Streng, D. R. (1995). Effects of fire regime and habitat on tree dynamics in north Florida longleaf pine savannas. Ecological Monographs, 65(4), 441-476.

Green, L.R. (1977). Fuelbreaks and other fuel modification for wildland fire control. USDA Forest Service, Agricultural Handbook No. 499. (Washington, D.C.)

Green L.R. (1981). Burning by prescription in chaparral. USDA Forest Service, Pacific Southwest Forest and Range Experiment Station, General Technical Report GTR-PSW-051. (Berkeley, CA)

Hall, J.R. (2012). The total cost of fire in the United States. National Fire Protection Association No. USS13.

Hertzberg, M., (1973). The theory of free ambient fires: The convectively mixed combustion of fuel reservoirs, Combust. Flame 21, 195-209.

Hertzberg, M., Cashdollar, K., Litton, C., & Burgess, D. (1978). Diffusion flame in free convection. Rep. Invest.-United States Bureau of Mines, 8263.

Heskestad, G. (1998). Dynamics of the fire plume. Philosophical Transactions A, 356(1748), 2815.

Horn, B.K., Schunck, B.G. (1981). Determining optical flow. Artificial Intelligence 17(1), 185-203.

Howard, L.N. (1966). "Convection at high Rayleigh number", in Applied Mechanics, Proceeding of the 11th Congress of Applied Mechanics, edited by H. Gortler (Springer, Munich).

Incropera, F. P., DeWitt, D. P., Bergman, T. L., and Lavine, A. S. (2007). Intorduction to heat transfer. John Wiley and Sons, pp 528.

Johansen, R.W. (1984). Prescribed burning with spot fires in the Georgia Coastal Plain. Georgia Forest Research Paper 49, Georgia Forestry Commission. (Macon, GA). Available from URL http://www.srs.fs.usda.gov/pubs/ja/1984/ja_1984_johansen_001.pdf (accessed 5/1/2013).

Karagozian, A. R., & Marble, F. E. (1986). Study of a diffusion flame in a stretched vortex. Combustion Science and Technology, 45(1-2), 65-84.

Karter, M.J. (2012). Fire loss in the United States during 2011. National Fire Protection Association No. FLX10.

Kaye, N.B. & Linden, P.F. (2004). Coalescing axisymmetric turbulent plumes. Journal of Fluid Mechanics 502, 41-63.

Khanna, V., Goel, R., & Ellzey, J. L. (1994). Measurements of emissions and radiation for methane combustion within a porous medium burner. Combustion science and technology, 99(1-3), 133-142.

Knapp, E. E., Keeley, J. E., Ballenger, E. A., & Brennan, T. J. (2005). Fuel reduction and coarse woody debris dynamics with early season and late season prescribed fire in a Sierra Nevada mixed conifer forest. Forest Ecology and Management, 208(1), 383-397.

Koschmieder, E. L. (1993). Bénard cells and Taylor vortices. Cambridge University Press.

Koseki, H., and Hayasaka, H. (1989). Estimation of thermal balance in heptane pool fire. Journal of fire sciences, 7(4), 237-250.

Kuo, K. K. Y., and Acharya, R. (2012). Fundamentals of Turbulent and Multi-Phase Combustion. Wiley.

Kuznetsov, A. V. (2011). Nanofluid bio-thermal convection: simultaneous effects of gyrotactic and oxytactic micro-organisms. Fluid Dynamics Research, 43(5), 055505.

Langmann, B., Duncan, B., Textor, C., Trentmann, J., & van der Werf, G. R. (2009). Vegetation fire emissions and their impact on air pollution and climate. Atmospheric environment, 43(1), 107-116.

Lee S.L. & Emmons, H.W. (1961). A study of natural convection above a line fire. Journal of Fluid Mechanics 11, 353-368.

List, E. J. (1982). Turbulent jets and plumes. Annual Review of Fluid Mechanics, 14(1), 189-212.

Liu, N., Liu, Q. Lozano, J.S., Shu, L., Zhang, L., Zhu, J., Deng, Z., Satoh, K. (2009). Global burning rate of square fire arrays: Experimental correlation and interpretation, Proceedings of the Combustion Institute, Volume 32, Issue 2, Pages 2519-2526.

Lozano, J., Tachajapong, W., Pan, H., Swanson, A., Kelley, C., Princevac, M., Mahalingam, S. (2008). Experimental investigation of the velocity field in a controlled, wind-aided propagating

fire using particle image velocimetry, Proceedings of the Ninth International Symposium on Fire Safety Science 255-256.

Lozano, J., Tachajapong, W., Weise, D.R., Mahalingam, S., Princevac, M. (2010). Fluid dynamic structures in a fire environment observed in laboratory-scale experiments. Combustion Science and Technology 182(7), 858-878.

Luo, K.H. (2004). "Instabilities, entrainment, and mixing in reacting plumes", European Journal of Fluid Mechanics B/Fluids 23, 443-460.

Macdonald R.W., Strom R.K., Slawson, P.R. (2002). Water flume study of the enhancement of buoyant rise in pairs of merging plumes. Atmospheric Environment, 36(29), 4603-4615.

Malalasekera, W.M.G., Versteeg, H.K., and Gilchrist, K. (1996). A review of research and experimental study on the pulsation of buoyant diffusion flames and pool fires, Fire and Materials 20, 261–271.

Martin, R.E., Dell, J.D. (1978). Planning for prescribed burning in the inland northwest. USDA Forest Service, Pacific Northwest Forest and Range Experiment Station, General Technical Report GTR-PNW-076. (Portland, OR).

Martínez-de Dios, J. R., André, J. C., Gonçalves, J. C., Arrue, B. C., Ollero, A., & Viegas, D. X. (2006). Laboratory fire spread analysis using visual and infrared images. International Journal of Wildland Fire, 15(2), 179-186.

Masters, R. A., Rasmussen, G. A., & McPherson, G. R. (1986). Prescribed burning with a helitorch on the Texas rolling plains. Rangelands, 173-176.

Maynard T., Princevac M., (2012). The application of a simple free convection model to the pool fire pulsation problem. Combustion Science and Technology 184(4), 505-516.

McAllister, S.M., Chen, J. Y., and Fernandez-Pello, A. C. (2011). Fundamentals of Combustion Processes. Springer.

McCaffrey, B.J., (1979). Purely buoyant diffusion flames: some experimental results. National Institute for Standards and Technology Report NSBIR 79-1910. (Washington, DC)

McCaffrey, B. J. (1983). Momentum implications for buoyant diffusion flames. Combustion and Flame, 52, 149-167.

McGrattan, K. B., Baum, H. R., Rehm, R. G., Hamins, A., Forney, G. P., Floyd, J. E., & Hostikka, S. (2000). Fire dynamics simulator: technical reference guide. US Department of Commerce, Technology Administration, National Institute of Standards and Technology.

McMurtry, P. A., Riley, J. J., & Metcalfe, R. W. (1989). Effects of heat release on the large-scale structure in turbulent mixing layers. Journal of Fluid Mechanics, 199, 297-332.

Meyer, R.E. (1982). Introduction to mathematical fluid dynamics. (Dover Publications, Toronto).

Morandini, F., Silvani, X., & Susset, A. (2012). Feasibility of particle image velocimetry in vegetative fire spread experiments. Experiments in fluids, 53(1), 237-244.

Morgan, W. J. (1972). Deep mantle convection plumes and plate motions. AAPG Bulletin, 56(2), 203-213.

Morton, B. R., Taylor, G. I. and Turner, J. S. (1956). "Turbulent gravitational convection from maintained and instantaneous sources". Proc. R. Soc. Lond. A 234, 1-23.

Morvan, D., Hoffman, C., Rego, F., Mell., W. (2011). Numerical simulation of the interaction between two fire fronts in grassland and shrubland, Fire Safety Journal 46(8), 469-479.

National Wildfire Coordinating Group (1996). Wildland fire suppression tactics reference guide (NWCG publication PMS 465) (Boise, ID).

Nelson Jr. R.M. (1993). Byram's derivation of the energy criterion for forest and wildland fires. International Journal of Wildland Fire 3(3), 131-138.

Nelson Jr., R.M. (2003). Power of the fire—a thermodynamic analysis. International Journal of Wildland Fire 12(1), 51-65.

Nelson Jr., R.M., Adkins, C.W. (1986). Flame characteristics of wind-driven surface fires. Canadian Journal of Forest Research 16(6), 1293-1300.

Nelson Jr., R.M., Butler, B.W., Weise, D.R. (2012). Entrainment regimes and flame characteristics of wildland fires. International Journal of Wildland Fire 21(2), 127-140.

O'Shea, P., Hussain, Z. M., & Sadik, A. Z. (2011). Digital signal processing: an introduction with MATLAB and applications. Springerverlag Berlin Heidelberg.

Orloff, L., De Ris, J., & Markstein, G. H. (1975). Upward turbulent fire spread and burning of fuel surface. In Symposium (International) on Combustion (Vol. 15, No. 1, pp. 183-192). Elsevier.

Pagni, P. J., & Peterson, T. G. (1973). Flame spread through porous fuels. In Symposium (International) on Combustion (Vol. 14, No. 1, pp. 1099-1107). Elsevier.

Paraschivoiu I. (2003). Subsonic aerodynamics. (Presses internationals Polytechnique, Montréal).

Pera, L., Gebhart, B. (1975). Laminar plume interactions. Journal of Fluid Mechanics 68, 259-271.

Pitsch, H. (2006). Large-eddy simulation of turbulent combustion. Annu. Rev. Fluid Mech., 38, 453-482.

Princevac, M., Fernando H.J.S, (2007). A criterion for the generation of turbulent anabatic flows, Physics of Fluids 19: 105102.

Puett, R. C., Hart, J. E., Yanosky, J. D., Paciorek, C., Schwartz, J., Suh, H., & Laden, F. (2009). Chronic fine and coarse particulate exposure, mortality, and coronary heart disease in the Nurses' Health Study. Environmental Health Perspectives, 117(11), 1702.

Pyne, S. J., Andrews, P. L., & Laven, R. D. (1996). Introduction to wildland fire. John Wiley and Sons.

Qui, X.L. and Tong, P., (2001). Onset of coherent oscillations in turbulent Rayleigh-Bénard convection, Physical Review Letters, 87.

Quintiere, J. G. (1989). Scaling applications in fire research. Fire Safety Journal, 15(1), 3-29.

Quintiere, J. G. (2006). Fundamentals of fire phenomena, John Wiley and Sons, West Sussex, England.

Quintiere, J. G. & Grove, B. S. (1998). A unified analysis for fire plumes. In Symposium (International) on Combustion (Vol. 27, No. 2, pp. 2757-2766). Elsevier.

Rehm, R.G., and Baum, H.R. (1978). The equations of motion for thermally driven, buoyant flows, Journal of Research of the National Bureau of Standards, Vol. 83, No. 3, 297-308.

Rehm, R. G., & Mell, W. R. (2009). A simple model for wind effects of burning structures and topography on wildland–urban interface surface-fire propagation. International Journal of Wildland Fire, 18(3), 290-301.

Ricou, F. P., & Spalding, D. B. (1961). Measurements of entrainment by axisymmetrical turbulent jets. J. Fluid Mech, 11(1), 21-31.

Rothermel, R. C. (1972). A mathematical model for predicting fire spread in wildland fuels. USDA Forest Service Intermountain Forest & Range Experiment Station Research Paper INT-115 (Ogden, UT).

Rothermel, R. C. (1983). How to predict the spread and intensity of forest and range fires Ogden, UT, USA: US Department of Agriculture, Forest Service, Intermountain Forest and Range Experiment Station.

Rothermel, R. C., (1984). Fire behavior considerations of aerial ignition. In Proceedings of a Workshop on Prescribed Fire by Aerial Ignition. Intermountain Fire Council, Missoula, Mont, USA.

Rothermel, R.C., (1991) Predicting behavior and size of crown fires in the Northern Rocky Mountains. USDA Forest Service, Intermountain Research Station Research Paper INT-438. (Ogden, UT).

Rouse, H., Yih, C. S., & Humphreys, H. W. (1952). Gravitational convection from a boundary source. Tellus, 4(3), 201-210.

Rouse H., Baines W.D., Humphreys H.W. (1953). Free convection over parallel sources of heat, Proceedings of the Physical Society, Section B 66, 393.

Schneider, M. E., & Kent, L. A. (1989). Measurements of gas velocities and temperatures in a large open pool fire. Fire Technology, 25(1), 51-80.

Sibulkin, M., & Hansen, A. G. (1975). Experimental study of flame spreading over a horizontal fuel surface. Combustion Science and Technology, 10(1-2), 85-92.

Sirignano, W. A., & Glassman, I. (1970). Flame spreading above liquid fuels: Surface-tension-driven flows. Combustion Science and Technology, 1(4), 307-312.

Smith R.K., Morton B.R., Leslie L.M., (1975). The role of dynamic pressure in generating fire wind. *Journal of Fluid Mechanics* 68(1), 1-19.

Sparrow, E.M., Husar, R.B., Goldstein, R.J. (1970). Observation and other characteristics of thermal, Journal of Fluid Mechanics 41, 793.

Stockstad, D. S. (1975). Spontaneous and piloted ignition of pine needles. USDA Forest Service Intermountain Forest and Range Experiment Station, Research Paper INT-194 (Ogden, UT).

Sugawa, O., & Takahashi, W. (1993). Flame height behavior from multi-fire sources. Fire and materials, 17(3), 111-117.

Sun, L., Zhou, X., Mahalingam, S., and Weise, D. R. (2005). Experimental investigation of the velocity field in buoyant diffusion flames using PIV and TPIV algorithm. Proc Int Assoc Fire Saf Sci, 8, 939-950.

Taylor, Z.J., Gurka, R., Kopp, G.A., Liberzon, A., (2010). Long-duration time-resolved PIV to study unsteady aerodynamics. IEEE Transactions on Instrumentation and Measurement 59(12), 3262-3269.

Tennekes, H., and Lumley, J.L. (1972). A first course in turbulence, MIT press, Cambridge.

Thomas, P.H., (1961). The size of flames from natural fires, Proceedings of the Ninth Symposium (International) on Combustion, 844-859, The Combustion Institute.

Thomas, P.H. (1963). The size of flames from natural fires. In Symposium (International) on Combustion (Vol. 9, No. 1, pp. 844-859). Elsevier.

Thomas, P. H., Baldwin, R., Heselden, A. J. M. (1965). Buoyant diffusion flames: some measurements of air entrainment, heat transfer, and flame merging. In Symposium (International) on Combustion (Vol. 10, No. 1, pp. 983-996). Elsevier.

Tieszen, S. R. (2001). On the fluid mechanics of fires, Annual review of fluid mechanics, 33(1), 67-92.

Tieszen, S. R., O'hern, T. J., Schefer, R. W., Weckman, E. J., & Blanchat, T. K. (2002). Experimental study of the flow field in and around a one meter diameter methane fire. Combustion and flame, 129(4), 378-391.

Turner, J. S. (1969). Buoyant plumes and thermals. Annual Review of Fluid Mechanics, 1(1), 29-44.

United States Army, Ft. Jackson Department of Environmental and Natural Resources Division (2007). Forest management. Retrieved from: http://www.jackson.army.mil/enrd/fo/Forest%20mgmt.htm

Van Wagner, C. E. (1967). Calculations on forest fire spreadby flame radiation, Department of Forestry and Rural Development , Petawawa Forest Experiment Station Rep. No. 1185, (Chalk River, ON).

Vogel, M., & Williams, F. A. (1970). Flame propagation along matchstick arrays. Combustion Science and Technology, 1(6), 429-436.

Wade D.D., Lunsford J.D., Dixon M.J., Mobley H.E., (1989). A guide for prescribed fire in southern forests. USDA Forest Service, Southern Region, Technical Publication R8-TP-11. (Atlanta, GA).

Weber, R. O. (1991). Modelling fire spread through fuel beds. Progress in Energy and Combustion Science, 17(1), 67-82.

Weckman, E. J., & Strong, A. B. (1996). Experimental investigation of the turbulence structure of medium-scale methanol pool fires. Combustion and Flame, 105(3), 245-266.

Weckman, E.J., and Sobesiak, A, (1988). The oscillatory behavior of medium scale pool fires", Proceedings of the 22nd International Symposium on Combustion, Pg 1299, The Combustion Institute.

Welker, J.R. & Sliepcevich, C.M. (1966). Bending of wind-blown flames from liquid pools. Fire Technology 2(2), 127-135.

Weihs, S.D. & Small, R.D. (1986). Interactions and spreading of adjacent large area fires, Pacific-Sierra Research Technical Report DNA-TR-86-214. (Los Angeles, CA).

Weise, D. R., and Biging, G. S. (1996). Effects of wind velocity and slope on flame properties. Canadian Journal of Forest Research, 26(10), 1849-1858.

Williams, F. A. (1969). Fire Res. Abstracts and Rev, 11, 1-22.

Wu, Y, Wu, S, Lu, S, Zhang, J, Cen, K. (2011). Novel methods for flame pulsation frequency measurement, Fire Technology 15-2684, 1-15.

Yedinak, K. M., Cohen, J. D., Forthofer, J. M., Finney, M. A. (2010). An examination of flame shape related to convection heat transfer in deep-fuel beds. International Journal of Wildland Fire, 19(2), 171-178.

Yih, C.S. (1952). Free convection due to a point source of heat. Proc. Isl U.S. Natl. Congr. Appl. Mech. pp. 941-947.

Yuan, T., Durox, D., Villermaux, E. (1994). An analouge study for flame flickering, Experiments in Fluids 17, 337-449.

Yuan L.M., Cox G., (1996). An experimental study of some line fires. Fire Safety Journal 27(2), 123-139.

Zhou, X. C., and Gore, J. P. (1995). Air entrainment flow field induced by a pool fire. Combustion and flame, 100(1), 52-60.

Zhou, X., Sun, L., Mahalingam, S., Weise, D. R. (2003). Thermal particle image velocity estimation of fire plume flow. Combustion Science and Technology, 175(7), 1293-1316.

Zhou X., Mahalingam S., Weise, D.R. (2005). Modeling of marginal burning state of fire spread in live chaparral shrub fuel bed, Combustion and Flame 143 (3): 183-198.

Zukoski, E. E., Kubota, T., Cetegen, B. (1981). Entrainment in fire plumes. Fire Safety Journal, 3(3), 107-121.

Zukowski, E.E. (1995). Properties of fire plumes, in Combustion Fundamentals of Fire (ed. G. Cox), Academic Press, London, 1995.

APPENDIX A: LABORATORY STUDY OF PARTICULATE EMISSIONS FACTORS OF PRESCRIBED WILDLAND FIRES [2]

1. Introduction

The practice of prescribed burning in wildland areas is a useful means for managing wildlife ecosystems and reducing the potential of severe wildfire [1]. However, the impact of prescribed fire emissions on surrounding communities is often problematic, as the release of biomass combustion products can have severe effects on local and regional air quality. Of particular concern is the dispersion of particulate matter of less than 2.5 μm in size (PM2.5), as it has been identified as a significant risk to public health [2].

A practical metric for determining the amount of pollutant released during a prescribed burn is the emission factor (EF), which is a measure of particulate production in relation to the amount and type of fuel burned. Emission factors are key components of pollution dispersion models, and serve as useful reference points for land and air pollution managers. EFs for some regional fuels, such as those found in Africa, have been well studied [3]. However, little recent data exist for fuels common to the southwestern United States, specifically those contained in chaparral. Emission factors have been published for chaparral [4], but they are not species-specific and were derived using older instrumentation. The objective of the research presented is to obtain EFs for specific chaparral species mixes, including chamise (Adenostoma fasciculatum), ceanothus (Ceanothus spp), manzanita (Arctostaphylos spp.), and California sagebrush (Artemisia californica) using state of the art techniques. Laboratory scale experiments using simulated brush loadings were used to obtain emissions data for each fuel type. Controlled laboratory conditions

---

provide the best possible means for obtaining emissions factors without influence from external factors. Variables in the field can include transient meteorological conditions, unpredictable fire behavior, and inhomogeneites in fuel density, composition, and moisture content. Some of these difficulties have been overcome through the use of mobile instrumentation platforms illustrated in [5], but steep terrain and plume buoyancy still presented significant challenges during the measurement period. In 2009-2010, field experiments to study the fuels presented here will employ similar methods.

2. Experimental Methods

2.1 Experimental Setup

Experiments were conducted in February 2009 in the Missoula Fire Sciences Laboratory, at the USFS Rocky Mountain Research Station in Missoula, MT. The combustion laboratory featured a fuel bed at the base of a 1.6 m diameter, 22 m high central exhaust stack. At the bottom of the stack, a 3.6 m diameter flue hood was attached directly above the fuel bed. A platform encircled the stack at an elevation of 17 m to allow for installation of sampling equipment. An environmental conditioning system introduced pressurized outdoor air to promote emissions entrainment through the stack. Mean flow velocity through the stack in the predominant flow direction was 1.5 m/s, as measured at platform height in the center of the duct, using a handheld anemometer. The Missoula FSL has been extensively used in previous wildland fuels emissions research, highlighted [3] and [7].

2.2 Sampling Equipment

Measurements of PM2.5 were obtained using DustTrak laser photometers (Model 8520, TSI, Inc.). Sampler flowrate was 1.7 L/min and particles were filtered through a PM2.5 size-

restrictive inlet. Instrument output was particulate concentration (mg m-3) with a measurement resolution of ±0.1%. Concentration logging interval was set to three seconds. Sampling equipment was placed on the upper platform, and Teflon tubing was used to connect the DustTraks to a measurement probe placed within the exhaust stack. Additionally, a separate DustTrak was placed within the combustion laboratory, away from the fire, to determine if a significant background particulate concentration could be detected. Flow through the stack was assumed to be well-mixed. A suite of chemical and particle characterization equipment accompanied the particle capture instruments. A summary of instrumentation is shown in Table 1. The additional instrumentation was used to obtain emissions factors using additional methods which will be published in the future.

Table 1. Summary of instrumentation

Instrument (Abbreviation)	Type of Measurement
Gases	
5 Gas Analyzer (5GA)	CO, SO_2, CO_2, O_2, NOx
Open-path FTIR (OP-FTIR)	CO_2, CO, CH_4, multiple species
Proton Transfer Reaction MS (PTRMS)	Aerosol composition
Canisters	Multiple species
TDS, DNPH, PUF/XAD	Selected species
Particulate	
Aerosol Mass Spectrometer (AMS)	Aerosol composition
Aerodynamic Particle Sizer (APS)	Particle size distribution
Fast Mobility Particle Sizer (FMPS)	Particle size distribution
Scanning Mobility Particle Sizer (SMPS)	Particle size distribution,

	composition
Micro Orifice Uniform Deposit Impactor (MOUDI)	Aerosol composition/size
Condensation Particle Counter (CPC)	Particle concentration
Dekati Mass Monitor (DMM)	Particle concentration, distribution
Portable Diffusion Charger (DC2000CE)	Particle surface area
Dustrak (DT)	Particle concentration
Proton Transfer Reaction MS (PTRMS)	Aerosol composition
Filter sampler (FS)	$PM_{2.5}$ mass
Filter sampler (FS)	Elemental/organic carbon mass

2.3. Fuel Bed Construction

The fuel bed was placed beneath the exhaust stack, consisting of a 2 m x 1 m metal table covered with thermal insulation. Electronic load cells supported the fuel bed to provide real-time fuel mass loss data. Fuels were arranged in an attempt to simulate their natural arrangement in the field and mass per unit area. Fuels were ignited using a butane torch and were allowed to burn to completion. Unfortunately, the natural sparse vertical arrangement of fuels were difficult to ignite, so fuels were piled in a predominantly horizontal arrangement which improved ignition success. The mass per unit volume likely differed from field conditions. This will be verified in conjunction with planned field measurements in November, 2009. The fuel bed arrangement is shown in Fig 1. Nine fuel types were tested (Table 2).
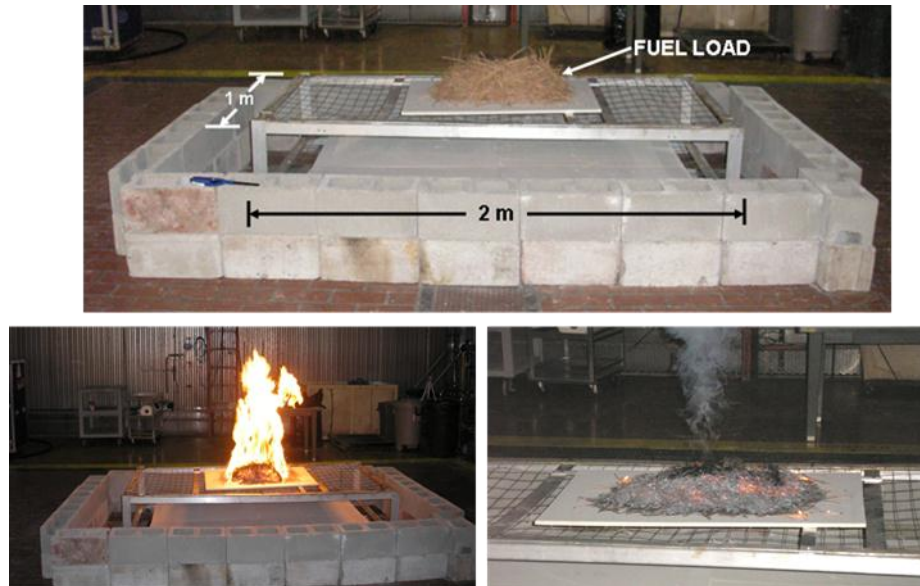
Fig 1. (a) Fuel bed prior to ignition; (b) Open flaming period; (c) Smoldering period. Note the significant

amount of residual ash.

Table 2. Composition of fuel types tested

Fuel type	Species
Chamise	Adenostoma fasciculatum, Quercus berberidifolia
Ceanothus	Ceanothus leucodermis
Maritime chaparral	Ceanothus impressus var. impressus, C. cuneatus var. fascicularis, Salvia mellifera
Coastal sage scrub	Salvia mellifera, Ericameria ericoides, Artemisia californica
California sagebrush	Artemisia californica, Ericameria ericoides
Manzanita	Arctostaphylos rudis, Arctostaphylos purissima
Oak savanna	Quercus emoryi, Eragrostis lehmanniana
Oak woodland	Quercus emoryi, Arctostaphylos pungens
Masticated mesquite	Prosopis velutina, Baccharis sarothroides

3. Calculation of Emissions Factors

The classical definition of the emissions factor, as described in [4], is as follows:

$$EF_X = \frac{m_X}{m_{burned}} \tag{1}$$

where EF_X is the emission factor of compound X, m_{burned} is the mass of dry fuel consumed (kg), and m_X is the total mass of pollutant X emitted (g). For a well-mixed duct, a method of obtaining m_X is proposed in [8]

$$m_X = \int_{t_0}^{t} \Delta C_X Q_{duct} dt \tag{2}$$

where ΔC_X is the concentration of pollutant measured within the stack at platform height (mg/m^3), Q_{duct} is the volumetric flow rate through the exhaust duct (m^3/s), t_0 is time of ignition (s), and t is the time at conclusion of smoldering (s). For this experiment, Eq (2) was computed using a simple trapezoidal integration routine based on a 3 second measurement interval.

The mass of dry fuel consumed is a topic worthy of discussion. Upon burn conclusion, a significant amount of matter remained on the fuel bed. The remaining mass is a mix of unconsumed dry fuel, partially burned fuel, and ash. The mass of residual matter varied by fuel type, but reached as much as 90% of dry fuel mass in some cases. For this reason, two types of emissions factors are presented

$$EF_1 = \frac{m_X}{m_{dry}} \tag{3}$$

$$EF_2 = \frac{m_X}{m_{dry} - m_{remaining}} \tag{4}$$

where m_{dry} is the total dry fuel mass at ignition (kg), and $m_{remaining}$ is the mass of residual matter remaining on the fuel bed at the end of the smoldering period (kg). By definition, emissions factors are to be obtained using the actual mass of fuel burned over the entire combustion period (ignition, flaming, and smoldering). However, fuel consumption is rarely absolute, even in laboratory scale experiments. Previous experiments [8, 9] used an alternate method of obtaining emissions factors; carbon mass balance. This method does not require pre- and post-burn weighing of biomass, but the instrumentation required to measure the necessary chemical species is significantly more advanced than that used in the direct method. This method also assumes that all carbon content of the biomass consumed during the fire is released into the atmosphere as measurable carbon compounds, as accounted for by the carbon biomass balance presented in [8].

An alternate method of obtaining emission factors was employed during the experiment, as described in [12]. This method uses Teflon membrane filters to collect particulate matter, size-segregated to only collect PM2.5. The filters are connected to the exhaust stack via a steel sampling line. The mass of PM2.5 emitted is then calculated using Eq (5):

$$m_X = m_{filter} \times \frac{Q_{duct}}{Q_{line}} \tag{5}$$

where m_{filter} is the amount of mass on the filter as measured post-burn (kg), and Q_{line} is the volumetric flow rate through the filter sampling line (m^3/s). The emissions factor is then obtained using Eq (1). A similar method of particle collection was also used to measure particulate matter emission from burning of California chaparral in a laboratory setting, as highlighted in [13].

3.1 Fuel Moisture

Fuel samples from the living plants contained water used for metabolic processes and dead fuels contained water absorbed from the atmosphere. Moisture content for all fuels was estimated using a fuel moisture analyzer (Computrac Inc., model MAX-1000). During moisture analysis, fuel samples (40 g) are heated to 150°C and initial mass loss due to moisture evaporation is determined. From the initial fuel mass loss, continuous extrapolations are made based upon a standard drying curve (via microprocessor). Once the measured mass losses are in agreement with the extrapolated values (as estimated by an algorithm based on moisture content), fuel moisture content is reported as a percentage of total fuel mass. Dry fuel mass in (3) was then obtained using the expression

$$m_{dry} = \frac{m_{total}}{1 + M} \tag{6}$$

where m_{total} is the total mass of moist fuel (g), and M is the moisture content reported by the fuel moisture analyzer, expressed as a fraction of total fuel mass. This technique provides a quick estimate of fuel moisture content; the preferred method typically uses larger samples and longer drying time in a convection oven set at 95°C. Moisture content for selected fuels is reported in Table 3.

Table 3. Fuel moisture content for selected southwestern chaparral fuels

Fuel type	Moisture content[a]
Ceanothus	9.21±0.75
Manzanita	8.87±2.98
California Sagebrush	8.36±2.30
Coastal Sage Scrub	9.44±2.76
Emory Oak Savannah	15.42±3.28
Chamise	7.79±1.02

a.Data represented as mean percentage of dry fuel mass ± 95% confidence interval

4. Results and Discussion

Typical $PM_{2.5}$ concentration profiles are shown in Fig. 2 for several fuel types listed in this study. In general, peak particulate concentration occurred within the first 200 seconds of burning, then exhibited a steep decline. However, maritime chaparral (Fig 2c) achieved an initial peak and decline within the 200 second interval, but was then followed by an even greater peak concentration. Within fuel types, concentration profiles exhibited similar behavior, except in cases of poorly sustained combustion. The concentration profiles were compared with those obtained in [11] (Fig 2d). Although the study used a different fuel (bamboo skewers), the authors of [11] also used the direct method of obtaining EFs in a laboratory setting. While the $PM_{2.5}$ concentration profiles from both experiments showed an initial rise in particulate concentration during the first 200 seconds of burning, the bamboo skewer fuel maintained a consistent particulate concentration through the flaming period. However, this experiment took place inside

of a wind tunnel, inside which the fire had fresh, unburned fuel at the flame front throughout the
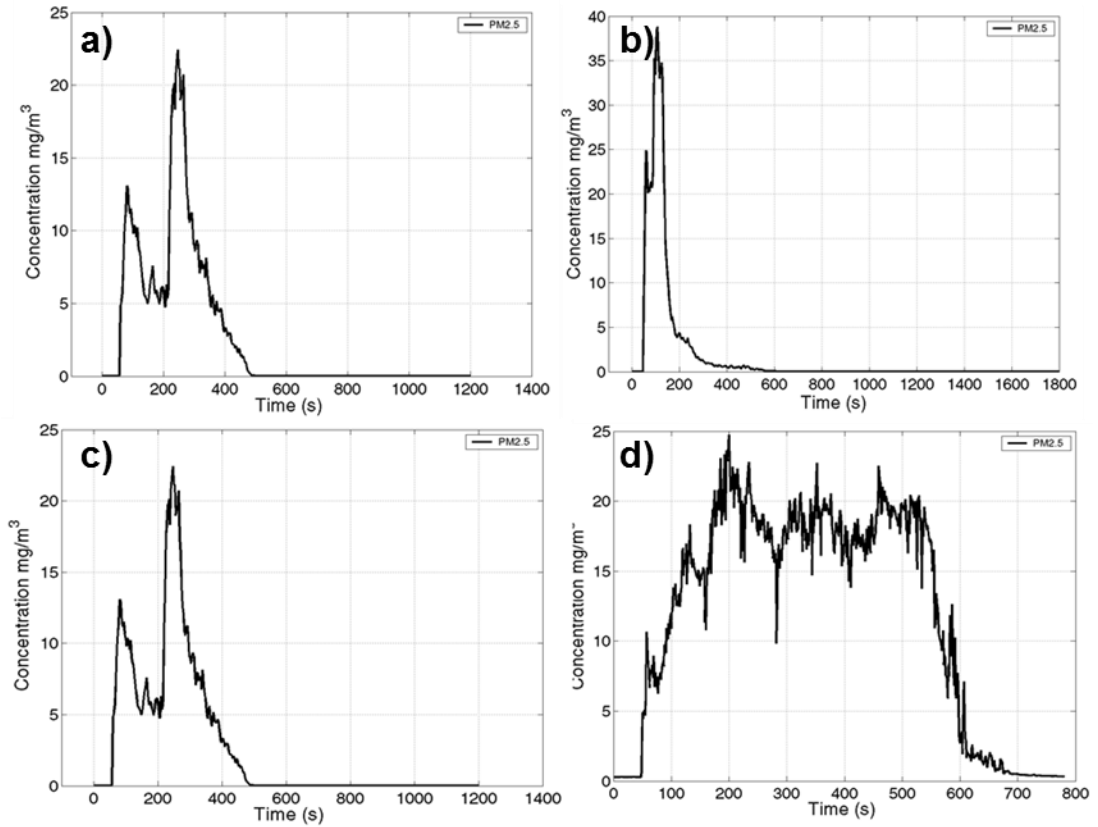
duration of the burn.

Fig 2. PM2.5 concentration profiles a) California sagebrush; b) Ceanothus; c) Maritime chaparral; d)

Bamboo skewers (high fuel loading) [11]

Table 4. PM2.5 Emissions Factors for selected southwestern chaparral fuels

Fuel type	$PM_{2.5}$ EF_1 (g kg^{-1})[a]	$P_{2.5}$ EF_2 (g kg^{-1}) [a]	$PM_{2.5}$ EF (g kg^{-1})[b] [12]	$PM_{2.5}$ EF (g kg^{-1})[c] [13]	$PM_{2.5}$ EF (g kg^{-1}) [6]
Ceanothus	1.85±0.37	2.54±1.20	5.29	67.65	N/A
Manzanita	1.04±0.19	1.13±0.23	2.29	87.37	N/A
California Sagebrush	3.60±0.25	3.89±0.30	4.49	N/A	N/A
Coastal Sage Scrub	2.71±0.50	2.87±0.54	3.11	47.27	N/A
Maritime Chaparral	2.56±0.60	2.71±0.66	0.58	N/A	8
Emory Oak Woodland	1.37±0.51	1.43±0.50	3.62	N/A	N/A
Emory Oak Savannah	0.67±0.17	0.75±0.19	1.63	N/A	N/A
Masticated Mesquite	1.18±0.10	1.26±0.11	1.54	N/A	N/A
Chamise	3.10±0.48	7.36±0.44	1.25	20.05	N/A

a.   Data represented as mean ± 95% confidence interval

b.   Data obtained from [12] using Teflon filter

c.   Data obtained from [13] using glass fiber filter

The mean emissions factor obtained for each fuel type is presented in Table 4. The EF for each fuel species cannot be compared directly to EPA AP-42, as data exists only for generalized chaparral and sagebrush for the Pacific southwest region. Moreover, the published values for chaparral were obtained using a field-based carbon mass balance method, as described in [8,9] The calculated emissions factors were compared to emissions factors obtained during the same experiment, using the Teflon filter methods described in [12] and the filter methods described in [13]. Both the values presented in this paper and in [12] were significantly lower than those obtained in [13]. However, some principle differences exist between the two experiments. The apparatus in [13] was of smaller scale (sampler height only 1.8 m above fuel bed), measurements only occurred only during flaming combustion, and fuel moisture content was higher (greater

than 50% of dry fuel mass for all fuels). Further analysis is required to address the discrepancy between the two experiments.

5. Summary and Conclusions

Experiments to determine $PM_{2.5}$ emissions factors for southwestern chaparral biomass fuels were carried out at the USFS Fire Sciences Laboratory in Missoula, MT. Particle concentration was measured using DustTrak laser photometers, and emissions factors were calculated using the direct method. Two separate emissions factors were obtained, using total dry fuel mass and net dry fuel mass consumed, respectively. The calculated emissions factors were compared to published values, as well as data obtained for identical fuels using filter methods. The amount of unconsumed fuel vs. ash needs to be quantified to provide a better understanding of emissions in relation to fuel consumption.

References

[1]   Biswell H, 1999. Prescribed burning in California wildlands vegetation management. University of California Press, Berkeley, CA..

[2]   Shusterman D, Kaplan JZ, Canabarro C, 1993. Immediate health effects of an urban. West J Med 158:133-138

[3]   Christian, T. J., B. Kleiss, R. J. Yokelson, R. Holzinger, P. J. Crutzen, W. M. Hao, H. Saharjo, and D. E. Ward, 2003, Comprehensive laboratory measurements of biomass-burning emissions: 1. Emissions from Indonesian, African, and other fuels, J. Geophys. Res., 108(D23): 4719

[4]   Hardy, C., Conard, S., Regelbrugge, J., Teesdale, D, 1996, Smoke Emissions From Prescribed Burning Of Southern California Chaparral, USDA Pacific Northwest Research Station, Research Paper PNW-RP-485

[5]   Miranda, A.I., Ferreira, J., Valente, J., Santos, P., Amorim, J.H, Borrego, C., 2005, Smoke measurements during Gestosa-2002 experimental field fires, International Journal of Wildland Fire, 14 : 107-116

[6]   U.S. EPA., Emission factors & AP 42. http://www.epa.gov/ttn/chief/ap42/

[7]   Chen, L.-W. A., H. Moosmuller, W. P. Arnott, J. C. Chow, J. G. Watson, R. A. Susott, R.E. Babbitt, C. E. Wold, E. N. Lincoln, and W. M. Hao, 2006, Particle emissions from laboratory combustion of wildland fuels: In situ optical and mass measurements, Geophys. Res. Lett., 33: L04803

[8]   Dhammapala, R., Claiborn, C., Corkill, J., and Gullett, B., 2006, Particulate emissions from wheat and Kentucky bluegrass stubble burning in eastern   Washington and northern Idaho, Atmospheric Environment, 40: 1007-1015

[9]   Delmas, R., Lacaux, J.P. and Brocard, D., 1995. Determination of biomass burning emission factors: Methods and results. Environmental Monitoring and Assessment. 38: 181-204

[10]   Ward, D.E and Hardy, C.C, 1989, "Emissions From Prescribed Burning Of Chaparral", Proceedings Of The 1989 Annual Meeting Of The Air And Waste Management Association, Anaheim, CA

[11]   Pan, H., Lozano, J., Tachajapong, W., Swanson, A., Kelley, C., Mahalingam, S., and Princevac, M., 2008, "Wind tunnel study of particulate emissions, fire spread and velocity field within the flame", 2008 Spring Meeting of the Western States Section of the Combustion Institute Los Angeles, CA

[12]   Hosseini, S., Li, Q., Miller, A., Cocker, D., Sharivastava, M., Weise, D., Hao, W., Yokelson, R., Jung, H, 2009, Chemical and Physical Characterization of Wood Smoke under Controlled Conditions. 2009 Fall Meeting of the Western States Section of the Combustion Institute, Irvine, CA

[13]   Weise, D., Ward, R., Paysen, T., and Koonce, A, 1991, Burning California Chaparral – An Exploratory Study of Some Common Shurbs and Their Combustion Characteristics, International Journal of Wildland Fire, 1 : 153-158

APPENDIX B: LABORATORY AND FIELD STUDY OF PARTICULATE EMISSIONS FACTORS OF PRESCRIBED WILDLAND FIRES[3]

1. Introduction

Prescribed fire, the deliberate burning of wildland areas, is an important tool for natural resource management. Prescribed burns allow the natural fire cycle to be emulated under controlled conditions, helping to preserve ecosystems and reducing wildfire risk by eliminating hazardous vegetation buildup. Unfortunately, prescribed fire is accompanied by undesirable side effects, principally the impact of smoke on local and regional air quality. To address this risk, many state and local governments require an air quality analysis to be performed prior to burning. Currently, the emissions inventories required to estimate the air quality impact of prescribed burns are limited, particularly for chaparral (shrub-type) fuels common to the southwestern United States. One of the primary emissions products of concern in wildland fire smoke is particulate matter of less than 2.5 μm in size ($PM_{2.5}$). $PM_{2.5}$ has been identified as a significant risk to public health (Shusterman et al., 1993). The emission factor (EF), a measure of pollutant production in relation to the amount and type of fuel burned, is the most commonly used quantity to estimate the impact of emissions-generating activities. In this paper, laboratory experiments to determine $PM_{2.5}$ emissions factors for specific species of chaparral fuels are described and compared with emissions factors obtained during a full-scale prescribed burn in southern California.

---

[3] Reprinted from T. Maynard, S. Hosseini, M. Princevac, H. Jung, D. Cocker, P.Tang, X. Tang, Q. Li, D.R. Weise, W.M. Hao, R. Yokelson, W. Miller, S.Mahalingam (2012), Laboratory and field study of particulate emissions factors of prescribed wildland fires, Presented at the 92nd American Meterological Society Annual Meeting (New Orleans, LA)

2. Experimental methods

2.1 Laboratory Experiments

Experiments were conducted in the Missoula Fire Sciences Laboratory, at the USFS Rocky Mountain Research Station in Missoula, MT. The laboratory has been widely used for biomass emissions studies (Christian et al., 2003; Chen et al., 2006) and is described in detail Maynard et al. (2010).

2.1.1 Sampling Equipment

Sampling equipment was placed on a platform 17 m above the fuel bed, surrounding the main exhaust stack (Figure 1). $PM_{2.5}$ emissions were measured using Teflon filters connected to the stack, as described by Hosseini et al. (2009). A size-selective $PM_{2.5}$ cyclone was installed upstream of the filters, and a new filter was installed prior to each burn. Additional instrumentation for the characterization of various gaseous and particulate species was also deployed using additional methods which are beyond the scope of this paper.

Fig. 1. a) Fire under laboratory flue, b) Looking up at instrumentation platform

165

2.1.2 Fuels and Fuel Bed

The chaparral fuels used were obtained from the California central coast, and are the most commonly occurring types in the region. Fuels were loaded to simulate their natural arrangement on a 2 m x 1 m fuel bed. Real-time mass loss was obtained using digital load cells. Fuels were ignited using a butane torch and were allowed to burn to completion.

Fig. 2. Selected chaparral fuels a) Chamise/Scrub oak, b) Ceanothus, c) Coastal Sage Scrub, d) Maritime chaparral

2.1.3 Calculation of Laboratory Emissions Factors

Christian et al. (2003) defined the emission factor as:

$$EF_X = \frac{m_X}{m_{burned}} \tag{1}$$

where EF_X is the emission factor of compound X, m_{burned} is the mass of dry fuel consumed (kg), and m_X is the total mass of pollutant X emitted (g). After each laboratory burn, the mass of $PM_{2.5}$

emitted was determined using the mass deposited on the filter multiplied by the relative amount of flow across the filter:

$$m_x = m_{filter} \times \frac{Q_{duct}}{Q_{line}}$$ (2)

where m_{filter} is the amount of mass deposited on the filter (g), and Q_{line} is the volumetric flow rate through the filter sampling line (m^3 s^{-1}). The emissions factor is then obtained using Eq. (1). Similar methods have been employed to measure particulate emissions of California chaparral in a laboratory setting, as demonstrated by Weise et al. (1991).

2.2 Field Experiments

Field measurements were performed during a prescribed burn at Vandenberg AFB in Lompoc, CA in November, 2009.

2.2.1 Site Description

The landscape surrounding the experiment site was characterized by rugged terrain with maritime chaparral and coastal sage as the dominant fuel types (Figure 3). The burn plot was approximately 150 acres with a moderate south-facing aspect.

Fig. 3. Representative terrain and fuels at Vandenberg AFB in Lompoc, CA (near Santa Barbara)

2.2.2 Instrumentation

A truck-based mobile laboratory was used for near-source emissions characterization, and was placed directly adjacent to the burn plot. Instrumentation included the Teflon filters described above, as well as a non-dispersive infrared (NDIR) analyzer to determine CO_2 concentration. Additional emissions characterization instruments were also deployed, but will not be discussed in this paper.

Meteorological conditions were measured at two sites near the burn area. A 10 m tower was deployed approximately 2 km south of the burn and contained two sonic anemometers, a net radiometer, laser photometers (to obtain $PM_{2.5}$ concentration), temperature/relative humidity probes, and soil heat flux sensors. A 3 m tripod was deployed directly adjacent to the burn area, and contained a single sonic anemometer and laser photometer.

2.2.3 Calculation of Field Emissions Factors

Since fuel consumption in the field cannot be reliably determined, it is generally not possible to use Eq. (1) to determine the emissions factor. However, since the laboratory emissions factor of CO_2 measured by our colleagues was seen to vary over a narrow range (~1750 g/kg), emissions factor of $PM_{2.5}$ can be determined by determining the amount of $PM_{2.5}$ released relative to CO_2:

$$EF(PM_{2.5}) = ER(PM_{2.5}) \times EF(CO_2) \tag{3}$$

where ER is the ratio of $PM_{2.5}$ to CO_2 concentration, and $PM_{2.5}$ concentration was obtained by dividing the mass deposited on the filter by the product of filter flow rate and measurement duration. Emissions factors were determined during four measurement periods of 60 minutes each.

2.2.4 Fire Behavior

Weather conditions at the time of ignition were WNW at 2-5 m/s with a temperature of 19°C and 50% RH. These conditions were not conducive to extreme fire behavior. The fire was ignited from the perimeter by hand. Flame lengths averaged 2-3 m, but sometimes exceeded 5 m in dense fuel stands (Figure 4). Active flaming occurred for approximately 5 hours.

Fig. 4. Typical fire behavior during Vandenberg AFB prescribed burn

3. Results and Discussion

3.1 Laboratory Experiments

A summary of emissions factors obtained during laboratory experiments is shown in Table 1. These values compare favorably with the measurements of Hardy et al. (1996), who measured emissions factors using an apparatus deployed above the flaming front of a field-scale prescribed burn. The measurements of Weise et al. (1991) were of smaller scale (sampler height only 1.8 m above fuel bed) and fuel moisture content was high (greater than 50% of dry fuel mass for all fuels).

Table 1. PM$_{2.5}$ Laboratory emissions factors for selected southwestern chaparral fuels

Fuel type	PM$_{2.5}$ EF (g kg^{-1}) (This study) [a]	PM$_{2.5}$ EF (g kg^{-1}) (Literature)
Chamise/Scrub Oak	7.38 ± 2.11	20.05 [b]
Chaparral[c]	5.46 ± 1.31	8.65 ± 0.60 [d]
Ceanothus	4.62 ± 2.08	67.65 [b]
Maritime Chaparral	4.10 ± 0.34	N/A
Coastal Sage	6.36 ± 0.72	47.27 [b]
California Sagebrush	6.87 ± 0.83	N/A
Manzanita	3.61 ± 1.17	87.37 [b]

a. Data represented as mean ± one standard deviation of the mean

b. Data obtained from Weise et al. (1991) using glass fiber filters

c. Southwestern chaparral fuel (multiple species)

d. Data obtained from Hardy et al. (1996) during field measurements using carbon mass balance method

3.2 Field Experiments

A summary of PM$_{2.5}$ emissions factors obtained during field experiments is shown in Table 2. Because fuels within the burn site were mixed, the values shown represent an average for all fuels. Throughout the burn, the emission factor was seen to increase, except during the last measurement period. The most likely explanation for this is the decrease in combustion efficiency

near the measurement location as the burn progressed. Christian et al. (2003) illustrated that an inverse relationship exists between combustion efficiency and particulate emissions production. During the first measurement period, fuels near the truck were actively flaming. However, as the burn progressed, the truck began to sample smoke from smoldering (i.e. less efficient) combustion.

Table 2. $PM_{2.5}$ Field emissions factors for southwestern chaparral at Vandenberg AFB

Local time	$PM_{2.5}$ EF $(g\ kg^{-1})$
1100 - 1200	5.27
1215 - 1325	7.57
1335 - 1450	14.13
1505 - 1605	3.49

5. Summary and conclusions

Experiments to determine $PM_{2.5}$ emissions factors for southwestern chaparral fuels were performed in the laboratory and during a full scale prescribed burn using two different methods. The calculated emissions factors were compared to published values, as well as data obtained for identical fuels using filter methods. The meteorological data obtained during this study is currently being used in computational modeling efforts to study the characteristics and effects of dispersion and pollutant transport from prescribed burns.

References

D. Shusterman , J.Z. Kaplan, C. Canabarro, West J. Med. (158) (1993) 133-138.

T.J. Christian, B. Kleiss, R. J. Yokelson, R. Holzinger, P. J. Crutzen, W. M. Hao,H. Saharjo, D.E. Ward, J.Geophys. Res., 108 (2003), 4719.

S. Hosseini, Q. Li,, A. Miller, D. Cocker, M. Sharivastava, D. Weise, W. Hao, R. Yokelson, H. Jung , Chemical and Physical Characterization of Wood Smoke under Controlled Conditions. Fall Meeting of the Western States Section of the Combustion Institute, Irvine, CA, 2009

D.R. Weise, D.E. Ward, T. Paysen, A. Koonce, Int. J. Wildland Fire 1 (1991) 153-158.

C.C Hardy, S. Conard, J. Regelbrugge, D. Teesdale, Smoke Emissions From Prescribed Burning Of Southern California Chaparral, Research Paper PNW-RP-85, USDA Pacific Northwest Research Station, 1996.